

THESE

En vue de l'obtention du : **DOCTORAT**

Centre de Recherche : **CENTRE DE RECHERCHE EN ENERGIE**

Structure de Recherche : **MECANIQUE DES MATERIAUX**

Discipline : **PHYSIQUE**

Spécialité : **MECANIQUE DES MATERIAUX**

Présentée et soutenue le 05/01/2019 par :

Abderrahim BENDADA

**VULNERABILITY ASSESSMENT FOR BUILDINGS AGAINST TSUNAMI
IN THE GULF OF CADIZ AND COMPARISON TO SEISMIC
VULNERABILITY ANALYSIS**

JURY

Mohammed KERROUM, P.E.S, Faculté des Sciences, Université Mohammed V, Rabat **Président**

Abdallah ELHAMMOUMI P.E.S, Faculté des Sciences, Université Mohammed V, Rabat **Directeur de Thèse**

Kamal GUERAOUI P.E.S, Faculté des Sciences, Université Mohammed V, Rabat **Rapporteur/Examineur**

Aomar IBENBRAHIM P.E.S, Institut Nationale de Géophysique, CNRST, Rabat **Rapporteur/Examineur**

Khalid ELHAROUNI P.E.S. Ecole Nationale d'Architecture, Rabat **Rapporteur/Examineur**

Année Universitaire : 2018/2019

TO MY PARENTS

TO MY WIFE

Acknowledgments

This work has been achieved through lots of struggle and efforts.

I would like to thank Allah the Merciful for his assistance and guidance that helped me complete my thesis with honor.

This thesis has been prepared in the Laboratory of Mechanics and Materials and directed by the professor Mr. ELHAMMOUMI Abdallah, head of this laboratory. I gratefully acknowledge the staff of this active and esteemed laboratory within the University of Mohammed V, Rabat for their assistance, patience and useful advices.

I am deeply indebted to my professor and director of thesis, Mr. ELHAMMOUMI Abdallah, who has been an excellent mentor and supporter in all this thesis phases, as well as a helper in any scientific ceremony, meeting or conference. I appreciate his noble work and thank him for all his efforts.

I would like to express the deepest appreciation to my professor and committee chair, Mr. KERROUM Mohammed, for his tireless guidance and benefic assistance.

In addition, I would like to thank my professor IBENBRAHIM Aomar, for his persistent help and continuous enthusiasm. Without his support, this work would not have been possible.

My thanks are also addressed to my professor Mr. GUERAOUI Kamal, for imparting his knowledge and expertise in this study.

I would also like to thank my professor, Mr. ELHAROUNI Khalid for his benefic advices and helpful support.

Many others have made this thesis successful, namely, Mr. SAMMOUDA Mohammed, Mr. MENLAYAKHF Samir, Mr. ALLAOUI Mohammed, and many other people whom I acknowledge their help and thank them plenty.

ABSTRACT

This work investigates the tsunami vulnerability of structures through numerical simulations of the impact. Our method is based on a structural analysis of the building frame and the exploitation of mechanical behavior results. Objective judgments of the building state in case of a tsunami attack is conducted through engineering references and methodologies like the displacement-base shear analysis, known for seismic analysis as the pushover curve. Interesting findings from the analysis of two test buildings introduced in this study provide a considerable asset in the assessment of tsunami vulnerability. One branch of the study develops an analysis of infill masonry walls' response for both types: in-plane and out-of-plane walls, while another branch details the reinforced concrete frame response as well as a CFD analysis of the tsunami attack. The RC behavior is fully discussed through an expanded explanation of results of the maximum displacements recorded, bending moment's distribution, nonlinear hinges reactions, and the decrease of building's stability.

Setting the assessment of tsunami vulnerability as the main objective, this study has reached its goals of illustrating seismic pushover curve, plotting tsunami capacity curve and fragility curves as well as justifying the findings with a logical interpretation and detailing the discussion of results.

Key Words (5) : vulnerability, building, tsunami, seismic analysis, pushover.

RESUME

La présente thèse traite le sujet d'analyse de la vulnérabilité tsunamique des structures en se basant sur des méthodes précises s'appuyant sur les règles d'ingénierie et les lois de la dynamique des structures.

Les trois éléments principaux de l'étude sont décrits : la connaissance du tsunami, ses forces et ses caractéristiques, les normes de dimensionnement des structures en béton armé et la méthode des éléments finis. En outre, une description de l'analyse de la vulnérabilité sismique est introduite puisque elle aide à comprendre la réaction de la structure suite à une sollicitation extérieure. Les caractéristiques du tsunami, les charges qu'appliquent la vague et la distribution de ces charges sur les obstacles rencontrés sont illustrées. En se basant sur ces éléments, une analyse détaillée sur la vulnérabilité tsunamique est développée sur deux niveaux: pour les bâtiments réguliers et pour les structures stratégiques pour l'évacuation comme les écoles. Plusieurs éléments de cette analyse sont traités, comme la réaction des murs en maçonnerie, l'étude de mouvement des éléments des portiques, ...etc. La déduction des déplacements et les déformations nous permet d'établir la courbe de capacité et les courbes de fragilité qui indiquent les probabilités des dommages que subiront les éléments structuraux et non structuraux et déterminent la vulnérabilité du bâtiment.

Mots-clefs (5) : vulnérabilité, bâtiment, tsunami, analyse sismique, pushover.

RESUME SOMMAIRE

La présente thèse traite le sujet d'analyse de la vulnérabilité des structures vis-à-vis du tsunami. En effet, la catastrophe de l'inondation de la vague de tsunami sur les zones côtières apporte des dégâts majeurs sur les structures existantes ainsi que des répercussions significatives sur la population et le tissu démographique. Le tsunami en outre est largement connu par la rapidité d'attaque et le temps limité pour la prévention. C'est dans cette perspective et dans le souci d'atténuer l'ampleur du danger de tsunami que cette étude est réalisée.

L'analyse de la vulnérabilité d'une structure consiste à quantifier et classer les dommages subis par ses éléments constructifs lors d'une sollicitation extérieure qu'est la vague de tsunami dans le cas présent de cette thèse. Cette quantification s'établit en faisant référence à au moins un paramètre de sollicitation comme le déplacement dans le cas d'une sollicitation sismique. Plusieurs paramètres peuvent influencer la mesure de la vulnérabilité et la détermination du degré de dommage subis par la structure. C'est en effet ce qu'a essuyé de nombreux chercheurs dans les domaines liés à la simulation de l'inondation de la vague de tsunami et la mesure de la vulnérabilité tsunamique de structures, comme Papathoma et al 2003, Benchekroun et al 2013. Des modèles d'estimation de vulnérabilité suggérés par ces chercheurs proposent des formules et des pondérations approximatives des éléments et paramètres qui peuvent influencer la vulnérabilité d'une région, à savoir : l'état de la structure existante, le rang d'exposition, l'entourage, les défenses maritimes à la côte... etc. Le résultat est exprimé en terme d'un facteur BV (building vulnerability) ou BTV (building tsunami vulnerability) qui regroupe tous ces paramètres selon leurs importance vis-à-vis la vulnérabilité mesurée. Un mappage de la zone d'inondation est ainsi établis où le facteur de vulnérabilité est calculé et réparti. Cette cartographie aide ainsi à localiser les régions les plus vulnérables et fragiles à l'inondation, pour prendre les décisions stratégiques de l'évacuation en cas d'une alerte future de tsunami.

Cependant, ces modèles se basent sur des approximations subjectives et des jugements généralement imprécis basés sur des verdicts visuels ou des estimations vagues des paramètres inclus dans le calcul du facteur de vulnérabilité. Par exemple, la détermination de l'état de la structure par les méthodes cités ci-dessus est faite suivant un sondage visuel pour voir le matériau supportant la structure (notamment le béton-armé, l'acier, le bois...etc) et

d'attribuer à chaque matériau un coefficient vague qui exprime sa résistance probable aux sollicitations de l'inondation, sans prendre en considération l'influence de la dynamique de la structure et le mouvement des portiques du bâtiment. Le jugement pourrait être erroné sans prendre effectivement les effets de la dynamique de la structure en considération. C'est pour cette raison que nous avons essayé à travers la présente étude, d'établir des méthodes objectives et précises s'appuyant sur les règles d'ingénierie et les lois de la dynamique des structures pour ainsi quantifier concrètement la vulnérabilité d'une structure attaquée par le tsunami.

Donnons l'exemple d'une structure située sur le premier rang près de la côte : cette structure se voit sollicitée par l'inondation de tsunami à travers divers forces s'appliquant sur les éléments du bâtiment. Ces forces qui sont des forces de contact du fluide formant la vague du tsunami, qui peut encercler le bâtiment, développent des actions sur les éléments structuraux et sur les murs (dans leurs plans et hors plans).

Les contraintes engendrées par ces forces créent des déplacements aux nœuds des portiques du bâtiment et des déformations de la structure porteuse. Les éléments verticaux sont sollicités en flexion composée puisqu'ils supportent la descente de charges des niveaux supérieurs et l'action du tsunami.

L'objectif est donc de déterminer les déplacements et les déformations lors de l'action du tsunami, qui sont dans notre étude les paramètres-clé pour quantifier la vulnérabilité de la structure et évaluer la fragilité du bâtiment.

Ce rapport débute par une introduction définissant la problématique du sujet de la thèse, l'objectif à atteindre, les limitations prévues dans l'étude, et finalement l'organisation de la thèse. Le chapitre suivant traite les trois éléments principaux de l'étude, à savoir : (1) la connaissance du tsunami, ses forces et ses caractéristiques, (2) les normes et les règles de l'art pour le dimensionnement des structures en BA et troisièmement (3) la méthode numérique de résolution (méthode des éléments finis).

Le troisième chapitre donne une description de l'analyse de la vulnérabilité sismique puisque le fondement de l'analyse sismique peut largement aider à comprendre la réaction de la structure vis-à-vis une sollicitation extérieure comme le tsunami ainsi que d'apporter une réflexion aux moyens de valorisation de la vulnérabilité tsunamique. Ce chapitre est suivi par une section qui décrit les caractéristiques du tsunami, la simulation de son inondation, les charges qu'appliquent la vague et la distribution de ces charges sur les obstacles rencontrés. Ces premiers chapitres aident à décortiquer et développer une analyse détaillée sur la

vulnérabilité tsunamique sur deux niveaux: pour les bâtiments réguliers (chapitre 5) et pour les structures stratégiques pour l'évacuation comme les écoles (chapitre 6). Pour ces deux chapitres, plusieurs éléments sont traités comme la réaction des murs en maçonnerie, l'étude de mouvement des éléments des portiques, le développement des rotules non-linéaires, l'évaluation des déplacements et des déformations...etc.

Pour illustrer la vulnérabilité d'une structure sollicitée au tsunami, nous avons étudié deux cas : un bâtiment de trois niveaux (R+2) et une école de quatre niveaux (R+3).

Les efforts de la vague sont calculés selon les formules proposées par la norme FEMA-P646 et sont par la suite introduites comme charges sur les éléments de la structure (les murs et les portiques). Après l'analyse de la réaction du bâtiment par la méthode des éléments finis, la déduction des déplacements et les déformations nous permet d'établir la courbe de capacité et les courbes de fragilité. Ces dernières courbes indiquent les probabilités des dommages que subiront les éléments structuraux et non structuraux et déterminent la vulnérabilité du bâtiment.

SUMMARY

Tsunami is a threatening catastrophe upon many coastal regions. The analysis of vulnerability of buildings against tsunami strike has become a crucial task for government authorities in order to prepare cities for immediate response and possibly evacuation plans as well as to bestow awareness and understandings on population about a possible tsunami event.

This work tries to investigate the tsunami vulnerability of structures through numerical simulations of the impact of an incoming wave. Our method is based on a structural analysis of the building frame and the exploitation of results about the mechanical behavior of the building. Objective judgments of the state of the building in case a tsunami attack is conducted through engineering references and methodologies like the displacement-base shear analysis, known for seismic analysis as the pushover curve. Additionally, the comparison of these findings to the observed data from previous tsunami events helps approving the retrieved results as well as recognizing the possible similarities and differences.

This study explains numerous basic elements which are fundamental in tsunami vulnerability analysis: tsunami simulations of propagation and inundation, building codes that are essential in designing the building frame and finally a complete comprehension of seismic vulnerability analysis which serves as an important leading guide in the analysis.

Interesting findings from the analysis of two test buildings introduced in this study provide a considerable asset in the assessment of tsunami vulnerability. One branch of the study develops an analysis of infill masonry walls' response for both types: in-plane and out-of-plane walls, while another branch details the reinforced concrete frame response as well as a CFD (computational fluid dynamic) analysis of the tsunami attack. The reinforced concrete behavior is fully discussed through an expanded explanation of results of the maximum displacements recorded, bending moment's distribution, nonlinear hinges reactions, stresses fluctuation and also the decrease of building's stability.

Setting the assessment of tsunami vulnerability as the main objective, this study has reached its goals of illustrating seismic pushover curve, plotting tsunami capacity curve and fragility curves as well as justifying the findings with a logical interpretation and detailing the discussion of results. Finally, a conclusion brings upon a general summary of the outcome of the work, explaining the advantage of the study method as well as directions for the development possible axis and future works.

Table of contents

Acknowledgments.....	2
ABSTRACT.....	3
RESUME.....	4
RESUME SOMMAIRE	5
SUMMARY.....	8
Table of contents.....	9
1. Introduction.....	11
1.1. Defining the problem	11
1.2. Objective.....	12
1.3. Limitations	14
1.4. Organization of the thesis	14
2. Study elements description.....	16
2.1. Introduction.....	16
2.2. Tsunami	17
2.3. Building design codes	17
2.4. Numerical analysis method (FEM).....	18
2.5. Conclusion	19
3. Analyzing seismic vulnerability.....	20
3.1. Introduction.....	20
3.2. Pushover analysis	21
3.3. RISKUE methodology for seismic vulnerability assessment.....	27
3.4. Conclusion	31
4. Tsunami characteristics.....	32
4.1. Introduction.....	32
4.2. Simulation of inundation.....	33
4.3. Tsunami loading	36
4.4. Distribution of tsunami forces.....	41
4.5. Conclusion	44
5. Assessing tsunami vulnerability for common buildings: focus on infill masonry.....	45
5.1. Introduction.....	45
5.2. Characteristics of the test building.....	46
5.2.1. Architectural plan.....	46
5.2.2. Frame elements design	46

5.3.	Infill masonry analysis	48
5.3.1.	Out of plane walls.....	48
5.3.2.	In plane walls.....	55
5.4.	RC frame analysis.....	59
5.4.1.	Equation of motion.....	59
5.4.2.	Time history.....	60
5.4.3.	Steps of analysis	62
5.4.4.	Results	62
5.5.	Conclusion	69
6.	Assessing tsunami vulnerability for a school building: comparison with seismic vulnerability	70
6.1.	Introduction.....	70
6.2.	Designing the test school building	71
6.2.1.	Architectural plan.....	71
6.2.2.	Frame elements design	72
6.3.	Simulation of the inundation.....	73
6.3.1.	Introduction.....	73
6.3.2.	Computational fluid dynamics (CFD).....	73
6.3.3.	Model characteristics	73
6.3.4.	Results and interpretation.....	76
6.4.	RC frame	79
6.4.1.	tsunami forces distribution	79
6.4.2.	Pushover curve.....	80
6.4.3.	Capacity curve for tsunami loading.....	81
6.4.4.	Fragility curve analysis	85
6.5.	Conclusion	87
7.	General Conclusion and direction for future research.....	87
	Conclusion Générale	89
	Practical example	93
	Appendix	95
	Bibliography	98
	List of figures.....	102
	List of tables	105

1. Introduction

Content

- 1.1. Defining the Problem
- 1.2. Objective
- 1.3. limitations
- 1.4. Organization of the thesis

1.1. Defining the problem

Tsunami has been increasingly considered as an alarming and threatening catastrophe that leads to many fatalities and economic losses. The powerful wave that strokes the shore of many coastal countries results with a large destructed field, collapse of buildings, deficiency of infrastructures, without counting the enormous number of deaths, injured people or diseases spread. These areas suffer also from a difficult ability to access to the inundated zones due to the debris, and the malfunctioning of some important facilities like power plants, water resources, or even a critical facility like nuclear plants (case of Fukushima power station:([Kawatsuma, Fukushima, and Okada 2012](#))). Therefore, these reasons influenced the public opinion and the decision makers to make a careful understanding about the phenomenon of tsunami, from its generation, propagation and inundation to the fragility measure whether for population or structures.

Many research studies ([Norwegian Geotechnical Institute 2013](#); [Omira et al. 2010](#)) analyzed the causes of the tsunami like rupture of the ocean's bed fault or giant landslides. Then, they simulated the behavior of the wave until its arrival to the coast where the inundation submerges a large land area. These simulations also provided some useful information about the run-up height, the estimated velocities in different distances from the shore, accelerations, maximum flooding limits, etc.

These studies are based on probabilistic or deterministic approaches. The first approach, the probabilistic, uses different data collected from the past tsunami events with numerous magnitude and frequencies to describe the future probable scenarios, while the second approach, deterministic, is based on a single-valued event to approximate the scenario-like mechanism. The probabilistic methods require large data from historical events and multi-sources analysis, this is why it cannot be used in a region with lack data, unlike the deterministic method, which is more suitable in this case.

The other part that helps understanding the tsunami threat is the human and construction vulnerability measures. One of the most known methods applied to assess vulnerability is the Papathoma method (Dall’Osso et al. 2009; Dominey-Howes and Papathoma 2007; Papathoma et al. 2003) which works on a “tsunami vulnerability assessment model” (PTVA1, and the revised versions PTVA2 & PTVA3). The authors propose a dynamic model that incorporates multiple parameters influencing the tsunami vulnerability (Dominey-Howes and Papathoma 2007). These parameters include the built environment (the buildings’ material and surrounding, number of floors...), sociological data (population density and distribution), economic data, and environment data (natural protection, defense walls...) ((Papathoma et al. 2003)). The method adds also some parameters for the day/night distribution of population, seasonal density and even the distribution of movable objects (tables and chairs). Such method requires a precise and meticulous work based on a good handling of GIS tools and surveys analysis. The obtained results are interesting and show the human vulnerability toward a tsunami threat. Later revised version of the PTVA model, seeking to refine the vulnerability study, makes some additional weighted elements like the water intrusion. However, this method does not correctly specify the state of buildings exposed to the threat and the input data is based on pure subjective judgment on the conditions of structures.

In order to emphasize the structure’s influence on vulnerability measure, other studies worked on multi-criteria methods that categorize the buildings according to a defined matrix classification. An example of this way of analyzing vulnerability is the BTV (building tsunami vulnerability) method explained by (Benchekroun et al. 2013). The authors explain that the BTV model attempts to predict the buildings’ tsunami vulnerability through the identification of factors that control the expected building damage. Three main parameters are introduced to calculate the BTV value, which are the construction condition, the building location and the water depth. Weight factors (F_{wi}) calibrate these parameters to amplify the influence of important ones than others: the building classification matrix defines and describes classes of buildings according to their “degree of resistance”: very weak, weak, medium, good and very good. Classes usually follow the number of stories of the building. The classification of the sea defense regroups regions with higher retaining elements like tetrapods and concrete walls. Finally, the water intrusion, which is based on inundation simulation, defines the limits of areas that would suffer from higher or lower water depths. The work’s results are summarized through a mapping with a GIS tool that shows the inundated zone and the vulnerability classes’ areas. Although the method is good at explaining the distribution of building’s vulnerability and giving a general idea about the consequences of a tsunami attack, it is based on the allocation of subjective opinions about the buildings’ classification with no precise defined limits between categories and with personal judgment of the resistance of buildings’ types to tsunami forces. Such subjectivity of classification could lead to erroneous results without counting its time consuming for large surveys.

1.2. Objective

In order to evaluate the vulnerability of buildings against the dangerous strike of tsunami wave, this study tries to establish an objective and technical method based on a software analysis of the structure put under tsunami forces. The key of this procedure is the use of the finite element method (FEM) to analyze the behavior of the structure frame. This simulation provides accurate results about the displacements and the reactions of various points in the structure frame. The method also allows

visualizing the deformations recorded for different elements of the structure through time. Furthermore, analyzing the building's behavior with much detail on its mechanical properties helps determining its capacity at resisting tsunami actions and permits an objective comparison with the "demand" of tsunami. Thanks to that, the assessment of vulnerability of structures against tsunami impact is fulfilled which allows understanding the tsunami's scenario.

The procedure of the method is as follows:

- ❖ Choosing a coastal area threatened by a probable tsunami attack.
- ❖ Analyzing the buildings' distribution all over the coast subject to the collision with the tsunami wave and recognize the existing types of buildings (RC, steel frame, masonry, etc.)
- ❖ Identify the inundation scenario and the wave characteristics in each zone of the shore, including the run-up height, velocities, accelerations and flooding limits. This is based on simulations previously studied and it is not subject to this study.
- ❖ Use the database of the frame element's mechanical properties, materials characteristics and tsunami forces to create a model of a building (or a group of buildings) in a structural analysis program, recognized as reliable in engineering design and loadings' calculations.
- ❖ Determine the capacity of the building at resisting tsunami actions when loaded by the tsunami forces.
- ❖ Plot the fragility curves for each level of vulnerability.
- ❖ Compare the plotted curves with statistical data from previous tsunami events in order to validate the suggested model.

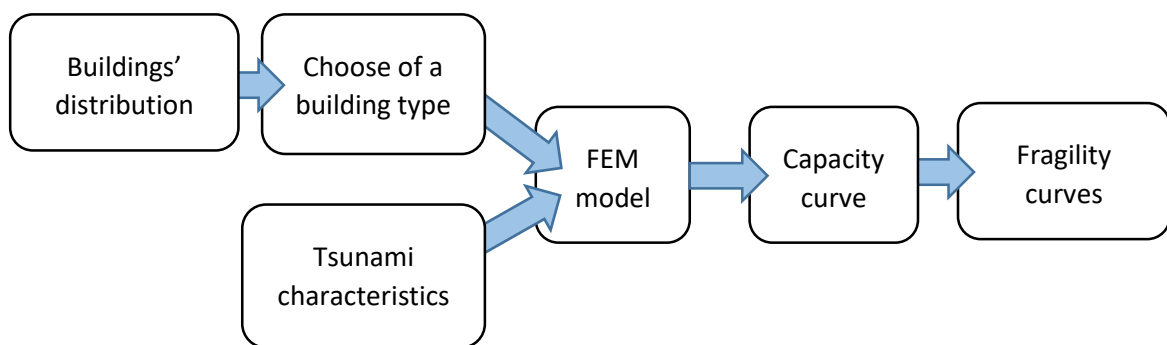


Figure 1: project organization

This study has integrated and accompanied different international projects for assessment of tsunami vulnerability (Inspired, ASTARTE). These projects emphasized the exchange of ideas and the collaboration between different teams. For this work, we have chosen the region of Tangier, north Morocco because it is subject to some developed analysis of generation, propagation and inundation of a probable tsunami in the Gulf of Cadiz. The study exploits the results about tsunami characteristics and inundation descriptions provided by these works. It is also worth mentioning that other studies analyzed the coastal buildings' distribution (Atillah et al. 2011; Benchekroun et al. 2013) and defined the categories and types of buildings near the shore. This has also saved the time for other surveys. We focus in this study on analyzing the buildings' reaction with a FEM model and assess the vulnerability of these structures.

1.3. Limitations

Considering the objective of this work, some assumptions are introduced to simplify the assessment of vulnerability. This concerns the following remarks:

- ❖ The analysis works on buildings with similar geometry forms. Buildings with irregular form or with complex geometry are excluded.
- ❖ The complex behavior of tsunami wave is simplified. The turbulent movement of water, deformations in topography and the rundown wave are not considered.
- ❖ Some complex phenomena related to the movement of water (like the scour) are not considered.

Further simplifications are introduced when necessary.

1.4. Organization of the thesis

This thesis consists of six chapters. It starts with a general introduction where the definition of the problem of tsunami vulnerability assessment is provided. This discusses the state-of-the-art of existing assessment methods and the advantages and inconvenients of the present vulnerability analysis process. The chapter also explains the aim of the thesis, which tries to give an objective way to determine the buildings' vulnerability using of the capacity curve. Some limitations are signaled so that the analysis of the finite element model could be smoothly achieved. Scope and organization of the thesis is presented in this chapter.

The second chapter describes the study elements. It gives an overview about the phenomenon of tsunami all over the globe with more attention to the case of the Gulf of Cadiz. The chapter summarizes the previous studies established in this region that concern the tsunami wave creation at the bed sea, the movement of the wave from oceanic waters to shallow waters, and the inundation in the city of Tangier, north Morocco. The chapter also discusses the current building design codes applied in the structural dimensioning task. These codes normalize the technical considerations taken into account when defining the cross-section design of the frame elements. Codes or "norms" applied in the region of Tangier are illustrated, which helps simulating the structure FEM model with more precision and realism. Finally, this chapter describes the FEM method and its benefits for accurate calculation issues.

The third chapter concerns the previous research studies that discussed the vulnerability of buildings when an earthquake strikes. In fact, the assessment of vulnerability for a tsunami risk has much resemblance with a seism risk case. Although the forces' application pattern is not identical for the two cases, the structure reaction remains under the law of the equation of motion. This helps defining the capacity curve and the fragility curves. The chapter explains the pushover method recognized as a noticeable tool to evaluate the capacity curve of a building under seismic loads. The concept of the method is illustrated and the steps that permit to plot the capacity curve are detailed. Next, a brief review about the RISKUE methodology ([Risk-Ue 2003](#)) that defines the vulnerability assessment procedure in seismic case is given. The two approaches LM1 and LM2 are compared and the use of the LM2 approach is explained as well.

The fourth chapter deals with tsunami characteristics. The simulation of inundation studied by (Omira et al. 2011) and others is explained. The process of simulation as well as the governing equations of fluid motion (Navier-Stokes equations) are introduced in order to comprehend the methodology of modelling the wave and tracking its movements. The following section presents tsunami forces with the aim of developing a generalized set of loadings formulas and temporal distributions. Combination of these forces is illustrated as well because it is important to understand the succession of steps of the wave's impact. Laboratory tests, listed after, come to validate the adopted formulas and propose the time history diagram usually followed by the wave forces.

The fifth and sixth chapters represent the core of the thesis and focus on the assessment of vulnerability for two types of buildings. The fifth chapter tries to investigate the vulnerability of common buildings with more interest in the infill masonry response to tsunami impact. The building introduced in this chapter is a working place of GF+2floors dimensioned and designed using building codes for the task of determining the cross sections of the frame elements. Explanation about the standards of dimensioning and loads application pattern is provided in this section. The work then is oriented into analyzing the infill masonry walls for its two types: out-of-plan walls and in-plan walls. For each type, existing models and mathematical representation is described, as well as the Eurocode'6 recommendations and suggestions. The results of the infill masonry reaction to tsunami solicitation are detailed, either by analytical solutions or FEM method. Another section of the chapter analyzes the RC frame response through developing the equation of motion and describing the time history integrated in the FEM model. The steps of the analysis are explained and fully detailed. Results show some general finding about maximum recorded displacements, hinges results and stresses variation through time. Capacity curve and fragility curves are plotted after with a comparison to statistical data from previous tsunami events, in order to validate the model and explain the points of similarities and differences.

The sixth chapter investigates the assessment of tsunami vulnerability for a school test building with more interest in seismic comparison. The school structure is a strategic building with an important role in the immediate tsunami evacuation plan. The first section of this chapter is dedicated to the representation of the school architectural plans and the explanation of the frame elements' cross-section design. A simulation on a CFD program, which helps understanding the flow characteristics and properties, is then introduced by defining the fluid properties such as velocity and creating a 3D model of the school building. Finally, the results of the CFD simulation are interpreted and explained with the illustration of the available features in the program results. The third section of the chapter investigates the RC frame behavior with the elaboration of capacity curve and fragility curves. A comparison to pushover curve and other fragility curve from statistical data of previous tsunami events is introduced in order to compare the tsunami and seismic actions on the building.

2. Study elements description

Content:

- 2.1. Introduction
- 2.2. The tsunami phenomenon
- 2.3. Building design codes
- 2.4. Numerical analysis method (FEM)
- 2.5. Conclusion

2.1. Introduction

This part of the thesis introduces the three main components influencing directly the study of tsunami vulnerability: (1) The tsunami phenomenon, (2) Building design codes and (3) Numerical analysis method (FEM).

First, an overview of the tsunami phenomenon is given, starting from its creation to the propagation and finally the inundation. The major factors that cause the tsunami are then detailed. Special attention is given to the mechanism of generation of tsunamis and the wave behavior through the successive phases of its lifetime. An additional chapter focuses on the consequences of the inundation on the shore especially in the study area: The Gulf of Cadiz.

In the second part, building design codes that help dimensioning structures are described. This part illustrates different design codes available and applicable in many countries. In fact, many countries, or groups of countries, choose to adopt their own building design code by unifying the procedures of calculations and dimensioning task. More attention is devoted to the Eurocode norm due to its importance in making the design procedure standards in the countries next to the Gulf of Cadiz (Morocco and Portugal). We illustrate different parts of this standard and the missions accomplished by each part. Next, we try to define the former norm, the limit state design, which is applied to dimension existing structures. We explain the components of this norm and describe the criteria considered when analyzing a structure element following this code.

The third part introduces the finite element method. First, we give an overview about existing methods to solve a mechanical problem. We explain the differences between these different methods and define the main functions fulfilled by each one. We focus more on the finite element method and

describe its strengths compared to other methods and also its shortcomings. We detail the steps that lead to the solution of mechanical problems with this method. Finally, we present the software SAP2000 that permits analyzing a structure with the finite element method and the features offered by this program. The study discusses benefits of this program and some important results extracted from its analysis.

2.2. Tsunami

Tsunamis are among the most devastating catastrophes that strike coastal cities. They are caused by a sudden disturbance in the sea bed like earthquakes or volcanic eruptions. The large amount of energy released by this disturbance spreads out the water column at a great speed. Series of waves are created from the epicenter of the fault in case of earthquakes and travel long distances without being noticed with high speed also. Tsunami waves are characterized by their length and high speed. When the tsunami wave arrives near coastal shorelines, the water column is reduced and the first waves become compressed because of the successive arrival of the series of waves. This results in a reduction in the wavelength of waves and consequently the abrupt increase of water height. As the energy accumulated in the compressed wave increases, the crest overturns at a certain moment and the wave collapses. The phenomenon is known as “the breaking waves”, but it is large and powerful in case of tsunamis. Some records of tsunamis show that the height of breaking tsunami waves could vary from 3m to 30m, which proves the danger of tsunami attacks on population and infrastructures.

In this study, we undertake an assessment of the vulnerability of buildings and structures in case of a tsunami attack. The focus is specifically accorded to buildings next to the shore in Morocco. This area, chosen as the study area, is located offshore SW Iberia and NW Morocco and characterized by a high seismicity and tectonic activity. This is why it is considered as an important tsunamigenic area in the Atlantic Ocean. Even if the most powerful and enormous tsunamis are located in the Pacific Ocean since it is hotbed to the continental and oceanic plates activity and volcanism, some coastlines in other regions are not safe from the threat of tsunamis and this is the case of the Gulf of Cadiz.

Over history, several tsunami events in the region of the Gulf of Cadiz have been recorded and described in the literature scripts (*El Mrabet 1991; Baptista & al 1998; Kaabouben & al 2009*). The most destructive tsunami mentioned in the history of this region was probably the November 1st 1755 tsunami that demolished the Lisbon city and caused many loss of lives. Moreover, some recent paleotsunami (*Luque & al, 2002*) and historical (*Baptista & al 1998*) studies in this region recognized the existence of previous tsunami events similar to the 1st 1755 tsunami. In fact, *Luque & al (2002)* recognized three deposits generated from past tsunamis. This emphasizes the consideration of the threat of future tsunamis that could strike the Gulf of Cadiz coastlines.

2.3. Building design codes

Building design codes define a set of rules that must be respected in a structural design. They highlight the restrictions, obligations and recommendations for every aspect in the process of building a structure such as the geometry of frame's elements, the level of resistance of materials, specific requirement for used materials (resistance to fire, low/high temperature/pressure, adaptability for salty or toxic environment, etc.). They indicate also the method of assembling frame elements and

mixing ingredient of materials like concrete, as well as diverse specifications for the security and environmental protection.

Building codes are considered as a law respected and enforced by authorities and various participants in the process of building structures. Architects, engineers, laboratories, constructors are all highly concerned in understanding the aims of building codes applied in their region and responsible for providing plans and buildings respecting the specifications of the adopted code.

In order to develop a building code, many laboratory tests and experiments are undertaken so as to know the characteristics of materials, their strength, ductility, consistence, cracks and failure mode, etc. The cost is very high regarding the importance of the acquired results. This is why many countries try to develop a united building code applied in all participating countries but with additional specifications for each country following its particular conditions and regional characteristics. The Eurocode is an example of this method. Other countries create their own building code or adopt a foreign code due to proximity considerations or conformity to local context. For the latter method, additional considerations are added for the local specifications.

In Morocco, the applied building code for concrete buildings is the BAEL91 and more recently the Eurocode, adopted for the Moroccan context. The BAEL91, is based on a limit state design procedure which considers two limit states to be respected: ULS (ultimate limit state) and SLS (service limit state). The former draws the boundaries where the structure becomes instable and incapable of bearing any additional load due to the overstress in frame elements or incapacity of an element for any further solicitation. This state usually indicates the limits after-which there is failure and rupture of the structure. The latter state highlights the necessary conditions for a building to assume a good functioning and serviceability in a given period. It determines a minimum required of material for example not to show any fractures or disorders in the working space. Both the ULS and SLS take into account some security coefficients and participate in the process of determining the characteristics of the building backbone.

The Eurocodes in the other hand introduce additional specifications to the structural design such as the aggressivity of the ambient environment. The characteristics of materials are reconsidered due to the recent development in materials' fabrication and the introduction of more elaborated technics to strengthen their resistance.

2.4. Numerical analysis method (FEM)

Nowadays, the use of computers and artificial intelligence has become widely common. The interaction with machine allows a considerable reduction of processes' time with elaborated and precise results. In the civil engineering domain, this numerical approach is quite useful.

The process of modelling and designing a structure, will it be a bridge, a building or a tank of water, requires a large base of knowledge and technics of the art of building. This also stands on a powerful mathematics and physics' knowledge to determine accurately the distribution of forces and stresses in a given frame. Note that the engineer must also bear in mind the diversity of building materials and the complexity of their functioning, limits and maneuverability. In order to overcome this challenge of designing a structure each time, the right tool is surely by exploiting the advantages of numerical simulations and calculations. This is where the finite element method was born.

The finite element method (FEM) is a handful tool that could deal with complex geometry and mechanical problems. The method is founded on three bases, which are:

- The approximation of a general output parameter
The structure shows diverse reactions due to external solicitations. In order to quantify these reactions, a mechanical parameter like displacement or base shear force could be helpful. The measure of this parameter allows the determination of over-stressed areas and dangerous zones where cracks and rupture of the element could occur. Thus, it is necessary to establish a mathematical model that links the solicitation to the reaction of each node in the structure. Note also that the introduction of boundary conditions where the displacement for example is null or where the rotation is null (for fixed links) is necessary to solve the problem.
- The Discretization of the elements:
The finite element method adopts its name because in this method, the frame elements are discretized in small elements with determined shapes (rectangles or triangles) and finite size. A mathematical model is applied to each finite element because it is easier to handle small sized shapes than to model the entire structure. It is important to note that the smaller the grid of elements is and how it is distributed, the more precise the results are.
- General equilibrium of the structure:
To each node in the finite element system, the mechanical equilibrium must be verified and respected. The equilibrium regroups a set of equations like the virtual work principle. These equations try to determine the relationship between external forces (described mathematically by a vector $\{F\}$ applied in some nodes of the structure) and output parameters like the displacement vector $\{u\}$ in each node. Mechanical properties are integrated in the stiffness matrix $\{K\}$ that describes the rigidity of the frame element. The system to solve is by far the following system:

$$[K]\{u\} = \{F\}$$

Stresses and deformations can be calculated later through appropriate formulas.

The FEM is a useful tool that simplifies the task of dimensioning and optimizing the structural backbone of a building. Some powerful software were built in order to simplify the introduction of a 3D frame of the building and the application of external loads. In this thesis, the work is achieved through simulations in the SAP2000 software, which is approved and considered reliable in structural analysis.

2.5. Conclusion

The base study elements that are tightly related to the analysis of vulnerability of buildings in the Gulf of Cadiz region are presented. This helps understanding the importance of this analysis and be aware of the threat of tsunamis in this area. In the first hand, the building design codes inform us about the structures' "backbone" and the frame elements constitution. In the other hand, the presentation of the finite element method gives an overview about this sophisticated method and its benefits in examining the behavior of structures. The outcome of these elements will be useful in the comprehension of the pushover method and the RISKUE methodology, described in the next chapter, and the building analysis in further chapters.

3. Analyzing seismic vulnerability

Content:

- 3.1. Introduction
- 3.2. Pushover analysis
- 3.3. RISKUE methodology for seismic vulnerability assessment
- 3.4. Conclusion

3.1. Introduction

Earthquakes are well-known natural catastrophes, caused by tectonic movements in the Earth's crust. They present a serious problem for many countries like Japan and the USA. This is the main reason behind adopting seismic design codes for buildings.

The mechanism of earthquakes is related to the movement of the Earth's plates. In fact, seismic waves result from the sudden release of energy when two blocks of fault move one with respect to the other. This energy is formed by the relative motion of plates that increases the stress in the boundaries of the fault. When the stress overcomes a specific limit, the energy stored is released, causing the sliding of the blocks. There are three types of fault sliding: the normal sliding, the thrust sliding and the strike-slip.

In order to minimize the casualties and economic losses caused by an earthquake, the seism - proofing or seismic design is a practice developed to construct buildings that withstand the motion of the ground. This practice has been adopted in many countries and implemented in the design codes for constructions of civil engineering structures. The buildings constructed under such standards suffer less from the stress created in the frame elements. The design code specifies the level required for material characteristics, the form and geometry of the building, specific construction assignments, etc.

Moreover, in order to analyze the vulnerability of a building to the seismic action, some recent approaches studied the risk scenario for a probable maximal earthquake event and proposed different methodologies to define different levels of damage for the structure. The concept of the methods consists on providing fragility curves that describe the damage rate of the frame elements, either structural or non-structural elements.

In the next section, we illustrate the nonlinear static procedure method called the pushover method that helps determining the capacity of buildings for resisting the seismic action. In a later section, we will describe the RISKUE approach for earthquake risk scenario and vulnerability analysis.

3.2. Pushover analysis

In order to determine the capacity of buildings to resist to seismic action, engineers use some elaborated methods to find out the bending moments and the stresses present in the frame elements. This helps dimensioning the frame elements' cross sections. Four methods, mentioned in EN'1998 (Standard 2005) section 4.4.1, are applied to evaluate the seismic action effects:

1. Lateral force analysis (static linear),
2. Linear dynamic procedure (linear),
3. Non-linear static (pushover) analysis,
4. Non-linear time history dynamic analysis.

	Linear	Nonlinear
Static	Force analysis	Pushover
Dynamic	Modal RSA	Time history dynamic analysis

Table 1 : methods of evaluation of a seismic action

Each method has its hypotheses and procedure.

1. **Lateral force analysis (static linear):**

This method allows modeling the structure with a linear elastic rigidity, where the yield level is the limit where the frame elements are responding. Due to the linearity of the method, seismic forces are distributed through pseudo lateral forces that describe displacements approximating the expected ones during a real earthquake event. The measure of displacement is a good indicator for damage in nonlinear zone than are forces. This model is applied when the fundamental period is the predominant one over other period values, and it assumes an excess of internal forces values due to the elimination of the inelastic response in calculations.

The procedure is based on three steps:

- Period determination: the fundamental period of the building is calculated by one of three methods: analytical (with eigenvalues analysis), empirical ($= C_t h_n^\beta$ where h_n is the height above the base to the roof level and C_t and β are coefficients shown in Table 2) or approximate method (by the Rayleigh-Ritz period determination method). For the Eurocode8, β equals $\frac{3}{4}$ for all frames.

Type of frame	Steel	Concrete	Steel eccentrically braced	Wood	Other frames
C_t	0.035	0.018	0.030	0.060	0.020
β	0.80	0.90	0.75	0.75	0.75

Table 2: coefficients of the empirical method for period determination

- The pseudo lateral force determination: this force represents the base shear force calculated according to FEMA 356 as follows :

$$V = KC_1C_mS_a(T)W$$

Where: K is a modification factor related to the expected maximum inelastic displacement to displacements calculated for linear response. ($C_1=1.5$ if $T < 0.1s$; $C_1=1.0$ if $T > T_c$; interpolated linearly between the two values, T_c is the period value shown in (Figure 2) indicating the transition between the constant acceleration segment to the constant velocity segment)

C_1 is related to the increased displacement due to the P-delta effects. (see FEMA356 section 3.3.1.3.1 for more details)

C_m is the effective mass factor to account for higher mode mass participation effects. (C_m equals 0.8 for concrete shear wall and pier spandrel, 0.9 for concrete moment frame, 1.0 for other frames)

$S_a(T)$ is the response spectrum acceleration value for the fundamental period T , given by Figure 2.

W is the effective seismic weight of the building including the total dead load and other gravity loads (FEMA 356 section 3.3.1.3.1)

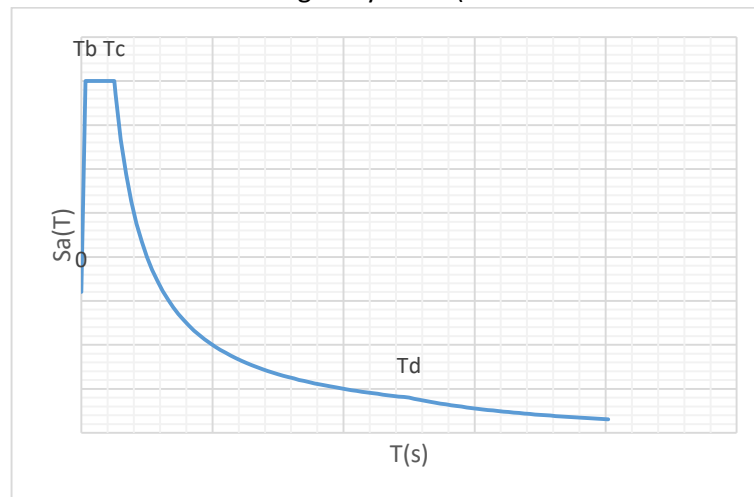


Figure 2: response spectrum (after Ringot, E. 2014)

Note that the Eurocode8 give the value of the pseudo lateral force as follows:

$$V = \lambda m S_a(T)$$

Where: λ is a correction factor equals to 0.85 if $T < 2T_c$ and the building has 2 stories, 1.0 elsewhere. (T_c is the period value mentioned in Figure 2)
 m is total mass of the building.

$S_a(T)$ is the response spectrum acceleration value given by Figure 2.

The Moroccan standard for seismic design (RPS2000) proposes the following formula to calculate the pseudo lateral force:

$$V = ASDIW/K$$

Where: A is the ground acceleration factor
 S is the coefficient related to the type of ground.
 D is a coefficient describing the dynamic acceleration.
 I is a coefficient related to the importance of the structure.
 W is the total weight of the building.
 K is the behavior coefficient related to the ratio between the expected inelastic response and the calculated elastic response.

The three formulas describe the same pseudo lateral force, but with different assumptions and influencing factors.

- Vertical distribution of seismic forces: the vertical distribution of the pseudo lateral force is given by the Eurocode 8 as follows:

$$F_x = \frac{w_x h_x^k}{\sum_1^n w_i h_i^k} V$$

Where: F_x is the lateral force applied to the floor level x .
 w_x, w_i are the portions of the total building weight assigned to the floor level x and i respectively
 h_x, h_i are height from the base to the floor level x and i respectively
 k is 2.0 if $T > 2.5s$, $0.5T + 0.75$ if $1.0s < T < 2.5s$ and 1.0 if $T < 1.0s$. (the RPS2000 v2011 takes $k=1$ for all values of period)

2. Linear dynamic procedure:

This method allows the analysis of seismic forces, the distribution over the height of the building and the response displacements through a linear elastic dynamic analysis. This assumes an elastic stiffness, and restrains the behavior of frame elements at yield level. The linear dynamic procedure includes two analysis methods, namely, the response spectrum analysis and the time history analysis:

- The response spectrum method uses peak modal response calculated from dynamic analysis of the mathematical model. Only modes contributing significantly to the response are considered, and that is by capturing over 90% of the participating mass of the building in each of the two orthogonal principal directions. These predominant modes are combined using rational methods to estimate the building response quantities. The combination method differs, if the periods are dependent, i.e. when two successive periods' ratio is lower than 0.9 or higher than 1.1, or not. If the predominant periods are dependent, the simple quadratic combination is used to calculate any response quantity R_i (forces, displacements...) as follows:

$$R_{max} = \sqrt{\sum_{i=1..N} R_i^2}$$

The complete quadratic combination is used in the other case:

$$R_{max} = \sqrt{\sum_{i,j=1..N} \beta_{ij} R_i R_j}$$

Where R_i is the response quantity (force, displacement...) for the N^{th} floor level and β_{ij} is a coefficient calculated as follows:

$$\beta_{ij} = \frac{8\sqrt{\omega_i \xi_i * \omega_j \xi_j} (\omega_i \xi_i * \omega_j \xi_j) \omega_i \omega_j}{(\omega_i^2 - \omega_j^2) + 4(\omega_i^2 + \omega_j^2)(\omega_i \xi_i * \omega_j \xi_j) + 4(\xi_i^2 - \xi_j^2) \omega_i^2 \omega_j^2}$$

Where ω_i, ω_j are the pulsation values for the i, j floor levels respectively, and ξ_i, ξ_j are the damping values for i, j floor levels respectively if different damping values are considered. The pseudo lateral force V mentioned in the previous method (the static linear method) is calculated through these combinations as well as the vertical distribution of seismic forces F_x mentioned in the same method.

- The time history method, uses a time-step-by-time-step evaluation of building response, using discretized recorded or synthetic earthquake records as base motion input. Response parameters are calculated for each time history analysis. If three or more time history analyses are performed, the maximum response of the parameter of interest is used for seismic design.

3. ***non-linear static (pushover) analysis***: when choosing the nonlinear static analysis (pushover), the mathematical model of the building considering nonlinear load-deformation characteristics of frame elements is put under monotonically increasing lateral load representing inertia seismic force until a target displacement is reached. This target displacement is intended to represent the maximum displacement likely to be experienced during the earthquake event. Moreover, because the mathematical model accounts for the inelastic response from the frame elements, the calculated internal forces are intended to approximate the real internal forces. This method is interesting for many reasons, namely:

- ✓ Evaluating the inelastic response of structural elements and the distribution of damage
- ✓ Determining the structural performance of either new or existing buildings.
- ✓ Approximating the real response of the building and avoiding the over-resistance coefficients.

The procedure of the method is detailed by the following steps, provided by ATC40 (Applied Technology Council (ATC) 1996):

- a) Determining the capacity curve: this is fulfilled by the following steps:
 1. Create a computer model incorporating nonlinear behavior of elements.
 2. Classify each element of the model as primary (structural elements) or secondary (non-structural elements)
 3. Apply lateral forces specified in the linear static method (the first method) if 75% of the total mass of the building participates in the fundamental mode. Elsewhere, the combination procedure, specified in the response spectrum method (linear dynamic method), for modes that succeeded to capture 90% of the total participating mass, should be applied.
 4. Calculate member forces for the combinations of vertical and lateral loads.
 5. Choose an element (or group of elements) of the building (joint in a moment frame, a strut in a braced frame, a shear wall..) and adjust the lateral force so that this element get stressed by 10% of its member strength
 6. Record the base shear and the roof displacement
 7. Revise the model using zero (or very small) stiffness for the yielding elements
 8. Apply a new increment of the lateral force so that another element (or group of elements) yields.

9. Add the increment of lateral force and the corresponding roof displacement to the previous totals to give accumulated values of base shear and roof displacement.
10. Repeat steps 7,8 and 9 until the structure reaches the ultimate point, such as: instability from P- Δ effect, significant distortions, an element (or group of elements) is reaching a lateral deformation level at which significant strength degradation begins, or a loss of gravity load occurs.
11. The responsible element (or group of elements) for reaching the ultimate point is eliminated, and the procedure restarts from step 3. Additional pushover curves are made so as to define the overall loss of strength of the structure, as explained by the [Applied Technology Council \(ATC 40\)](#) in Figure 3 and Figure 4.

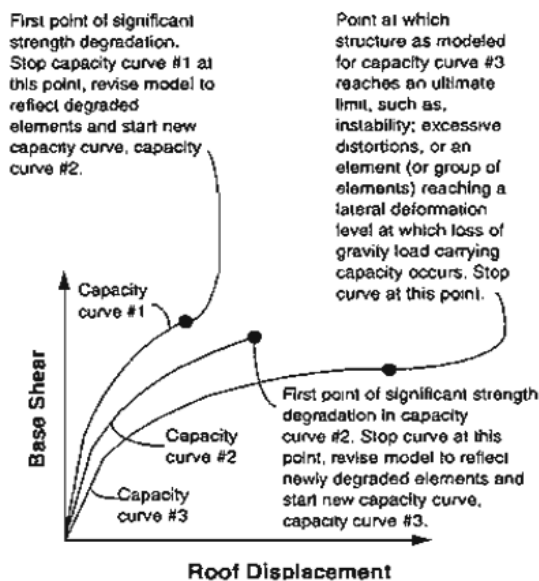


Figure 3: capacity curves required to define the strength degradation (after ATC 40)

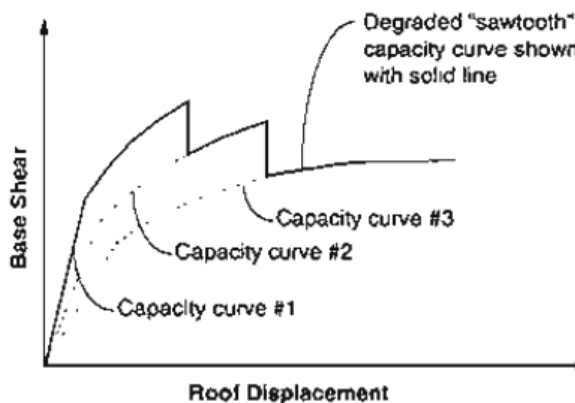


Figure 4: capacity curve with global strength degradation modeled (after ATC 40)

- b) Determining the seismic demand: the seismic demand is evaluated through a response spectrum. A response spectrum presents the maximum response of single-degree-of-freedom systems (SDOF) as a function of their periods. In fact, it is interesting to work with a response spectrum since it avoids the temporal

information. Practically, an acceleration response spectrum (Figure 5) helps defining elastic forces through the following equation:

$$F = m\gamma(T)$$

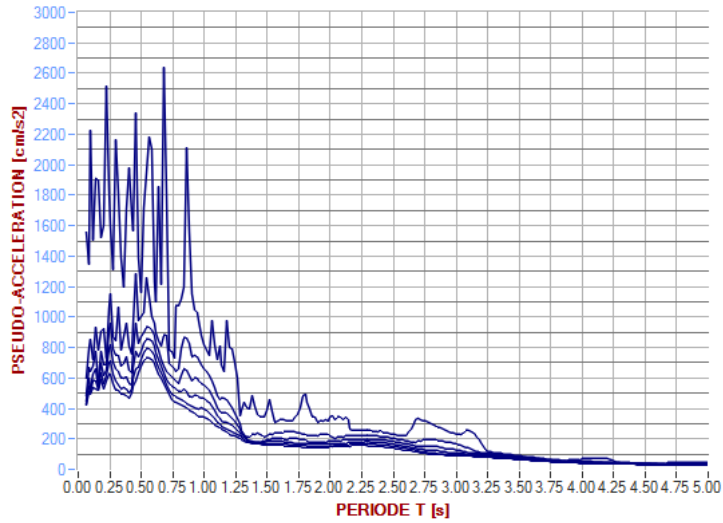


Figure 5: acceleration response spectrum (after Ringot, E. 2014)

Recently, design and assessment procedures focus more on displacements and deformations which are considered to be more relevant parameters. This is the reason behind using the displacement response spectrum (Figure 6), plotted by following the simple relationship equation:

$$S_a(T) = \omega^2 S_d(T)$$

Where S_a and S_d are the spectral acceleration and spectral displacement respectively, and $\omega = 2\pi/T$.

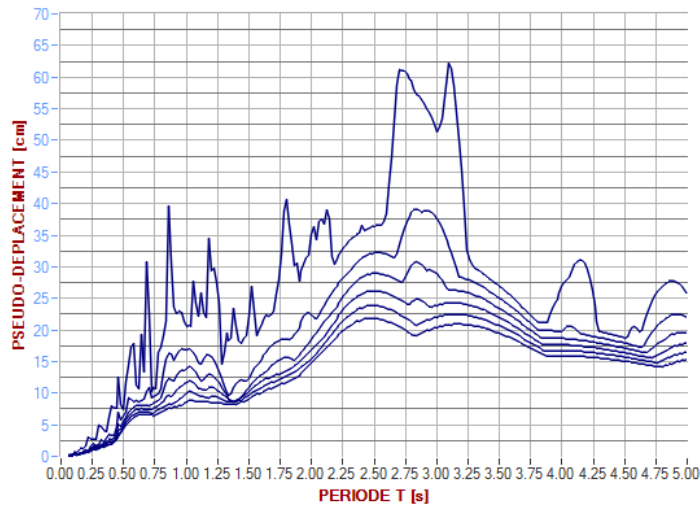


Figure 6: displacement response spectrum (after Ringot, E. 2014)

Another transformation to ADRS (acceleration-displacement response spectrum) has become significantly important. The ADRS (Figure 7) shows the spectral acceleration vs spectral displacement. The advantage of this form is that capacity and demand curves can be plotted in the same diagram allowing graphic resolution.

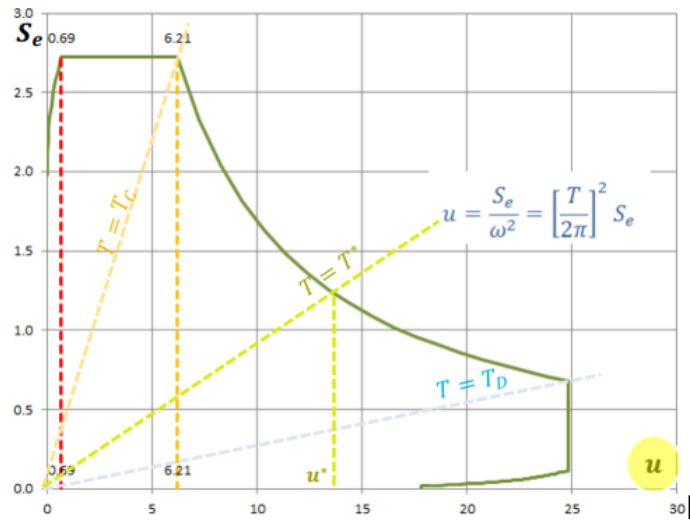


Figure 7: Acceleration-displacement response spectrum (ADRS) (after Ringot, E 2014)

Note that the use of the response spectrum assumes that the building's model is simplified from multi-degree-of-freedom (MDOF) to simple-degree-of-freedom (SDOF), since the masses are supposed concentrated in the floor levels and the mass of walls is divided between the two levels above and below.

It is worth mentioning that the response spectrum depends on many factors namely: the site conditions, dumping value, real seismic spectrum input... this is why it is normalized and imposed by authorities in seismic design codes.

4. **Non-linear time history dynamic analysis:** the basis of the nonlinear dynamic procedure is similar to those for the nonlinear static procedure (pushover). The main exception is that the response calculations are carried out using Time History Analysis. With the nonlinear dynamic analysis, the design displacements are not established using a target displacement, but instead are determined directly through dynamic analysis using ground motion time histories. Calculated response can be highly sensitive to characteristics of individual ground motion; however, more than one ground motion record should be adopted to carry out the analysis. Since computer model incorporates inelastic behavior of elements, the calculated forces will be reasonable approximations of those expected for real earthquake event.

3.3. RISKUE methodology for seismic vulnerability assessment

The European RISK-UE project (an advanced approach to earthquake risk scenarios with applications to different European towns) was launched in 1999. It dealt with the assessment of earthquake scenarios based on the analysis of their global impact at a city scale within a European context. Moreover, the project developed a new methodology for creating earthquake scenarios by concentrating on principal features of European cities to identify the vulnerability of urban systems, with regard to the historical, functional and social context of buildings. Similarly, other projects have been proposed to fulfill the vulnerability assessment objective, like HAZUS (1990) in the USA and RADIUS(1990), worldwide. The RISK-UE project was carried out in seven European cities: Barcelona, Bitola, Bucharest, Catania, Nice, Sofia and Thessaloniki.

The project was organized and operated through seven work packages as follows:

- WP01: European distinctive features, Geographic Information System (GIS) inventory, database and building typology;
- WP02: Seismic hazard assessment, both at regional and local level;
- WP03: Urban system analysis. Aimed at highlighting weak points under normal conditions, during crisis and recovery periods;
- WP04: Vulnerability assessment of current buildings;
- WP05: Vulnerability assessment of old town centers, historical monuments and buildings;
- WP06: Vulnerability assessment of lifeline facilities and essential structures;
- WP07: Seismic risk scenarios.

For the aims of this thesis, the methodology of WP04 for vulnerability assessment of current buildings is interesting. More precisely, current building denotes multi-story buildings that have been designed and constructed by respecting a certain level of seismic protection as specified by building codes and standards. The Risk-UE WP04 team focused on two main objectives:

- Define vulnerability models that describe the relation between potential building damage and adopted seismic hazard solicitations.
- Develop the corresponding fragility models and damage probability matrices that express the probability of exceeding a given damage state as a function of spectral parameters.

Vulnerability is regularly defined as:

“The degree of damage/loss to a given element at risk, or set of such elements, resulting from the occurrence of a hazard”.

Building vulnerability is:

“A measure of the damage a building is likely to suffer from, given that it is subjected to ground shaking of specified intensity”

Vulnerability function (or fragility models) of an element at risk represents:

“The probability that its response to seismic loading exceeds its various performance limit states defined based on physical and socio-economic considerations”.

There are two main approaches for generating vulnerability relationships:

- The first approach: LM1, is based on damage data obtained from field observation after an earthquake or from experiments. It is suitable, if the seismic hazard properties are not detailed in the urban environments, and the seismic intensity is adequately estimated.
- The second approach: LM2, is based on mechanical models of the structure, either through detailed time-history analysis or through simplified methods. It is used in case of the presence of detailed local seismicity studies, expressed in terms of site-specific spectral quantities such as spectral acceleration, velocity and displacement.

In both approaches, suitable seismic parameters controlling the building response are used, as well as the identification of different damage states, the damage progress and the probability of exceeding a damage level. The “seismic excitation-damage states” relationships are defined by specific probability distributions of damage and are expressed by means of “fragility models” or “damage probability matrices”.

The LM2 method is suitable for this thesis analysis, since it conjugates technical information to refined fragility curves, and also because Moroccan authorities have made huge efforts in determining details about the seismic data over the entire kingdom territory. The steps of the method are described as follows:

- Define the capacity model of the building and convert it in capacity spectrum
- Determine the seismic demand spectrum for the site
- Calculate the expected building response (performance) by intersecting capacity and demand spectra, and determine the intersection (performance) point.
- Establish the corresponding fragility curves through conditional probabilities and determine the rate of damage states for the determined performance point.

Note that the fragility curves are plotted in terms of conditional probability of exceeding a certain damage state (ds) that defines the spectral displacement value ($S_{d,ds}$) and a specific hazard parameter (β_{ds}). LM2 method considers four damage states denoted as: Minor, Moderate, Severe and Collapse. An example of the suite of fragility curves for different damage states is shown in Figure 8. The conditional probability is expressed by the following formulas:

$$P(ds > Sd) = \Phi \left[\frac{1}{\beta_{ds}} \ln \left(\frac{S_d}{S_{d,ds}} \right) \right]$$

with S_d is the spectral displacement and $S_{d,ds}$ is spectral displacement value corresponding to the damage state (ds), and equals to:

$$Sd1=0.7 Dy$$

$$Sd2=Dy$$

$$Sd3=0.5 Dy+0.25 Du$$

$$Sd4=Du$$

and the parameters β_{ds} (lognormal standard variation) equal to:

$$\beta_{ds1}=0.25+0.07\ln(\mu_u);$$

$$\beta_{ds2}=0.2+0.18\ln(\mu_u);$$

$$\beta_{ds3}=0.1+0.4\ln(\mu_u);$$

$$\beta_{ds4}=0.15+0.5\ln(\mu_u)$$

where Dy and Du are the displacements of the yield and ultimate points respectively, which are provided by the capacity curve. The parameter μ_u equals Du/Dy .

Steps of the pushover curve plot is displayed in Figure 9.

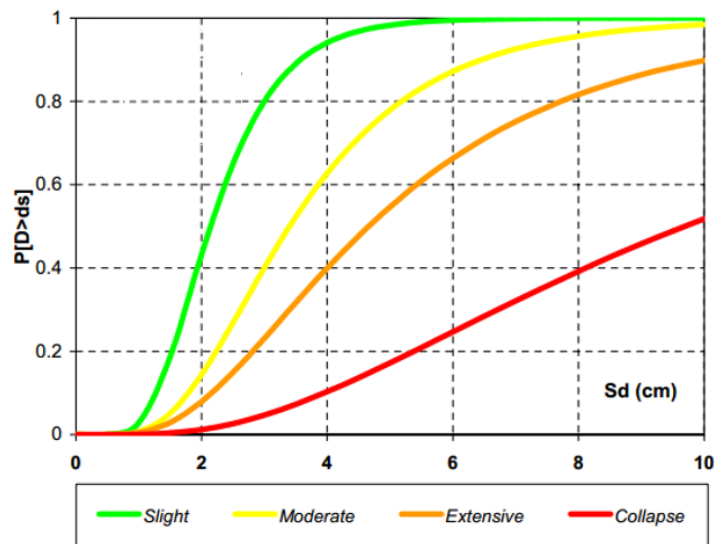


Figure 8: example of fragility curves (after Risk-Ue 2003)

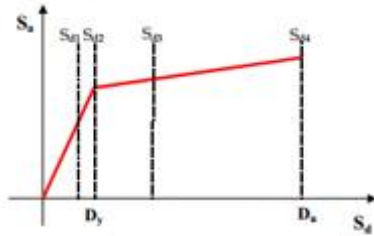
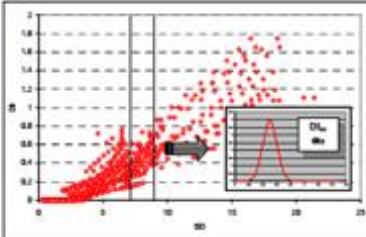
Steps	Pushover / CBA	Nonlinear Dynamic
STEP 1:	Define/model capacity spectra (bilinear model)	Define/model dynamic capacity spectra (bilinear model)
STEP 2:	Define damage threshold levels (criteria)  $\overline{Sd}_1 = 0.7D_y$ $\overline{Sd}_2 = D_y$ $\overline{Sd}_3 = D_y + 0.25(D_u - D_y)$ $\overline{Sd}_4 = D_u$	Corralte global damage index (DI) vs spectral displacement (S_d) and calculate mean damage index (DI_{av}) and its tandard deviation (σ_{DI}) 
STEP 3:	Calculate cumulative probability (CP) for being in or exceeding certain damage state (k) at certain S_d level (beta distribution Table 3.8.1) $P(D \geq D_k) = 1 - P_\beta(k)$ $P_\beta(k)$ - beta distribution	Calculate cumulative probability (CP) for being in or exceeding certain damage index at certain S_d level (normal distribution) $P[DI \geq DI_K] = 1 - \Phi \left[\frac{DI_K - DI_{av}}{\sigma_{DI}} \right]$ $DI_k = 0, 0.1, 0.25, 0.4, 1.0$
STEP 4:	Perform regrssion analysis for S_d - CP for each damage degree and calculate median value of the spectral displacement ($\overline{S}_{d,ds}$) and lognormal standard deviation (β_{ds})	
STEP 4A:	Calculate directly β_{ds} as a function of ultimate ductility μ_u $\beta_{S_{d1}} = 0.25 + 0.07 \ln(\mu_u)$ $\beta_{S_{d2}} = 0.2 + 0.18 \ln(\mu_u)$ $\beta_{S_{d3}} = 0.1 + 0.4 \ln(\mu_u)$ $\beta_{S_{d4}} = 0.15 + 0.5 \ln(\mu_u)$	
STEP 5:	Fragility curves are defined with the steps: 1) 1, 2 and 4A for pushover or CBA only; or 2) 1, 2, 3, 4 for both types of analyses	

Figure 9: principal steps to plot fragility curves (after Risk-Ue 2003)

3.4. Conclusion

This chapter has explained with detailed information, the seismic analysis procedures, available in current design and verification methods, as well as the vulnerability assessment tools proposed by Risk-UE. Understanding the mechanism behind the building response to an earthquake excitation is helpful to accomplish the vulnerability assessment in tsunami case. Furthermore, the plot of fragility curves for tsunami hazard reveals interesting in terms of a correct comparison between the two hazards and a preparation for tsunami evacuation plans. In the next chapters, a methodology for tsunami vulnerability assessment is proposed, with much resemblance to the procedures mentioned earlier (especially the pushover analysis and Risk-UE LM2 method).

4. Tsunami characteristics

Content:

- 4.1. Introduction
- 4.2. Simulation of inundation
- 4.3. Tsunami loading
- 4.4. Distribution of tsunami forces
- 4.5. Conclusion

4.1. Introduction

Tsunami waves hold a great kinetic energy that inflicts tremendous pressures and forces on structures and poses a threat to human safety. Apart from seismic lateral forces that buildings experience during the acceleration of the soil, tsunami-induced forces cause additional loads on the frame elements. Tsunami is not a simple version of flooding, but it is more devastator with aggressive solicitation on structures. Figure 10 shows some failures among frame elements on buildings attacked by the December 2004 tsunami in Thailand and Indonesia. It has been observed that the damage degree on structures is far more consistent if structural elements (columns, beams, ...) are broken than if it was for non-structural elements. Clearly, distinguishing between structural and non-structural elements is necessary due to the functions of each group: while non-structural elements have the main role of protecting from aggressive weather, temperature variation, sound pollution, ..., structural elements are bearing descending loads, which makes the building in a critical state if their failure occurs.

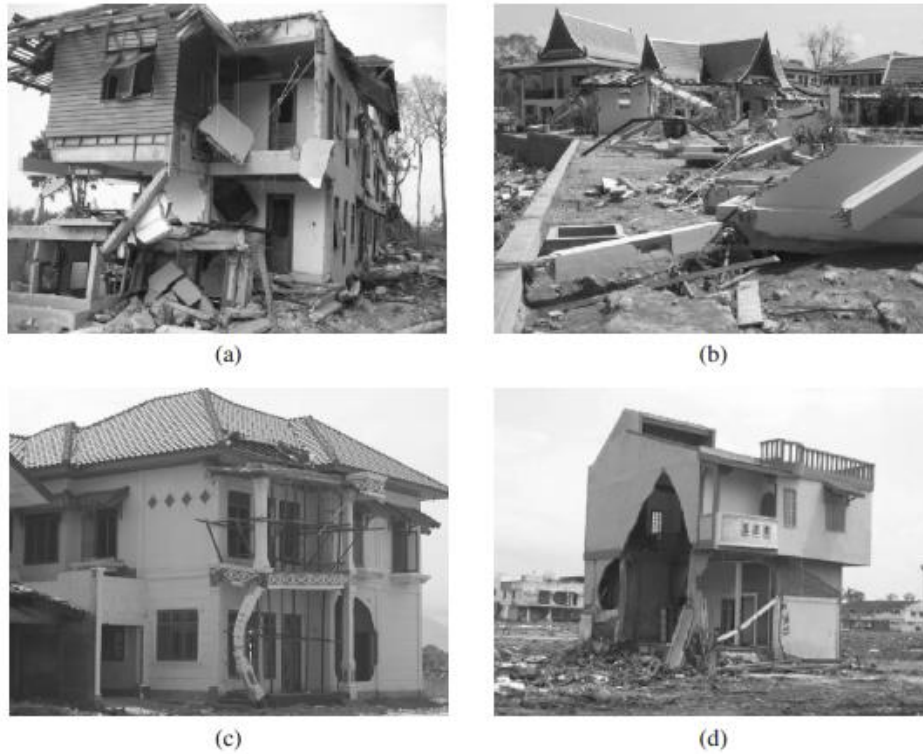


Figure 10: Tsunami damage in Thailand and Indonesia (December 2004 Indian Ocean tsunami): (a) severe structural damage, Khao Lak, Thailand; (b) column failure of a reinforced concrete frame, Thailand; (c) column failure due to debris impact, Banda Aceh, Indonesia; (d) failure of infill walls, Banda Aceh, Indonesia. (after Nistor et al. 2010)

In the following section, results of the inundation simulation studied by previous works is shown as well as the theoretical knowledge which these numerical simulations are based on. Next, a presentation of tsunami forces is introduced with an objective of developing a generalized set of loading formulas, movement equations and temporal distributions. Combinations of these forces, listed in the following section, is illustrated because it is important to understand the successive steps of the wave's impact. Additionally, laboratory tests are described in order to validate the adopted formulas.

4.2. Simulation of inundation

In order to understand the action and distribution of tsunami forces on buildings, a simulation of propagation and inundation of tsunami on shore is surely helpful. It can also predict some useful characteristics of the wave such as velocity, flow depth and run-up.

It was from 1950 that the investigation about the generation and propagation of long waves such as tsunamis started. Initial models like [Hall and Watt \(1953\)](#) attempted to construct an approximation of the propagation of one single long wave by solving a simplified canonical problem. In 1966-1967, [Peregrine](#) succeeded at establishing the basic mathematical theory of tsunamis as well as the calculation of the evolution of simplified undulate bore. A remarkable work over 1970 lead by [Houston and Gracia \(1974\)](#) used, for the first time more realistic geophysical initial conditions for submarine earthquakes in order to plot a deep ocean propagation of tsunamis from Alaska and Chile towards the USA coasts. The increasing development of numerical methods over the decades of 1980s and 1990s

helped significantly in solving more complex propagation problems (Borrero & al 2006). Moreover, the Catalina workshop in USA (1990) showed the progress in tsunami's propagation research and discussed the best method to validate the available numerical and analytical tools. The workshop emphasized the use of numerical shallow water equations to solve the problem of propagation and suggested the validation of the numerical results with laboratory results that were established four years later. Some of the successful models adopted are COMCOT, MOST and TSUNAMI-N2 codes.

So, in order to simulate the propagation of tsunami wave, the most adequate method is the use of numerical shallow water equations (SWEs). In fact, governing equations concerning the motion of compressible fluids are Navier-Stokes equations that reflect Newton's conservation of momentum in three directions. Another equation of conservation of mass is added to the previous three equations to form a four-coupled differential system linking the pressure and the three components of velocity. The shallow water equations (SWEs) are derived from the depth average integration of the Navier-Stokes and mass conservation equations, illustrated by the following equations:

$$\rho \left(\frac{\partial u}{\partial t} + u \frac{\partial u}{\partial x} + v \frac{\partial u}{\partial y} + w \frac{\partial u}{\partial z} \right) = - \frac{\partial p}{\partial x} + \mu \left(\frac{\partial^2 u}{\partial x^2} + \frac{\partial^2 u}{\partial y^2} + \frac{\partial^2 u}{\partial z^2} \right) + \rho g_x$$

$$\rho \left(\frac{\partial v}{\partial t} + u \frac{\partial v}{\partial x} + v \frac{\partial v}{\partial y} + w \frac{\partial v}{\partial z} \right) = - \frac{\partial p}{\partial y} + \mu \left(\frac{\partial^2 v}{\partial x^2} + \frac{\partial^2 v}{\partial y^2} + \frac{\partial^2 v}{\partial z^2} \right) + \rho g_y$$

$$\rho \left(\frac{\partial w}{\partial t} + u \frac{\partial w}{\partial x} + v \frac{\partial w}{\partial y} + w \frac{\partial w}{\partial z} \right) = - \frac{\partial p}{\partial z} + \mu \left(\frac{\partial^2 w}{\partial x^2} + \frac{\partial^2 w}{\partial y^2} + \frac{\partial^2 w}{\partial z^2} \right) + \rho g_z$$

$$\frac{\partial \rho}{\partial t} + \frac{\partial(\rho u)}{\partial x} + \frac{\partial(\rho v)}{\partial y} + \frac{\partial(\rho w)}{\partial z} = 0$$

Where ρ is the density of fluid, t is time, g is gravity, μ is dynamic viscosity, u, v and w are the component of velocity in x, y and z directions respectively.

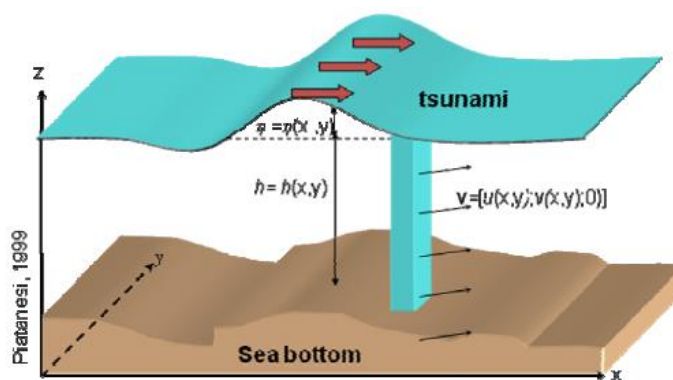


Figure 11: The shallow water, long waves, approximation for tsunami propagation. presents the free surface elevation, h denotes the water depth and u and v are the velocity components in x - and y - directions, respectively. (after Piatanesi & al 1999)

The shallow water equations are resolved by using a finite difference method with respect of boundary and initial conditions. Three main steps are important in this procedure:

- Creating a grid that allows the determination of approximative values in specific points at different time-steps.
- Discretizing differential equations in the grid model using the finite difference approximations in order to have an algebraic system of equations.
- Solving the algebraic system.

It is worth mentioning that the more the dimensions of the grid cells are small, the more precise and accurate are the obtained values. However, it is much time-consuming if the calculations are very important. In addition, the finite difference model requires some detailed data about the bathymetry and topography in order to properly simulate the inundation. Although the bathymetry's three coordinates could be integrated without complex problems because it is supposed hardly variable, the topography may reveal some additional problems due to the urban tissue. Within a large area, the outcome of the interaction between the wave and obstacles such as buildings, breaking walls, movable objects (transport vehicles, cargos...) is hard to predict.

Some studies such as (Norwegian Geotechnical Institute 2013; Omira & al 2011; RMSI 2012) have worked on some advanced simulation models that describe the generation and propagation of the tsunami wave in the Gulf of Cadiz. The areas affected are the coasts of Morocco and Portugal. The topography inserted in these models does not consider the built and structures. However, the results of these works may give an idea about the flow depth and velocity of the wave in the inundated areas. Figure 12 and Figure 13 show the simulation of the creation of tsunami of the South West Iberia source and the resulting inundation onshore. From these references, an average of the value of the flow depth, in the Gulf of Cadiz-Moroccan coasts, may be considered between 6-8m and the velocity of the wave could be estimated by 6-7m/s (Omira & al 2011).

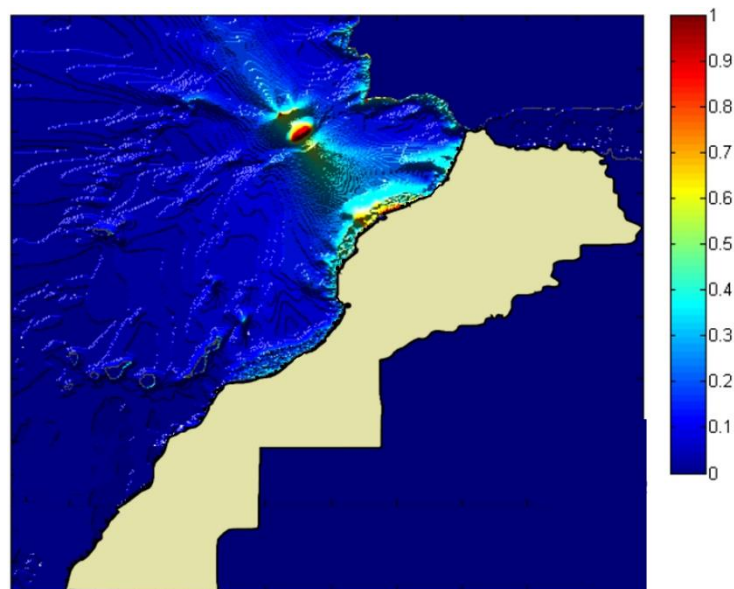


Figure 12: computed extreme water surface from South West Iberia source to local areas (after RMSI 2012)

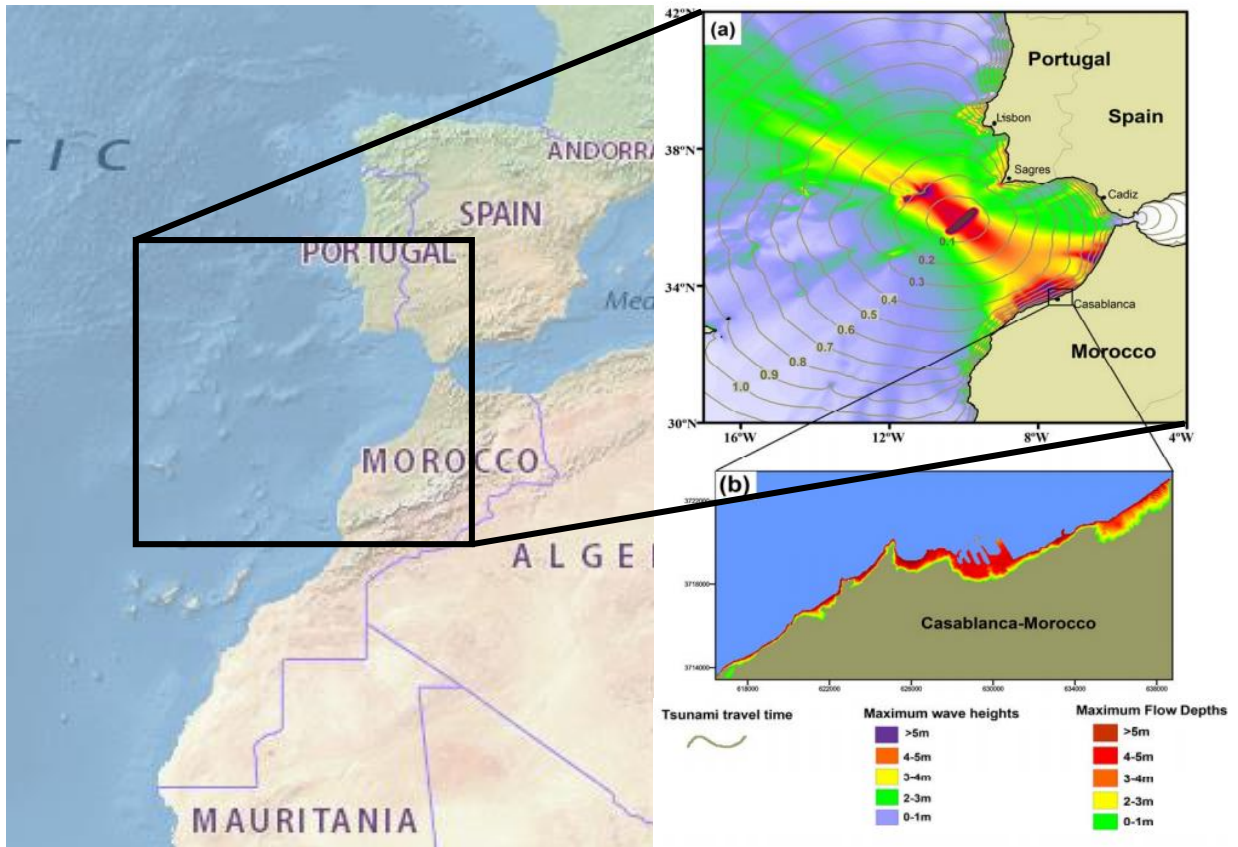


Figure 13: Omira 2011 model: (a) maximum wave heights and flow depths generated from South West Iberia source (b) inundation onshore (after Omira & al 2011)

4.3. Tsunami loading

In an effort to understand tsunami mechanisms and induced solicitation on structures, some guidance was provided by current available standards and codes. An accurate comprehensive theory about the development of tsunami waves and their propagation on land, such as those described for seismic waves, is a very challenging task since many factors influence the wave's characteristics. FEMA P-55 Coastal Construction Manual (FEMA 2011) illustrates some of these factors that tsunami loads are determined with:

- the magnitude of the earthquake responsible of tsunami or triggering event
- the location of the triggering event
- the configuration of the continental shelf and shoreline
- detailed bathymetry
- the upland topography

Another difficulty that rises when comparing tsunami forces to seismic ones, is the contact mode in both cases. Earthquakes wave travel through the ground and spread according to the nature and obstacles in types of soils. Buildings receive the shakings at the level of foundations as an excitation of the ground acceleration. Thus, the seismic forces are distant or, properly saying, are non-contact forces. However, tsunamis apply contact forces on the structure frame. Each frame element may experience an additional stress due to the pressure of water filled by sediments, debris impact, buoyancy, scour....

Apart from similarities/differences with seismic load, tsunami forces are, in general practice, compared with riverine flooding and storm surge. FEMA P-55 Coastal Construction Manual (FEMA 2011) section 7.2.2 specifies that:

“Tsunami loads on residential buildings may be calculated in the same fashion as other flood loads; the physical processes are the same, but the scale of the flood loads is substantially different in that the wavelengths and run-up elevations of tsunamis are much greater than those of waves caused by tropical or extratropical cyclones ... When the tsunami forms a bore like wave, the effect is a surge of water to the shore. When this occurs, the expected flood velocities are substantially higher...and if realized at the greater water depths, would cause substantial damage to all buildings in the path of the tsunami. Designers should collect as much data as possible about expected tsunami depths to more accurately calculate tsunami flood forces.”

FEMA P-646 (FEMA P-646 2008) notes also in section 6.1 that:

“Very little guidance is provided in currently available structural design codes, standards, and guidelines on loads induced by tsunami inundation. Established design information focuses primarily on loads due to rising water and wave action associated with riverine flooding and storm surge. While little specific guidance is provided, the presumption is that currently available flood design standards are to be used in designing for tsunami load effects”

Indeed, in the design of flooding, buildings and structures have to resist the effects of floodwaters, such as flood depths, pressures, velocities, impact, uplift forces, etc.... However, there are significant differences between tsunami inundation and flooding. A major point of difference is the increased flow velocity for tsunami waves, which results with much greater velocity-related loads on structures. As an example of the high level of energy contained in tsunami waves, some fishing boats, containers, large cars and even planes have been observed carried with the current and struck with buildings. FEMA P-646 notes that size, mass and stiffness of this type of debris, which is not considered in flooding design, may need to be considered in tsunami forces.

Another critical point of contrast between flooding and tsunami is the mechanism of scour. Tsunami involves two types of scour: shear-induced scour, which consists of soil transport due to the flow velocity. This is similar to that observed for flooding. An additional type of scour is liquefaction-induced scour that results from rapid drawdown as the water recedes (FEMA P-646). Pore pressure causes liquefaction of the soil because of lack of time to dissipate, resulting with greater scour than in the flooding case. Unfortunately, scour problems are not discussed in this thesis.

With regard to many aspects of differences between tsunami and earthquake in first hand and tsunami and flooding in other hand, it may be concluded that tsunami represents far more threat to buildings with greater loading magnitude. Loading forces can be determined, though, with a certain level of confidence due to the resemblance to flooding mechanism- although the scale proportion is much important- hence an approximation of tsunami forces is essential to evaluate the response of buildings to tsunami. This approximation involves forces related to hydrodynamic, hydrostatic and buoyancy effects. Moreover, formulas and equations for tsunami forces are prone to be subject to many laboratory tests, in order to validate their correctness.

In this perspective, FEMA P-646 2008, which provides guidelines for design of structure for vertical evacuation from tsunami, have been developed in order to correctly identify the expected magnitude, form and pattern of tsunami forces with respect to physics laws, to observed consequences from past tsunami events and also, especially, to results from accurate laboratory results. Tsunami forces, according to FEMA P-646, include:

- hydrostatic forces;
- hydrodynamic forces;
- impulsive forces;
- buoyant forces;
- debris impact forces;
- debris damming forces;
- uplift forces; and
- additional gravity loads from retained water on elevated floors.

Before illustrating these forces and their expressions, an assumption is made for the density of tsunami water due to the transport of suspended sediments, and is taken 1.2 times the density of fresh water i.e. $\rho_s=1200\text{kg/m}^3$.

- Hydrostatic forces:

The pressure of standing or slowly moving water on structural components' interfaces causes hydrostatic forces. It acts perpendicular to the surface of the element. Hydrostatic forces are important for long structures such as sea walls. The expression of hydrostatic force is given by equation:

$$F_h = \frac{1}{2} \rho_s g b h_{max}^2 \quad \text{Equation 1}$$

Where ρ_s is the fluid density including sediment (1200kg/m^3), g is the gravitational acceleration, b is the breadth (width) of the wall, and h_{max} is the maximum water height above the base of the wall at the structure location. If the structural component with height h_w is fully submerged, the resultant hydrostatic force can be written as follows:

$$F_h = \frac{1}{2} \rho_s g (h_{max} - \frac{h_w}{2}) b h_w \quad \text{Equation 2}$$

Where h_{max} (the effective height), is the vertical difference between the design tsunami runup elevation R and the base elevation of the component, z_w as shown in

$$h_{max} = R - z_w \quad \text{Equation 3}$$

It is worth mentioning that FEMA P-646 code considers a safety coefficient for the value of tsunami runup elevation $R^*=R/1.3$ because the objective of the code is designing new tsunami evacuation buildings. However, for the evaluation purpose, this coefficient is ignored. Hydrostatic force distribution according to Equation 3 is shown in Figure 14:

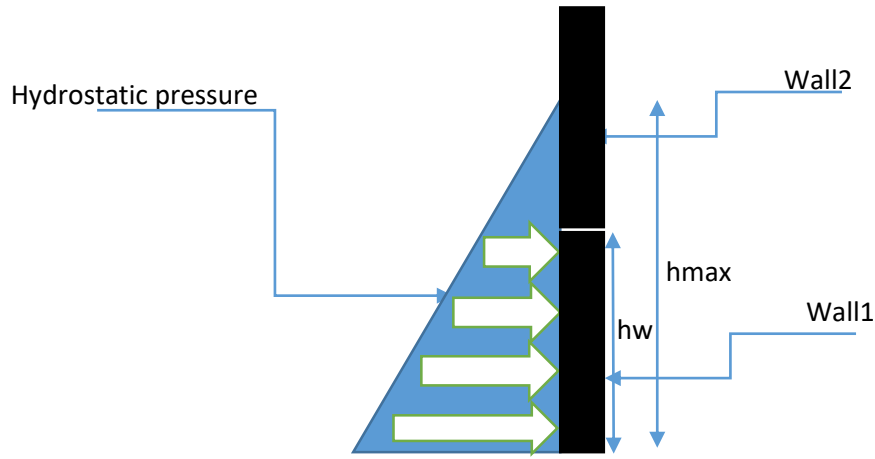


Figure 14: hydrostatic force distribution and location of resultant

- Hydrodynamic forces;

The application of hydrodynamic forces on the structure occurs when water flows around the structure or structural components. These forces are function of fluid density, flow velocity and structure geometry.

Hydrodynamic forces can be computed as follows:

$$F_d = \frac{1}{2} \rho_s C_d B (hu^2)_{\max} \quad \text{Equation 4}$$

Where ρ_s is the fluid density including suspended sediment (1200kg/m^3), C_d is the drag coefficient, B is the breadth of the structure in the plane normal to the direction of flow (i.e. the breadth in the direction parallel to the shore), h is the flow depth, and u is the flow velocity at the location of the structure. For forces on components, B is taken as the width of the component. It is recommended that the drag coefficient be taken as $C_d=2.0$ for rectangular columns and $C_d=1.2$ for cylindrical columns, as proposed by Arnason(2005) (Figure 15).

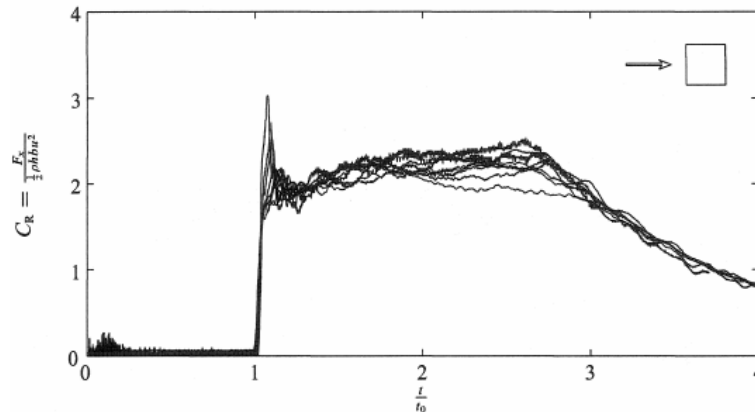


Figure 15: calculation of drag coefficient on rectangular columns due to hydrodynamic force (after Arnason 2005)

Moreover, the expression $(hu^2)_{\max}$ represents the momentum flux per unit mass. It is important to mention that $(hu^2)_{\max}$ does not equal $h_{\max}u_{\max}^2$. The maximum flow depth, h_{\max} and maximum flow velocity, u_{\max} , at a perpendicular site may not occur at the same time. The hydrodynamic forces must be based on the parameter $(hu^2)_{\max}$, which is the maximum momentum flux per unit mass occurring at the site at any time during the tsunami.

As for the value of $(hu^2)_{max}$, FEMA p-646 suggest firstly a detailed numerical simulation model for an accurate calculation of the value. However, an estimation of the value can be given by the following equation

$$(hu^2)_{max} = gR^2(0.125 - 0.235\frac{z}{R} + 0.11\left(\frac{z}{R}\right)^2) \quad \text{Equation 5}$$

Where g is the acceleration due to gravity, R is the runup elevation, and z is the ground elevation at the base of the structure. These parameters are illustrated in Figure 16. It is also worth mentioning that the velocity and the water depth expressions, illustrated by (Yeh 2007) and based on (Peregrine and Williams 2001) formulas, are as follows:

$$\eta = \frac{1}{36\tau^2}(2\sqrt{2}\tau - \tau^2 - 2\zeta)^2 \quad \text{and} \quad v = \frac{1}{3\tau}(\tau - \sqrt{2}\tau^2 + \sqrt{2}\zeta) \quad \text{Equation 6}$$

Where : $\eta = \frac{h_{max}}{R}$; $v = \frac{u}{\sqrt{2gR}}$; $\tau = t \tan \alpha \sqrt{\frac{g}{R}}$; $\zeta = \frac{z}{R}$; $h_{max}=R-z$ is the water depth, R the maximum runup, u the flow velocity, g the gravitational acceleration, α is the beach slope, t is time and z is the ground elevation at the base of the structure as mentioned earlier.

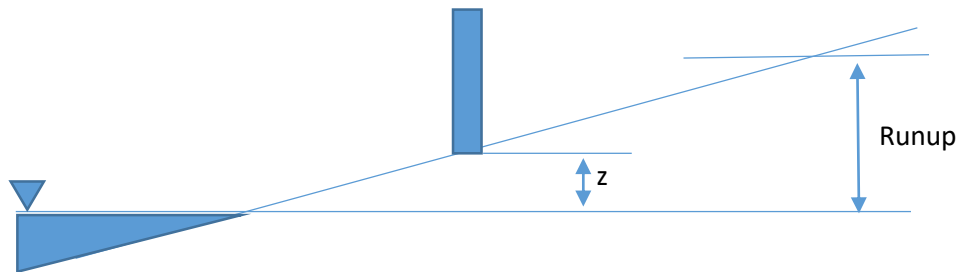


Figure 16: runup and z elevation parameters

Hydrodynamic force is distributed as shown in Figure 17 :

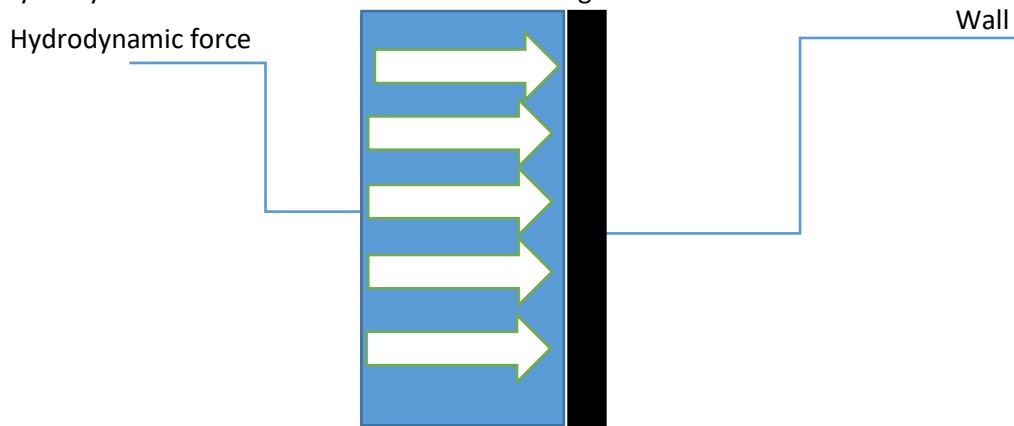


Figure 17: hydrodynamic force distribution

- Impulsive forces;
Impulsive forces are caused by the surge of water and its impact on a structure. A surge of water happens on shore after a bore was formed offshore. Differences between bore and surge forms are illustrated in Figure 18 and Figure 19. For more details, please refer to FEMA P646.

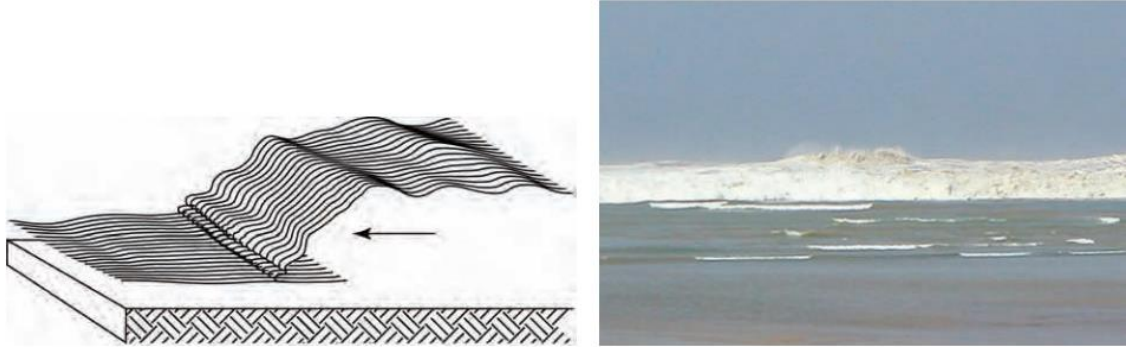


Figure 18: bore formation offshore (FEMA P646)



Figure 19: surge form when tsunami rush up on shore (after FEMA P646)

Previous studies, like Ramsden (1993), Arnason (2005) and Yeh (2007) discussed the formation of surge and its magnitude. They suggested that impulsive forces are greater than hydrodynamic forces by 1.5. The expression of impulsive forces is shown in

$$F_s = 1.5F_d \quad \text{Equation 7}$$

Impulsive forces strikes frame elements first, followed by the impact of hydrodynamic forces.

- **Buoyant forces;**
Buoyant forces try to lift the frame elements due to the buoyancy of water. Buoyant forces are expressed as follows:

$$F_h = \rho_s g V \quad \text{Equation 8}$$

Where ρ_s is the fluid density including suspended sediment (1200 kg/m^3), and V is the volume of water displaced by the building, i.e. the volume below the level of h_{\max} as determined by Equation 3.

Other types of forces are fully described in FEMA646

4.4. Distribution of tsunami forces

When a tsunami strikes a building's frame elements, the forces mentioned above do not act simultaneously. Different situations and scenarios could be plotted in order to understand the succession of forces impact:

- First of all, the water mass pushes the building through the impulsive force on vertical frame elements such as wall, columns, etc. This is caused by the leading edge of the surge of water. As explained above, the bore wave onshore arrives with a great kinetic energy that is characterized by a steep and flattened form. However, when approaching the shallow waters, the bore breaks and begins to form the surge. The surge or impulsive force is supposed 1.5 of the drag force (hydrodynamic force) applied on an element. Moreover, the impulsive force has very short duration loads and once the leading edge of the wave has passed a structural member, it will no longer apply the impulsive force but rather a sustained drag-hydrodynamic force.
- The hydrodynamic force is applied on all structural members after the impact of the impulsive force. The direction of this force follows the direction of velocity and flow of flooding. If the position of the building and its architectural plan are available, it could be advantageous to work on a time-stepped simulation of the flooding so as to identify the direction of the flow and the velocity punctual values. This simulation is provided by advanced CFD (computational fluid dynamics) on a 3D model of the building by using the supposed incidence velocity magnitude.
- Regarding the hydrostatic force, it should be noted that, by definition, this force is applied by steady or slowly moving water. This case does not correspond to the tsunami inundation, where the wave moves with a great velocity. The FEMA P646 recommends applying hydrostatic forces on large elements like walls. However, it could be supposed that inundated columns could have the hydrostatic force applied on them because, first for precaution even though the value of the hydrostatic force is not too important compared to hydrodynamic and surge forces, and secondly, columns' materials density differ from water density and so the vertical pressure of water increases at the bottom of the water mass. The hydrostatic force is not applied until the leading-edge front wave passes and the elements are submerged.
- Uplift forces due to buoyancy and hydrodynamic uplift force have the effect of reducing the total dead weight on structural elements.
- The mass of water retained applies an additional weight on slabs and consequently on structural elements that support this slab. Generally, columns bear the dead loads, live loads, seismic loads and in some cases wind loads. Tsunami load on slabs should be calculated as an accidental action.
- Debris influence on elements is punctual. An element reaction to the debris impact can be estimated through calculating the momentum of the projected element, which depends on its mass and stiffness. In case of buildings located near the shore, only large debris like cargos could be interesting, because small debris are not carried by the wave.
- Debris dam act like a wall against the flow of the wave. Like the debris description above, debris dam is not interesting in case of buildings near the shore unless there are large debris like cargos.

Another important factor that should be carefully analyzed is the temporal distribution of tsunami forces mentioned in the previous section. A detailed numerical simulation should handle the variation of the forces' magnitude through time. When the wave travels from the first rank of columns until the last one, additional forces are applied to different columns but not with the same value. So, in order to describe this temporal variation, the analysis of laboratory experiments is necessary.

Various research teams have held important experiments simulating the impact of long-type waves on a prototype model of buildings. Among some of those interesting experiments are those elaborated by ([Lukkunaprasit & al 2009](#); [Nistor et al. 2010](#)). On summary, their 3-dimensional experiments consist on generating a tsunami wave in the laboratory by a sudden release of water through a controlled gate

(Figure 20). Sensors are placed on the front of the building model to measure the pressure received from the wave impact and its variation through time. Experiments could investigate different building models with different characteristics such as the material used for the built (wood, plastic...) and the existence of opening. The parameters of the wave such as the wave height could be measured as well.

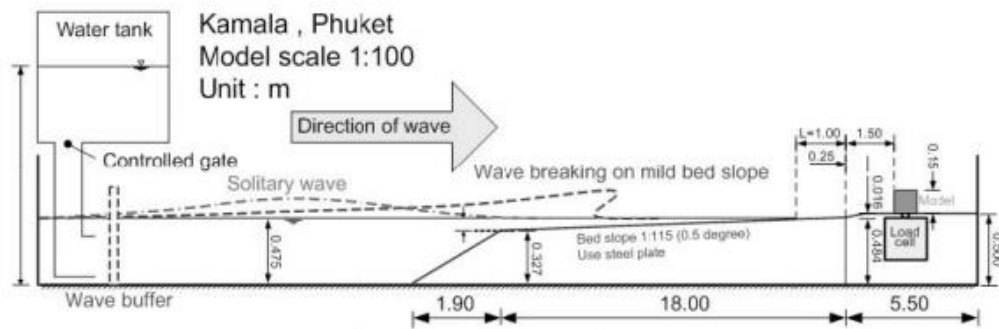


Figure 20: experiment simulating the tsunami wave impact on a building prototype (after Lukkunaprasit & al 2009)

As for the results of these laboratory experiments, (Nistor et al. 2010) tried to plot the variation of the resulting base shear force and pressure through time. Figure 21 illustrates the time history of the base shear force and pressure detected with the sensors on the building prototype. Similarly, (Lukkunaprasit & al 2009) plotted the recordings of different pressure gauges and the maximum force (Figure 22).

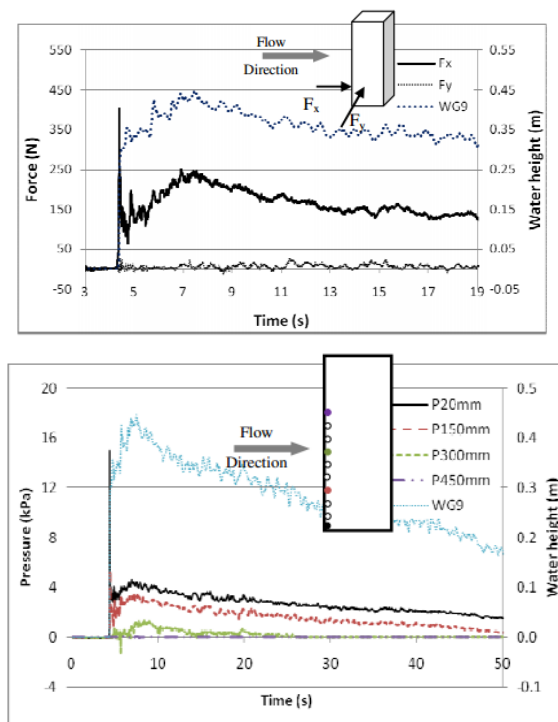


Figure 21: time history of base shear forces (up) and pressure (above) (after Nistor et al. 2010)

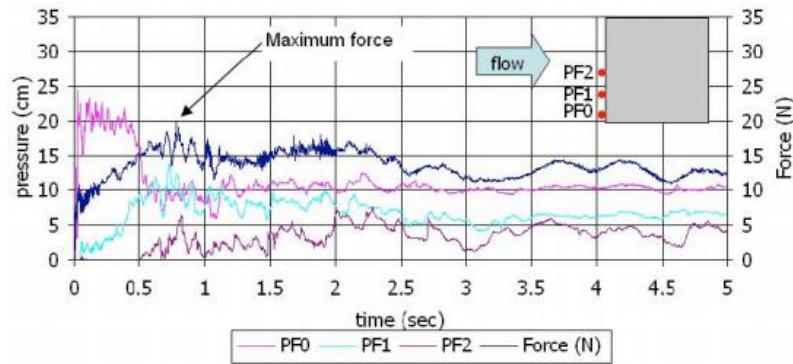


Figure 22: time history of maximum sensed force and different pressures detected (after Lukkunaprasit & al 2009)

The time history recordings from the previous studies are important for this thesis goal since they simulate the reaction of a real building to the tsunami impact. Although the scale of the forces magnitude in these experiments is smaller than the real tsunami wave, the temporal variation may be similar because in both experiments, the surge force shows the maximum impact on the building, followed by the hydrodynamic force which is less pressuring on the sensor gauges. A simplified model of the time history is introduced later on the structural software simulation taking into account the effective values of tsunami forces on one hand and their temporal variation on the other hand.

4.5. Conclusion

This chapter discussed and presented tsunami characteristics. A first presentation of the inundation simulation helped recognize some tsunami parameters such as velocity and wave height. The second section illustrated tsunami loadings on building's frame elements and described the major important forces of tsunami waves following the report of FEMA-P646. Additionally, the distribution of tsunami forces is shown and some laboratory tests are described. Through the previous study elements description (chapter 2), the analysis of seismic vulnerability (chapter 3) and the tsunami characteristics description (chapter 4), the assessment of tsunami vulnerability is ready to be studied in the next chapters.

5. Assessing tsunami vulnerability for common buildings: focus on infill masonry

Content:

- 5.1. Introduction
- 5.2. Characteristics of the test building
- 5.3. Infill masonry analysis
- 5.4. RC frame analysis
- 5.5. Conclusion

5.1. Introduction

In this chapter, a test building of two stories is dimensioned following local standards and analyzed under tsunami loading. The test building is chosen with a simple architectural plan in order to help understand the structure's response to a tsunami solicitation. Moreover, the influence of infill masonry walls is discussed in this chapter for out-of-plane and in-plane walls.

This chapter includes firstly an explanation about the dimensioning of the cross sections of different frame elements. The application of building codes recommendations mentioned in earlier chapters is necessary to make a satisfactory model of the building in the structural analysis program.

The second part of this chapter deals with infill masonry response to the impact of tsunami waves. In order to reach this objective, explanations about previous mechanical models of infill masonry walls for both types: out-of-plane or in-plane walls is provided. The mechanical behavior of these two types is illustrated with a presentation of the codes recommendations. Additionally, a FEM model for in plane walls is presented as well as the analytical resolution of out-of-plane failure mode. The RC frame is then analyzed through developing the governing equation of motion, the time history and the steps of analysis followed through procedure. Finally, the results are described and discussed.

5.2. Characteristics of the test building

5.2.1. Architectural plan

The test building considered in this study is a reinforced concrete (RC) building that has two floors. It is designed as a working place and composed of two working rooms and a directory (office) room per floor (Figure 23). The total area of each floor is approximately 200m². Moreover, the ground floor is 4m high and the other floors are 2.8m high. The terrace is not accessible.

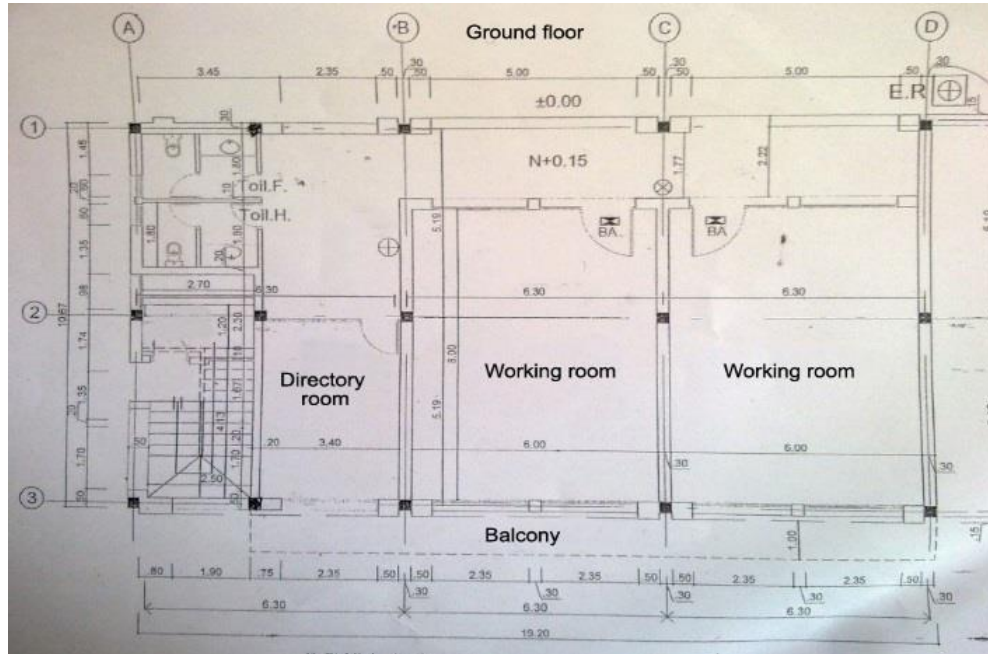


Figure 23: architectural plan of the test building

5.2.2. Frame elements design

In order to determine the frame elements' cross-section correctly, it is important to provide an overview about the characteristics of materials. Table 3 represents the principal characteristics for these materials.

For the task of pre-dimensioning the frame elements, the cross sections for columns were chosen 25*25(cm), for the bearing-loads beams 25*50(cm), for the non-bearing-loads beams 25*30(cm) and for the shell depth: 20cm. The building is considered fully supported by the fixed foundations (all DOF are restrained).

	Parameter	Mean value	unit	Stress-strain curve
concrete	Weight per unit volume	2500	Kg/m ³	
	E : modulus of elasticity	31000	MPa	
	Specified compressive strength f_c'	25	MPa	
	U: Poisson ratio	0.2	-	
steel	Weight per unit volume	7850	Kg/m ³	
	E : modulus of elasticity	210000	MPa	
	Yield strength	500	MPa	
	U: Poisson ratio	0.3	-	

Table 3: characteristics of materials

According to the BAEL'90 instructions, the building's structural elements should bear different recommended combinations of dead load, live load, seismic load and other loads like wind or snow if needed. These combinations are explicated as follows (DL=dead load, LL=live load, WL=wind load, EL=earthquake load):

- 1.35 DL
- 1.35 DL+1.5 LL
- 1.35 DL±1.5 WL
- 1.00 DL±1.5 WL
- 1.35 DL+1.35 LL±1.35 WL
- 1.00 DL±1.00 EL
- 1.00 DL+1.5*0.3 LL±1.00 EL

The structure is dimensioned with the SAP2000 software after considering the appropriate loads' values for this working place building. The software provides the required amount of reinforcing rebar and considers the stress and strain limits for the structural frame elements. Particular attention is assigned to the seismic dimensioning, which is established by the static linear method due to the simplicity of the building's frame. Wind and snow loads are not considered. Moreover, the software

helps identifying the values of moments and shear in any location within the frame in order to anticipate the critical rupture zones. After the dimensioning task, the software allows experimenting the tsunami forces on the building. In the next chapters, infill masonry and reinforced concrete elements of the building are analyzed towards tsunami action.

5.3. Infill masonry analysis

For an RC structure type, which is the most common type of buildings constructed nowadays in Morocco, the infill masonry has an important role to fulfil. This infill masonry is used for its sonic and thermic protection, but also important for increasing the building's stiffness and supporting its capacity towards seismic solicitation. Many previous studies have worked on infill masonry walls and proposed some advanced models that describe its mechanical behavior (Milani 2011; Pande & al 1990; Puglisi & al 2009)).

Walls of masonry are non-structural elements of regular RC buildings. Two types of walls are to be considered: out of plane and in plane walls. In this chapter, the infill masonry is analyzed for both types with a description of the proposed models to recognize the response of the infill masonry walls against an action (seismic or tsunami solicitation) and the norms suggestions to simplify the calculations of wall's resistance.

5.3.1. Out of plane walls

Out-of-plane infill masonry walls are the walls perpendicular to the flow direction. They have a weak inertia when facing the wave force. Additionally, the mechanical connection between different elements of infill masonry, namely bricks and mortar, is weak compared to reinforced concrete. This weakness resides in the heterogeneity of materials which forms many rupture zones. Out of plane walls receive also a great amount of tsunami impact force due to the surface exposure compared to in plane walls. This influences significantly the resistance of this type of infill masonry wall against tsunami impact and make it more vulnerable.

5.3.1.1. *Micro & macro model analysis*

Many studies discussed the micro and macro models for the infill masonry in order to approach its behavior. The micro model consists on choosing an elementary cell (or bloc) formed with masonry elements (brick and mortar) that can be successively repeated. On the other hand, a macro model considers the totality of the masonry wall with average values of its materials' characteristics regardless of their heterogeneity. (Lourenço 2000; Milani & al 2005) proposed a model for the out-of-plane masonry using a micro discretization of the wall panel and a simplified homogenization of the cell element (Figure 24). The elementary cell is subdivided along the thickness in several layers and the stress fields are equilibrated for each layer. The boundary conditions and the admissibility constraints are implemented as well. A use of a FE analysis code is also proposed in order to determine the out-of-plane failure surface. In addition, the authors discussed the experiments held by McMaster University (Gazzola & al 1986) on five wallets of masonry with different geometry shapes and boundary conditions. The out-of-plane pressure is applied via air bags in order to assure the uniformity of the distribution of load. Among the wallets, a case of a panel simply supported (WII) shows some interesting results regarding the displacement of the center of the wall when the pressure increases (Figure 25). From this pressure-displacement curve, an elastic linear phase could be recognized until the pressure reaches 3 Mpa. The displacement is not significant in this phase because it does not surpass 1.5mm. A sudden crack-displacement is recorded after. The displacement is linear to the applied pressure after this crack and stops at a pressure peak equals 6.6 Mpa. The wall is assumed to

be heavily damaged after this peak because the displacement of the center increases even though the applied pressure is not very important.

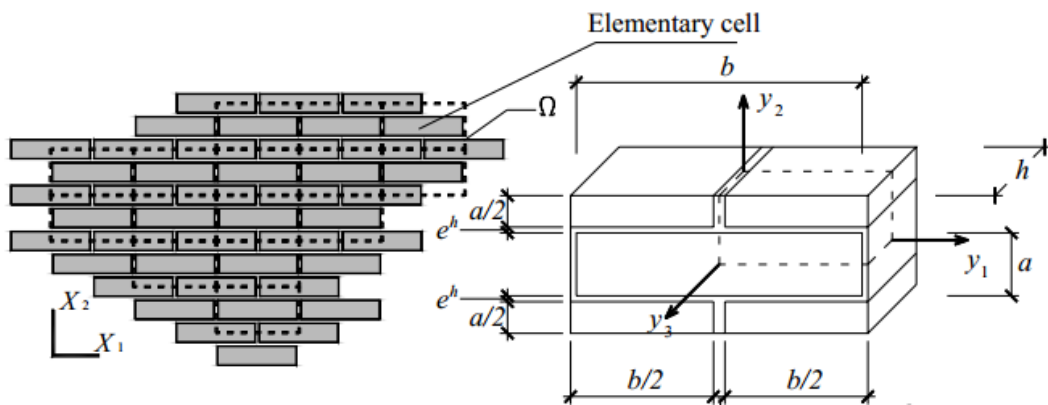


Figure 24: micro model proposed by (Milani, Lourenço, and Tralli 2005)

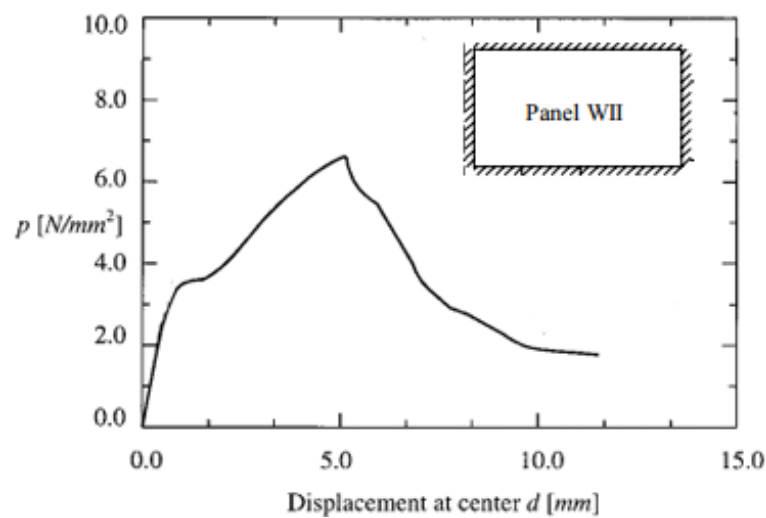


Figure 25: recording of the displacement of the wall's center due to the pressure p (after Lourenço 2000)

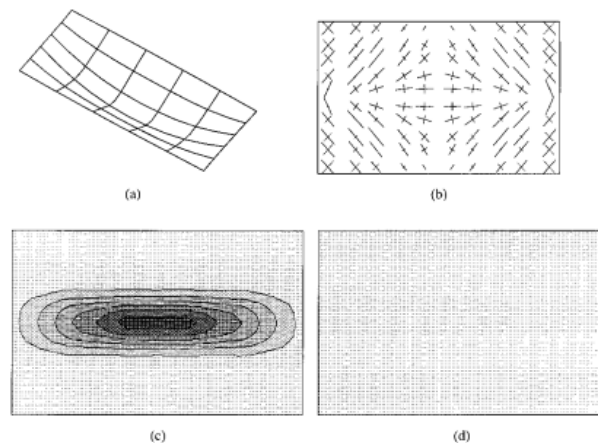


Figure 26: results of analysis at pressure p equals 6.6Mpa (peak) (a) deformed mesh (b) principal moments (c) plastic strain in bottom and (d) in top face. (after Lourenço 2000)

5.3.1.2. Mechanical behavior

The behavior of the masonry out-of-plane wall is based on plate theory. Plates are defined as plane structural elements with a small thickness compared to the planar dimensions. The typical thickness

to width ration of a plate structure is less than 0.1. This assumption helps identifying the displacement field as follows:

$$u_1(x) = u_1^0(x_1, x_2) - x_3 \frac{\partial \omega^0}{\partial x_1}$$

$$u_2(x) = u_2^0(x_1, x_2) - x_3 \frac{\partial \omega^0}{\partial x_2}$$

$$u_3(x) = \omega^0(x_1, x_2)$$

Where x_1, x_2 are the Cartesian coordinates on the mid-surface of the undeformed plate, x_3 is the coordinate for the thickness direction, u_1^0 and u_2^0 are the in-plane displacements of the mid-surface, and ω_0 is the displacement of the mid-surface in the x_3 direction. Moreover, the stress-strain relations are:

$$\begin{bmatrix} \sigma_{11} \\ \sigma_{22} \\ \sigma_{12} \end{bmatrix} = \frac{E}{1-\nu^2} \begin{bmatrix} 1 & \nu & 0 \\ \nu & 1 & 0 \\ 0 & 0 & 1-\nu \end{bmatrix} \begin{bmatrix} \varepsilon_{11} \\ \varepsilon_{22} \\ \varepsilon_{12} \end{bmatrix}$$

The development of governing equations in moments terms (see appendix) shown as follows:

$$M_{11,11} + 2M_{12,12} + M_{22,22} = 0$$

leads to the governing equation of displacement using the stress-strain relations. We obtain the following Lagrange equation:

$$\Delta^2 \omega = \frac{-q}{D}$$

Or, in expanded form:

$$\frac{\partial^4 \omega}{\partial x^4} + 2 \frac{\partial^4 \omega}{\partial^2 x \partial^2 y} + \frac{\partial^4 \omega}{\partial^4 y} = -\frac{q}{D}$$

Where ω is the deflection of the plate, q the solicitation on the plate and D is the bending stiffness of the plate introduced above. The resolution of this equation through Fourier series leads to the general solution expressed with the trigonometric terms: sine and cosine though it depends on the boundary conditions. For example, the deflection of a simply-supported plate with a general load is expressed as follows:

$$\omega(x, y) = \frac{1}{\pi^4 D} \sum_{m=1}^{\infty} \sum_{n=1}^{\infty} \frac{a_{mn}}{\left(\frac{m^2}{a^2} + \frac{n^2}{b^2}\right)^2} \sin\left(\frac{m\pi x}{a}\right) \sin\left(\frac{n\pi y}{b}\right)$$

Where w is the deflection, D the bending stiffness, a_{mn} coefficients of q in Fourier sum, a and b dimensions of the plate.

A more detailed explanation is provided in the appendix.

The Eurocode 6, dedicated to masonry, suggests that there are two failure modes for an unreinforced infill masonry supported by three or four edges, which corresponds to a plane of failure perpendicular or parallel to the bed joint (Figure 27). The characteristics f_{xk1} and f_{xk2} are the flexural strength of the masonry parallel/perpendicular to bed joint. These characteristics should be extracted from laboratory tests or by a FEM reliable model. The calculation of the design moment, M_d , is based on the plate theory results mentioned above with an integration of some additional factors. The design moments M_{d1}/M_{d2} when the failure occurs parallel/perpendicular respectively to the bed joint are:

$$M_{d2} = \alpha_2 W_d l^2$$

$$M_{d1} = \alpha_1 W_d l^2 = \mu M_{d2}$$

Where:

- $\alpha_1 = \mu \alpha_2$ is a bending moment coefficient which depends on:
 - The orthogonal ratio μ
 - The degree of fixity at the edge of the panel
 - And the height to length ratio of the panel
- μ is the orthogonal ratio of the flexural strength of masonry, $\mu = \frac{f_{xk1}}{f_{xk2}}$
- l is the length of the masonry panel.
- W_d is the applied load per unit area.

On the other hand, the moment of lateral resistance of a masonry panel is :

$$M_{Rd} = \frac{f_{xk} * t^2}{6 * \gamma_m}$$

Where

- f_{xk} is the flexural strength of masonry in the considered direction (f_{xk1} for parallel and f_{xk2} for perpendicular directions)
- t is the thickness of the panel
- γ_m is a security coefficient.

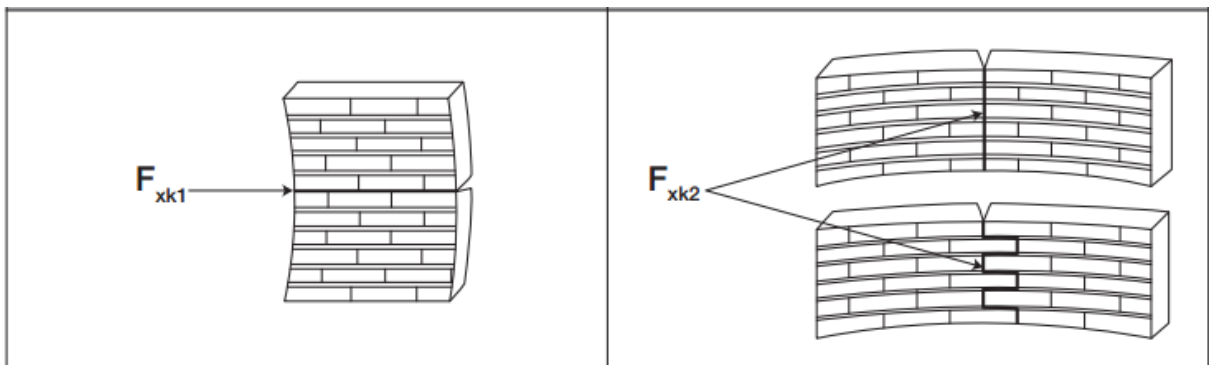


Figure 27: failure modes of unreinforced masonry: (left) parallel or (right) perpendicular to bed joints (after Eurocode 6)

In his study, Bui (2013) worked with a reliable software "3DEC" to determine the characteristics f_{xk1} and f_{xk2} for a masonry wall under out of plane solicitation. His work shows how the failure of the

wall occurs and how the pressure of failure depends on the H/L ratio. For a masonry wall simply supported by four edges (WII), the failure mode is shown in Figure 28. The characteristics f_{xk1} and f_{xk2} are calculated according to the EN 1052-2 recommendation that suggests increasing the loading on a specific inner bearing location shown in Figure 29. After finding out the rupture force, f_{xk1} and f_{xk2} are determined by the following formula:

$$f_{xk} = \frac{3 \cdot F \cdot d}{b \cdot t^2} \text{ (Mpa)}$$

Where:

- F: rupture force in case of a loading parallel/perpendicular to bed joint;
- d: spacing between the inner bearing
- b: height or width of the masonry specimen perpendicular to the direction of span
- t: width of masonry unit.

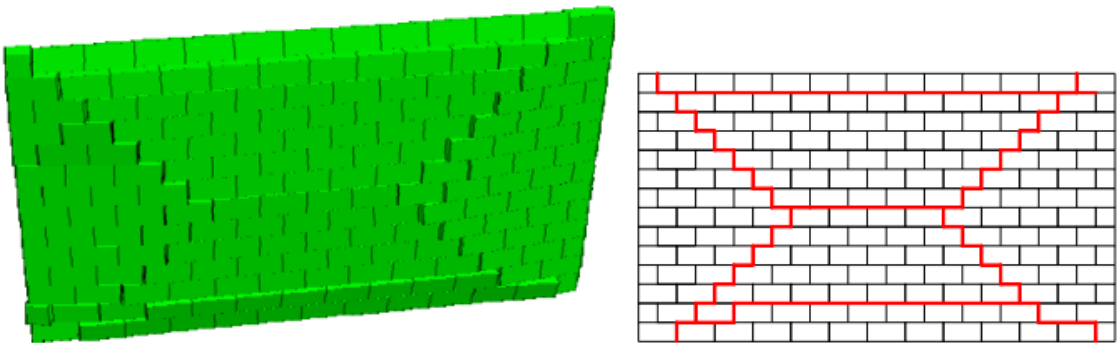


Figure 28: failure for a simply supported masonry panel (WII) (after Bui 2013)

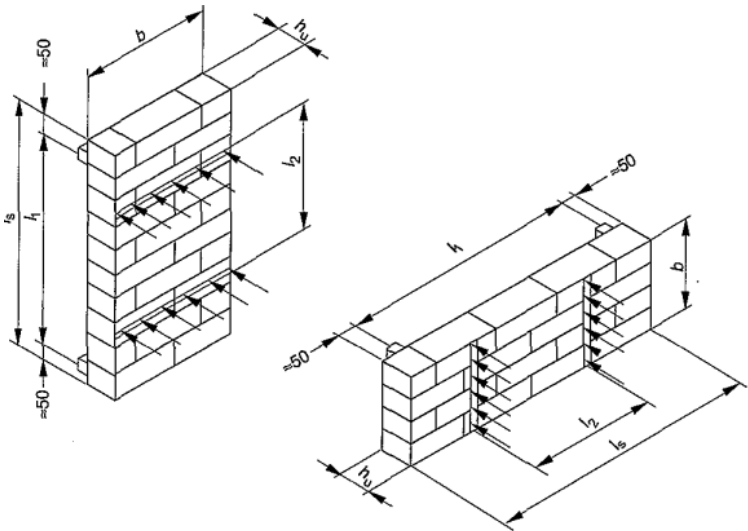


Figure 29: determination of f_{xk1} and f_{xk2} characteristics according to EN 1052-2 norm (see EN 1052-2 norm for more details)

The results of the FEM of a masonry panel 5000*2800 (mm²) with material characteristics specified in Table 4 are illustrated in Figure 30. Furthermore, this could be useful to determine the walls that fail at resisting to the tsunami’s impulsive force.

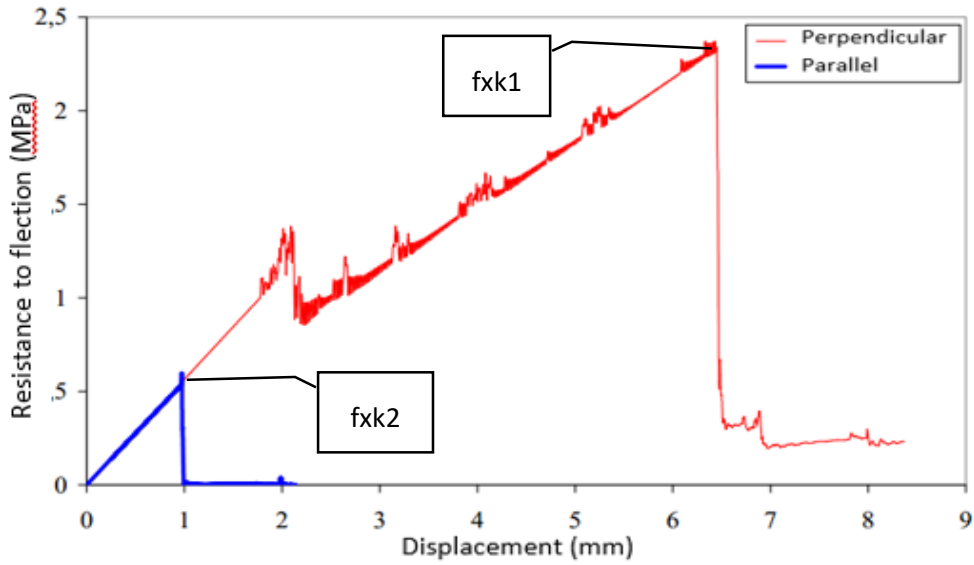


Figure 30: FEM in "3DEC" software to determine f_{xk1} and f_{xk2} (after Bui 2013)

Bloc		Interface			
Young modulus	Poisson coefficient	Tension resistance	Cohesion	Rubbing angle	Dilatation angle
$E(N/mm^2)$	ν	$T(N/mm^2)$	$C(N/mm^2)$	φ	ψ
15000	0.2	0.157	0.5966	0.36	0

Table 4: characteristics of masonry material (after Bui 2013)

Bui (2013) investigated the pressure variation when the H/L ratio varies (Figure 31).

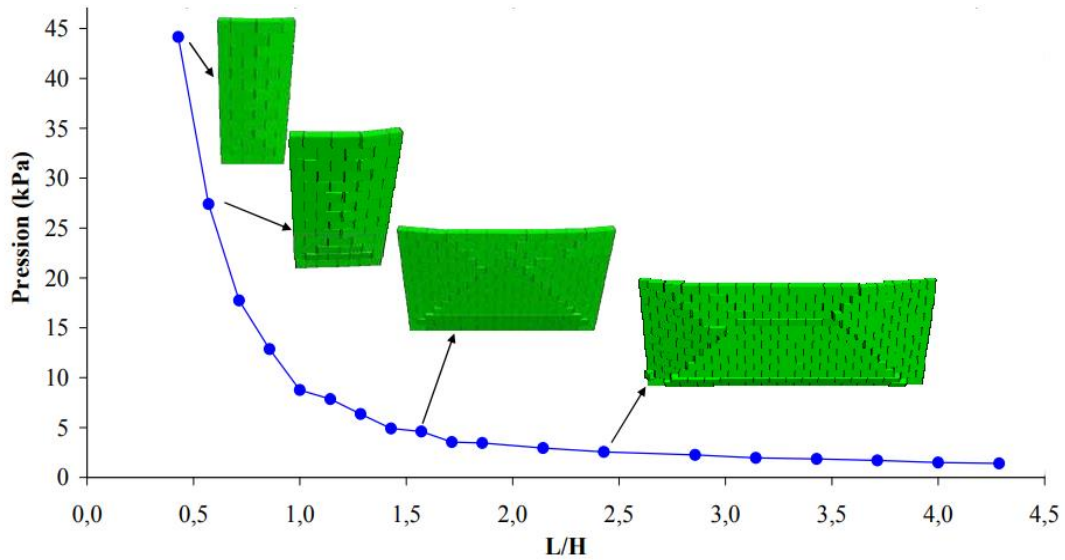


Figure 31: behavior of masonry panels simply supported by 3 edges (after Bui 2013)

The results of this chapter are developed in the next section.

5.3.1.4. Out of plane walls results

The infill masonry walls are simply supposed to be supported by three edges without bearing any loads. When investigating the wall's reaction to tsunami wave, we are interested specifically in the impulsive force that strikes and damages the wall. For this objective, the impulsive forces are calculated for different heights following the FEMA P'646 method. The effective height h_{max} that determines the surface pressuring the wall depends on R; the run-up level and z; the height at the site of the wall (building) by the relation:

$$H_{max}=R-z$$

These two parameters influence the level of resistance of the infill wall.

On the other hand, the maximum pressure that the infill masonry panel can withstand could be calculated through the Eurocode formulas mentioned earlier that define the solicitation and resistance moments of the wall, shown as follows:

$$M_{d2} = \alpha_2 W_d l^2$$

$$M_{Rd} = \frac{f_{xk} * t^2}{6 * \gamma_m}$$

If the wall doesn't fail, then

$$M_{d2} < M_{Rd}$$

Which means that:

$$W_{edmax} = \frac{f_{xk2} \cdot t^2}{6 \cdot \gamma_m \cdot \alpha_2 \cdot l^2} = \frac{f_{xk1} \cdot t^2}{6 \cdot \gamma_m \cdot \alpha_1 \cdot l^2}$$

Because $\mu = \frac{f_{xk1}}{f_{xk2}} = \frac{\alpha_1}{\alpha_2}$

The results for the infill masonry panel of the test building described in section 5.2.1, which has an area of approximately 5*2.8 m², are shown in Figure 32.

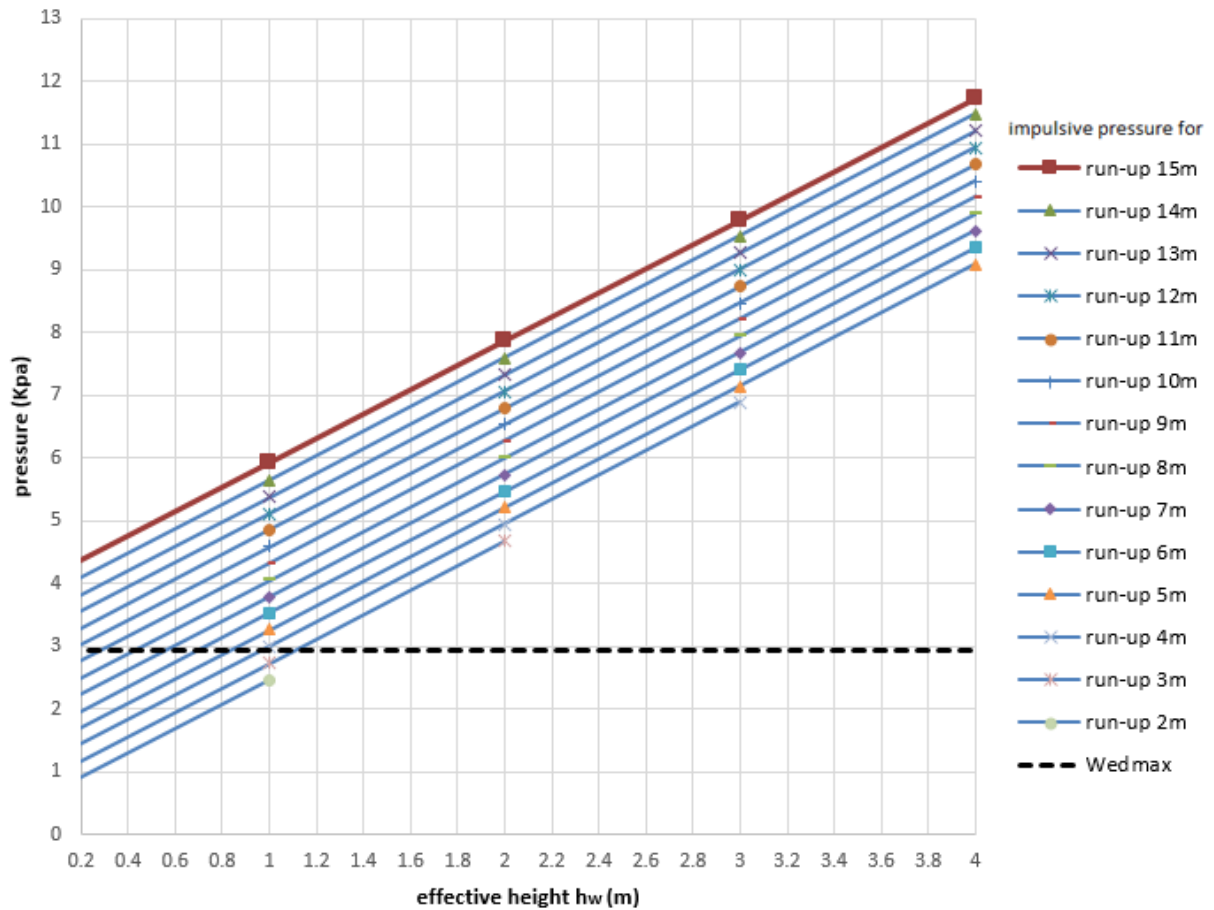


Figure 32: Variation of pressure of the impulsive force for different run-ups by the effective height, Wedmax is the maximum bearable pressure.

In fact, these results could be interpreted as follows: for a high run-up of 15m for example, a building at $z=14\text{m}$ above the normal sea level (so the effective height on the infill wall is $h_{\text{max}}=R-z=1\text{m}$) is struck by an impulsive pressure of 6 kpa. This pressure is above the limit of the infill wall's resistance which is $\text{Wedmax}=2.95\text{ Kpa}$ (retrieved from Figure 31 for a masonry wall of $5*2.8\text{m}^2$). As a result, the infill wall will crumble.

On the other hand, a building located in $z=2\text{m}$ with a tsunami run-up of $R=3\text{m}$ ($h_{\text{max}}=1\text{m}$) might not fail at resisting the impulsive pressure of 2.8 Kpa, which is under the capacity of wall's resistance boundary ($\text{Wedmax}=2.95\text{Kpa}$).

Regarding the case of this thesis and the considered location chosen as a study area (city of Tangier), the works of [Benchekrroun et al. \(2013\)](#) and the [Norwegian Geotechnical Institute \(2013\)](#), that simulated the inundation in the Gulf of Cadiz zone, indicated that the average run-up height in this area is 7-8m. So, the infill walls of buildings in this area might highly fail at resisting the wave impact due to the tremendous impulsive pressure.

5.3.2. In plane walls

In plane walls are the walls parallel to the direction of the wave incidence. In case of seismic solicitation, the in-plane walls help increase the rigidity of the building frame and resisting the seismic force. Unlike the out of plane walls, the in-plane walls dissipate the seismic energy differently and that by changing the lateral-load mechanism from predominant frame action to predominant truss action (Figure 33). Some studies focused on the infill masonry walls' response in the seismic case because

analyzing the pattern of dissipating the seismic force could provide a helpful information about reinforcing the rigidity of new RC buildings and also finding solutions for existing ones.

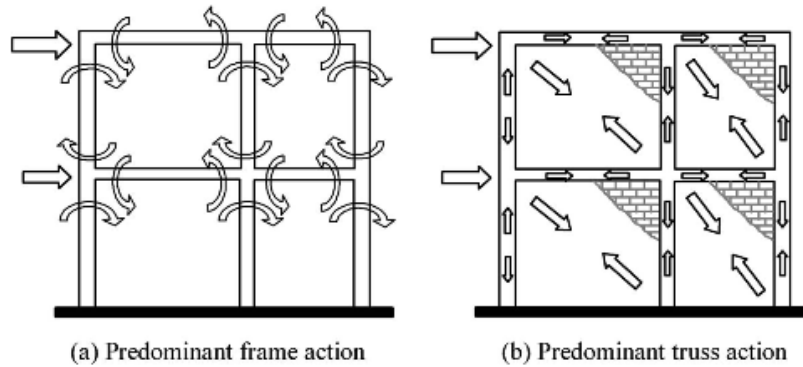


Figure 33: change in lateral load transfer mechanism by in-plane walls (after kaushik & al 2006)

In this chapter, we try to analyze the reaction of in-plane masonry walls against tsunami forces, and make a comparison with the seismic solicitation case.

5.3.2.1. Previous models studies

Many research studies have analyzed infill masonry walls under a seismic shear force oriented parallel to the wall's plane direction. Predicting the behavior of these infill walls, which are composite materials, is established through one of three major models. The first is the "microscopic" level, where the elemental matrix is constituted from a unit of bricks and adjacent mortar (Buhan & al 1994; Milani 2011; Zucchini & al 2002). The second considers a "mesoscopic" level, where the elementary unit is a simple layer of consecutive brick-mortar (joints) system that can be reproduced vertically to give the wall its height (Pande & al 1990). Finally, the macroscopic level where the wall is considered as a plate, with a hypothesis of a good and valid homogenization transformation (Al-chaar 2002; Asteris et al. 2011). This last method is the most suited for this analysis case because the objective is to recognize globally the reaction of in-plane walls against a lateral force of tsunami scale without detailing the deformation of infill masonry elements.

Mainstone & al (1970) have worked on the macro-model and suggested a replacement of the shear wall by an equivalent diagonal strut (

Figure 34) with geometrical parameters (Fema306) as follows:

$$\frac{w}{d} = 0.175\lambda_h^{-0.4}$$

where :

- d is the length of the strut frame (in)
- $\lambda_h = h_{col} \sqrt[4]{\frac{E_{inf} t_{inf} \sin(2\theta)}{4EI h_{inf}}}$,
- h_{col} = column height between centerlines of beams (in);
- E_{inf} = modulus of elasticity of the masonry panel;
- EI = flexural rigidity of the columns;
- t_{inf} = thickness of the infill panel and equivalent strut (in);

- h_{inf} = height of infill panel; and θ = angle, whose tangent is the infill height-to-length aspect ratio (in),
- $\theta = \tan^{-1}\left(\frac{h_{inf}}{L_{inf}}\right)$ in which L_{inf} = length of infill panel.

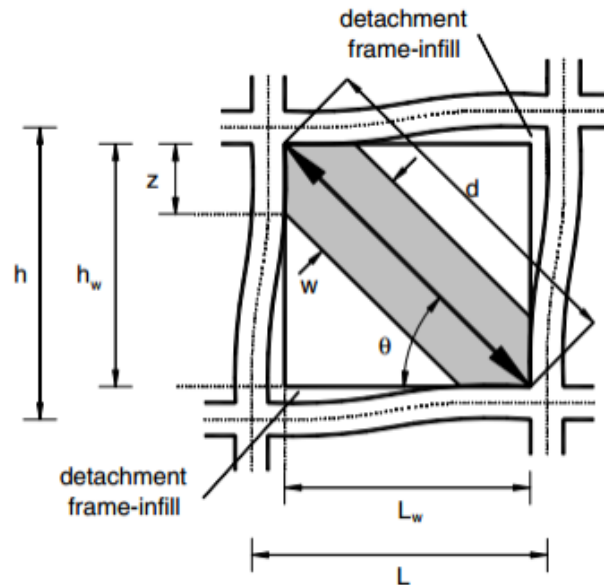


Figure 34: diagonal strut model for masonry walls following (after Mainstone & al 1970)

5.3.2.2. Eurocode recommendation

The Eurocode 6 recommends that the shear capacity should be checked for the shear forces generated by the diagonal strut action of the in-. However, the Eurocode doesn't specify the geometric and strength characteristics of the diagonal strut, except recommending the wall's minimum thickness for 240mm and the maximum slenderness ratio (height/thickness) for 15.

Other codes such as FEMA306 recommends using the equation provided by Mainstone & al (1970) introduced in the previous chapter. In addition, FEMA306 identifies four possible failure modes that indicate the damage pattern and potential crack which could occur for in-plane walls. These failure modes are: the corner crushing mode, diagonal compression, sliding shear, diagonal cracking and frame failure modes (Figure 35).

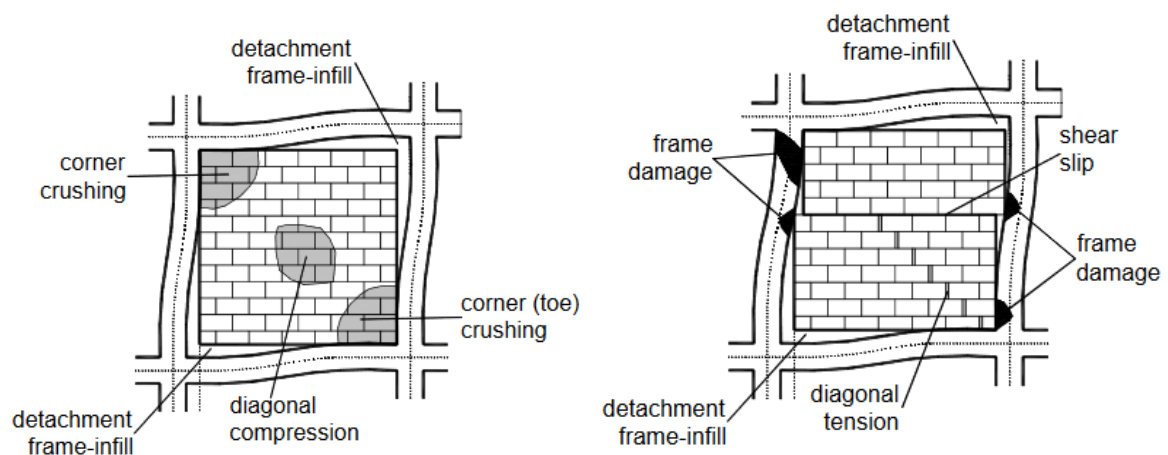


Figure 35: all failure modes of in-plane infill masonry (after Kumar & al 2017)

5.3.2.3. FEM results

In order to compare the reaction of in-plane masonry walls to seismic solicitation (that leads to the diagonal strut model) and the tsunami impact, we carried a finite element model (FEM) of the masonry panel of the test building adopted in this study and introduced in chapter 5.2. Considering the test building's frame geometry, the in-plane masonry walls have almost $5.00 \times 2.80 \text{ m}^2$. The beam is $40 \times 25 \text{ cm}^2$ with a concrete type C25/30. Columns are $30 \times 30 \text{ cm}$ with C25/30 as well. The masonry panel, as a matter of simplification, has an elasticity modulus of $E_m = 15000 \text{ MPa}$ and a Poisson ratio $\nu = 0.2$ (Bui 2013) with an average density of $D = 2000 \text{ kg/m}^3$. The seismic solicitation is applied on the top corner joint of the concrete frame parallel to the wall's plane. However, the tsunami impact is distributed uniformly along the column length (Figure 36). The forces are increased linearly through time.

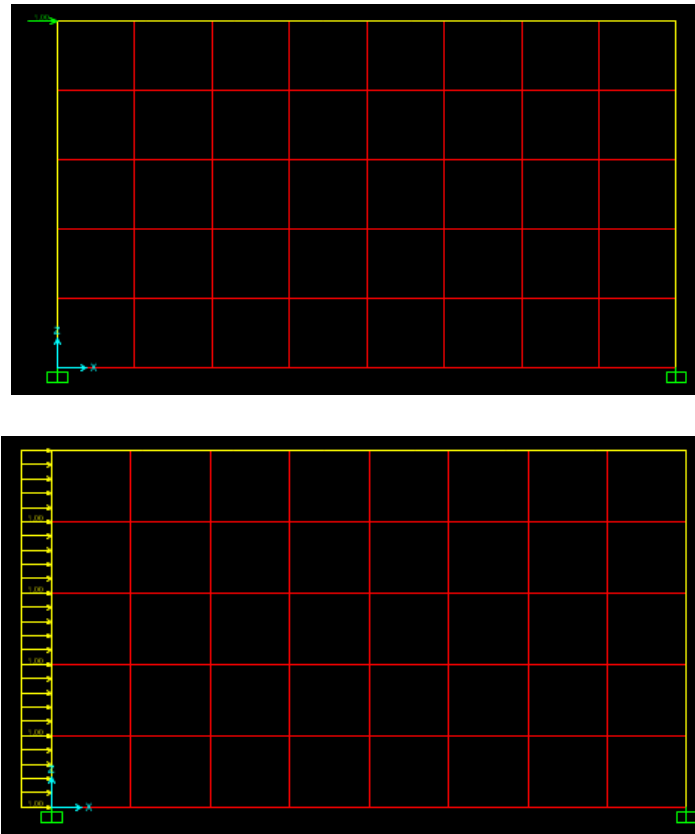
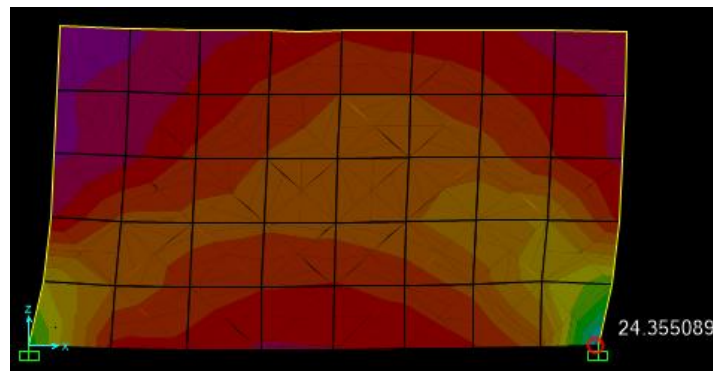


Figure 36: force application pattern for (top) seismic and (bottom) tsunami solicitations

The masonry panel is discretized in order to determine more precisely the values of stresses. Figure 37 shows the stress values in the masonry panel for the same time step. The maximum values of stress are indicated as well as the deformed shape of the concrete frame.



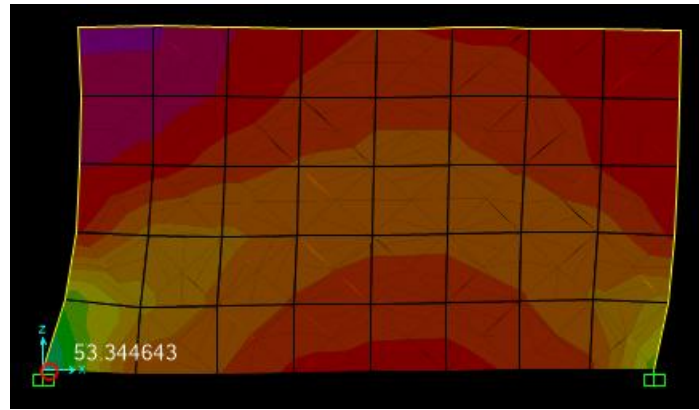


Figure 37: stress distribution in (top) seismic and (bottom) tsunami solicitations at the same time step (KPa)

Figure 37 shows that the masonry panel should handle much greater stress in case of a tsunami impact compared with a seismic solicitation. The recorded stress for this step of time shows that tsunami forces impose approximately a double strain on the masonry panel than the seismic force. Moreover, in the seismic case, the energy of solicitation is dissipated through a compressive pattern where the bottom right joint receives the most recorded stress. This favors Mainstone & al (1970) model which suggests the diagonal compressive strut, because it works similarly to the observed mechanism. However, the stress indicated in the tsunami case is maximum in the left bottom joint, which means that the energy is dissipated through a different pattern and that the diagonal compressive strut model might not fit the tsunami case model. This may be caused by the frame deformation which is different between the two cases. In the seismic case, the columns work as a cantilever system due to the concentrated floor mass on the top edge joints. However, in the tsunami case, the left column receives a distributed loading along its length. This causes a flexion of the column and consequentially more strain on the adjacent area of the masonry panel.

5.4. RC frame analysis

In this section, we analyze the response of the test building described in chapter 5.2 to a tsunami impact.

5.4.1. Equation of motion

The equation of motion of a multi-degree-of-freedom (MDOF) system subjected to excitations $\underline{P}(t)$ is given as follows:

$$\underline{\underline{M}}\ddot{\underline{U}} + \underline{\underline{C}}\dot{\underline{U}} + \underline{\underline{K}}\underline{U} = \underline{P}(t) \quad \text{Equation 9}$$

Where $\underline{\underline{M}}$ is the mass matrix, $\underline{\underline{C}}$ the damping matrix, $\underline{\underline{K}}$ the rigidity matrix and \underline{P} the input forces matrix. \underline{U} is the instantaneous displacement vector.

Equation 9 is transformed to the simplified form using the modal analysis:

$$m_j (\ddot{y}_j + 2\xi_j \omega_j \dot{y}_j + \omega_j^2 y_j) = p_j(t) \quad \text{Equation 10}$$

with:

- $\underline{U}(t) = \sum_{j=1}^n y_j(t) \underline{D}_j$;
- $p_j(t) = \underline{D}_j^t * \underline{P}(t)$;
- $\omega_j = \sqrt{\frac{\underline{D}_j^t \underline{K} \underline{D}_j}{\underline{D}_j^t \underline{M} \underline{D}_j}}$;
- $m_j = \underline{D}_j^t \underline{M} \underline{D}_j$;
- $c_j = \underline{D}_j^t \underline{C} \underline{D}_j = 2\xi_j m_j \omega_j$ and
- $k_j = \underline{D}_j^t \underline{K} \underline{D}_j$

where \underline{D}_j is the J^{th} eigenvector calculated from the modal analysis.

By applying the integral of Duhamel to Equation 10, the temporal displacement is given by:

$$y_j(t) = \frac{1}{m_j \omega_{DJ}} \int_0^t p_j(\tau) e^{-\xi_j \omega_j (t-\tau)} \sin[\omega_{DJ}(t-\tau)] d\tau \quad \text{Equation 11}$$

where $\omega_{DJ} = \omega_j \sqrt{1 - \xi_j^2}$

5.4.2. Time history

Chapter 4.4 discussed the temporal variation of tsunami forces obtained from laboratory experiments. The results of these experiments are important because they provide a global idea about the main impact of a tsunami wave and the fluctuation of tsunami forces' magnitude. The time history integrated into FEM model is a simplified plot inspired from various laboratory results and considering many important points:

- The layout of pressure curve: the curve maintains a constant value for several seconds in the beginning but drops after. The maximum value recorded for the first few seconds of the impact is due to the impulsive force of tsunami wave. The hydrodynamic force is succeeding the impulsive force but with a less magnitude (Figure 38)
- The traveling time of the wave from a row of columns (parallel to the wave incidence direction) to the next row: This depends on the velocity of the wave that could be revealed from previous works of inundation simulation of the shore. As discussed in chapter 4.2, propagation and inundation studies in the gulf of Cadiz indicated that the average velocity of tsunami wave is 6-7m/s. that means that the waves reaches the next row of columns in approximately 1s because the distance between successive rows of columns is 5,2 m (chapter 5.2.1). Figure 39 shows how the tsunami force changes for each raw of columns considering the delay of loading. this result suppose that out-of-plane infill masonry walls collapse promptly as retrieved from results of chapter 5.3.1.
- The magnitude of impulsive and hydrodynamic forces could be calculated through FEMA-P646 formulas as described in chapter 4.3. Indeed, tsunami forces: impulsive force and hydrodynamic force depend on the effective height that put the loading on the building frame. Although the laboratory curves could not determine the real value of the wave force that strikes the building's columns, it helps getting an overview about the variation of tsunami forces.

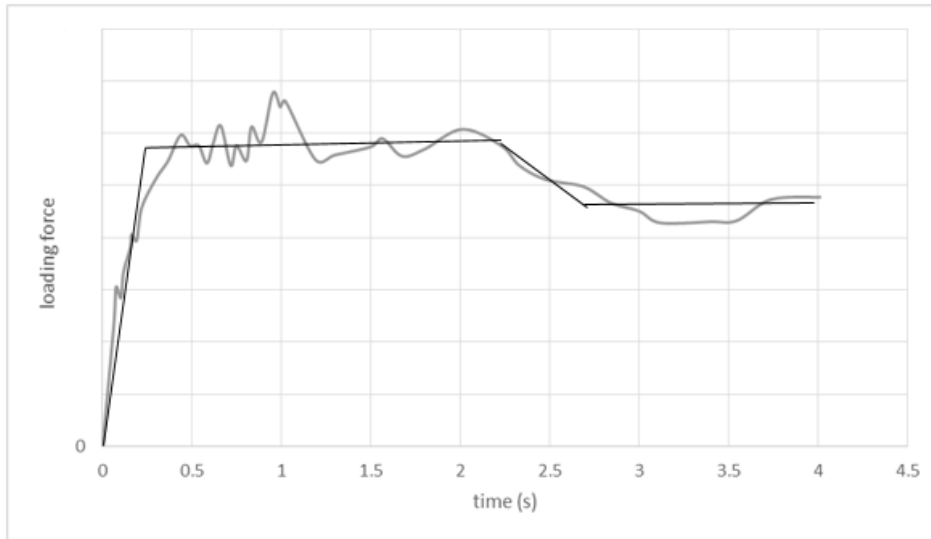
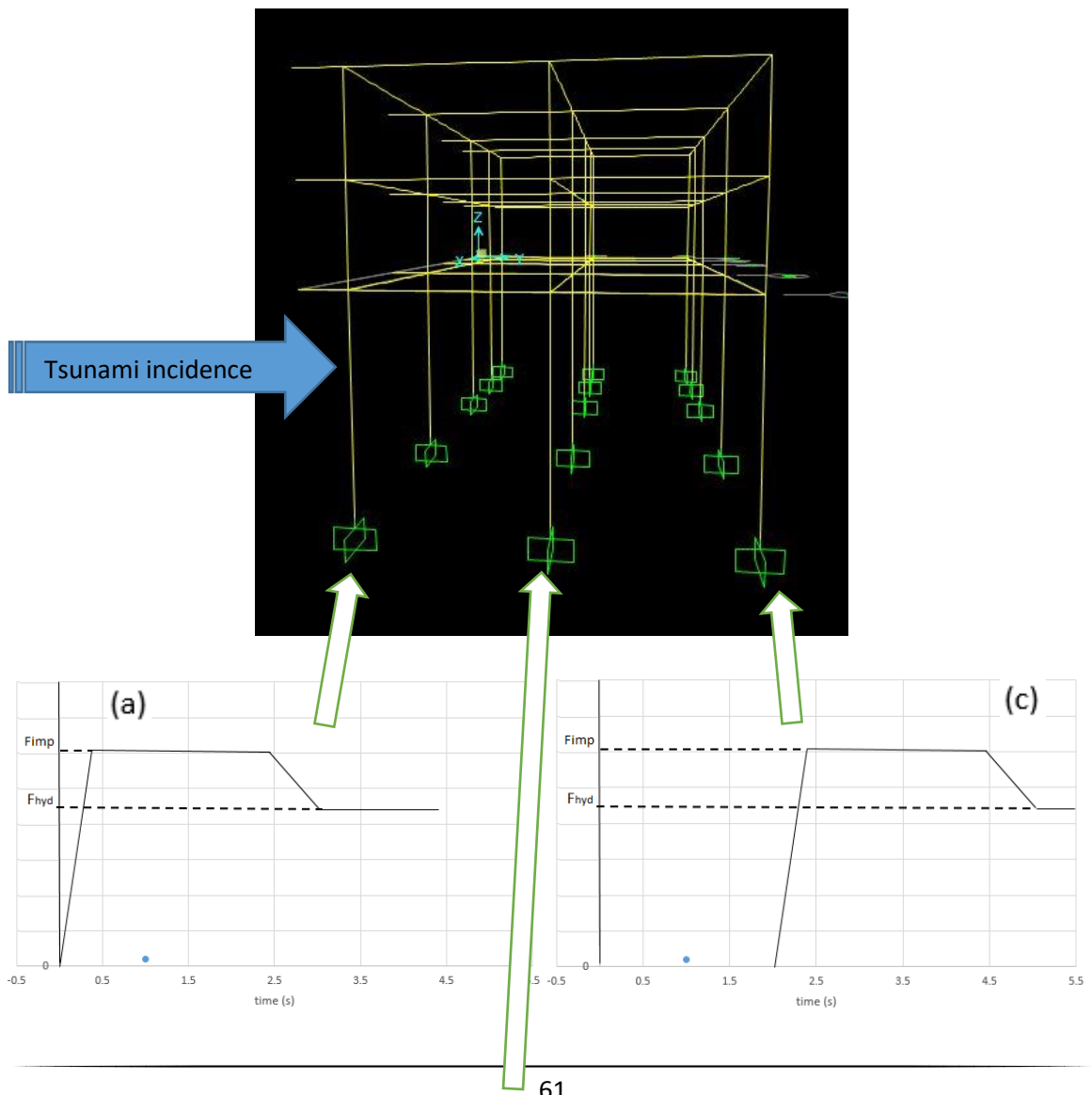


Figure 38: time history in the FEM model

The simplified plot (Figure 38) respects the ratio between the impulsive force and the hydrodynamic force suggested by FEMA P646, which is $F_{imp}=1.5F_{hyd}$. Moreover, the introduction of this simplified plot into FEM program minimizes as described in Figure 39 the consumption of compilation-time without threatening the validity of results.



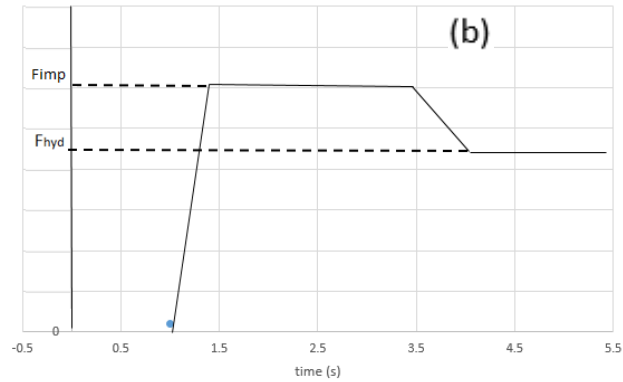


Figure 39: time history for each row of columns considering the delay of impact (F_{imp} impulsive and F_{hyd} hydrodynamic)

5.4.3. Steps of analysis

The analysis is conducted through the determination of maximum displacement in the building frame for each step of loading with tsunami forces: impulsive force and hydrodynamic force. In fact, the tsunami forces' values change according to each "effective" height step. The building is 10m height and the step chosen is 1m. So, for each effective height step, we change the loading of tsunami forces and run the software analysis then retrieve the maximum displacement as well as other results described later.

Another important point that should be explained is the influence of run-up height on tsunami forces. As mentioned in chapter 4.3, the expression of hydrodynamic force (ie, impulsive force because $F_{impulsive} = 1.5 F_{hydrodynamic}$) depends on R , the run-up height and z , the base elevation of the building. So, for two tsunami run-ups and two base elevations, the tsunami force change even if the effective height, which is the difference between the run-up and base elevation, is the same. Because of this important factor, one should consider firstly the run-up height of tsunami wave, then the effective height, ie the base elevation z because $z = R - h_{eff}$.

For this analysis, we have chosen two values of run-up height: 5m and 12m. However, the analysis could not reach floors above the ground floor for the case of $R=5m$, because the ground floor's height is 4m. We also suggested the analysis of the building frame for the 5m run-up case while changing the ground floor height: 4m, 5m and 6m height. We seek a comparison between these cases to better understand the impact of tsunami on the building frame.

5.4.4. Results

5.4.4.1. General results

After applying the tsunami loading on the building frame and running the analysis, the software provides a detailed information on the movement characteristics such as displacements in 3 directions and rotations around 3 axes. Figure 40 shows these characteristics in case of 7m effective height ($R=12m$). The tsunami impact follows the y direction, which is the reason the displacement U_2 is important compared to the U_1 and U_3 values. Moreover, the left side of the frame is displaced much more than the right side. This may be caused by the fact that the number of columns in the left side is more important and consequently, the loading on the left side due to tsunami forces applied on these columns is greater than the right side, where columns are fewer.

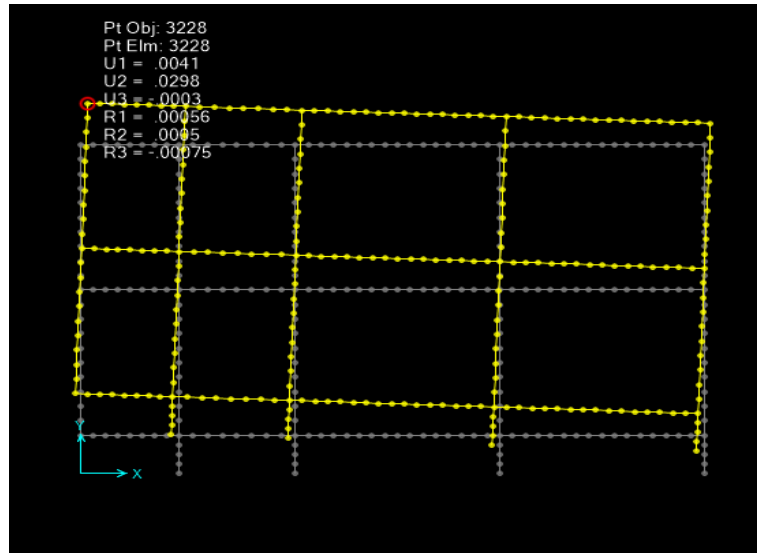


Figure 40: maximum displacement of the building frame (case of 7m effective height at the top floor)

The bending moments in the frame columns are shown in Figure 41. Columns of the ground floor resist to the impact moments more than other floors. In fact, the ground floor's columns are under a compound bending moment because of vertical loads that apply a compression stress and the flexion bending of tsunami forces. The column located in C-2 axe shows an important recorded moment compared to other columns. This may be caused by the important vertical load supported by this column even though its dimensions are greater than other columns (results from dimensioning the cross sections of columns).

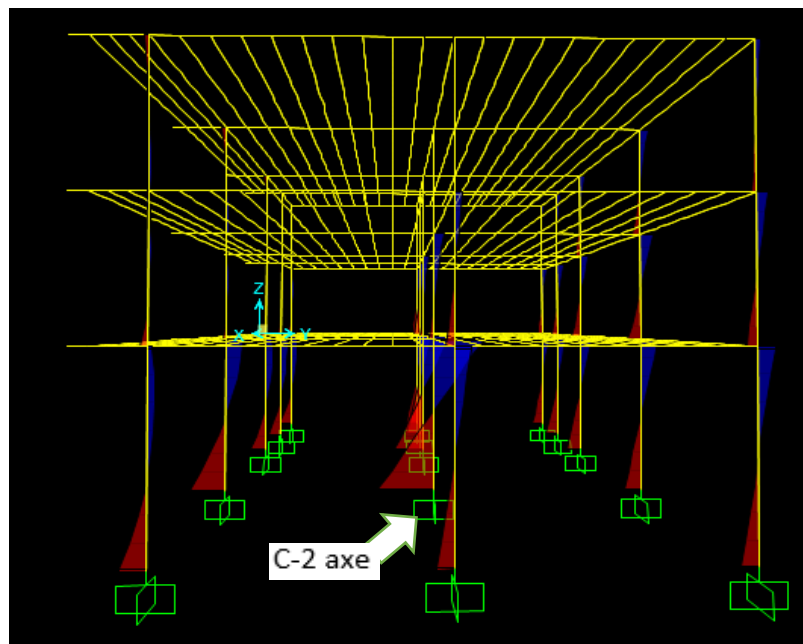


Figure 41: bending moments in columns (case of 7m effective height)

Figure 42 illustrates the deformed shape of the building frame where normally the maximum displacement occurs at the top floor. In some cases, the maximum displacement could be recorded at another floor level due to the excessive tsunami force. In order to monitor the variation of tsunami forces and also the movement characteristics (displacements and rotations), the use of nonlinear hinges is important. Figure 42 shows also some hinges deformed to some level of plasticity. In fact, hinges define the plastic behavior of the frame element through analyzing the deformation-force or

moment-rotation interaction (other interactions like stress-strain or moment-curvature could also be analyzed). The curves analyzed allow to recognize different levels of frame plasticity: (IO) immediate occupancy, (LS) life safety, (CP) collapse prevention as shown in Figure 43. When the curve layout exceeds the C-D points, the collapse of the element is highly predictable. This can be proven by the stress variation through time. A comparison of the variation of S11 stress between a 4m and 5m effective height cases is shown in Figure 44. Due to the greater tsunami force of the 5m case, the S11 stress (axial stress) reaches the limits allowed to concrete frame much faster than the 4m effective height case. It is also because the software could not solve the equation of movement mentioned in chapter 5.4.1 and could not invert the stiffness matrix that the analysis stops. This could prove that the element reach a failure state and can't handle any additional stress. As for reminder, Figure 45 shows how the stability of the building frame decreases due to the inversibility of stiffness matrix.

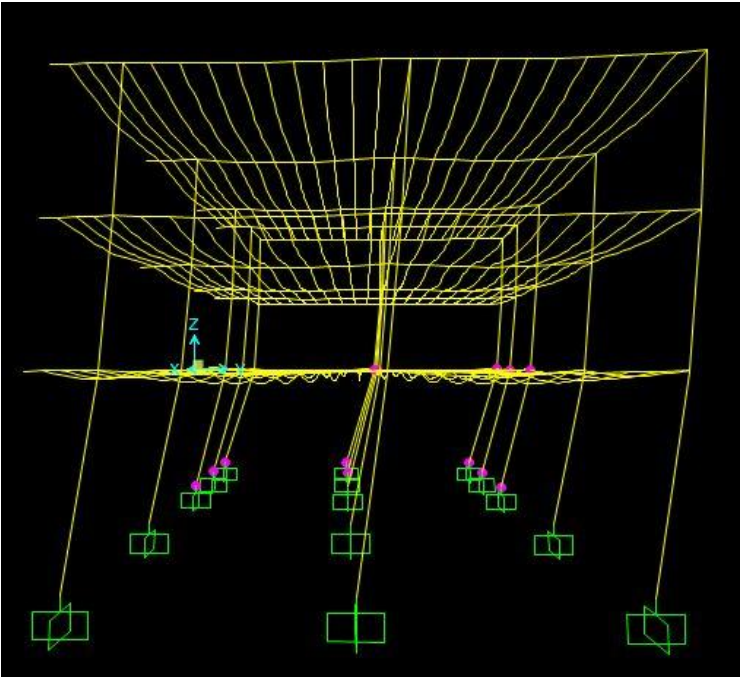


Figure 42: deformed shape of the building frame and state of hinges (case of 7m effective height)

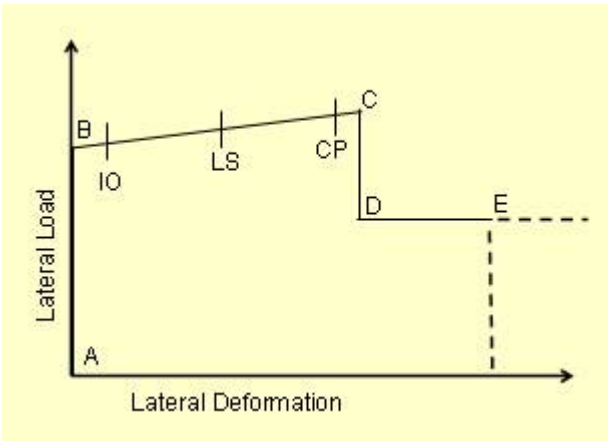


Figure 43: acceptance criteria (IO, LS and CP) for a force-deformation interaction of hinges (after SAP2000 help menu)

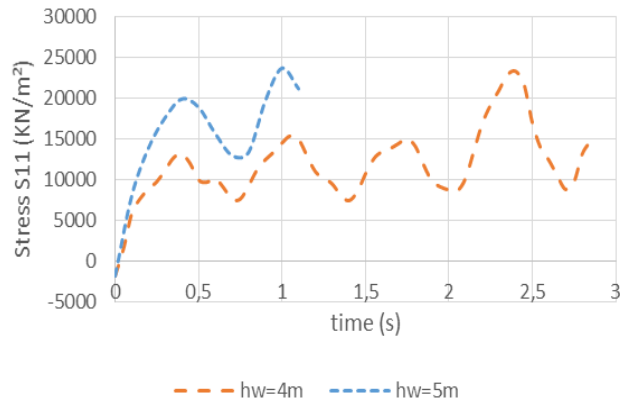


Figure 44: S11 stress recorded in a ground floor column for a 4m and 5m effective height cases

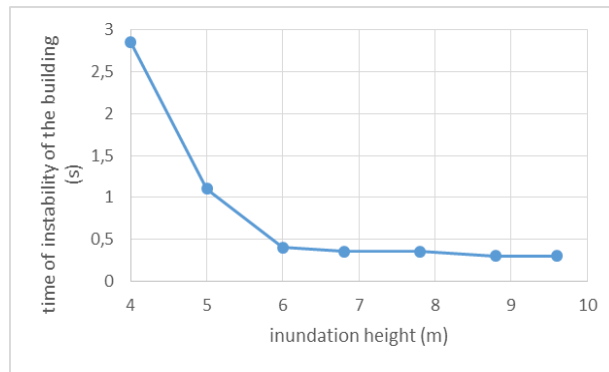


Figure 45: decrease of building stability by level of effective inundation height

5.4.4.2. Capacity curve

The capacity curve that describes the force-deformation of the building are retrieved from the software results for each effective height step. Results of deformation and base shear force for each time step (a time history analysis) are sorted in order to recognize the maximum values recorded by the simulation. As previously mentioned, we have analyzed the cases of a ground floor (GF) with different heights: 4m, 5m and 6m. The tsunami run-up is chosen as 5m and 12m. The capacity curve for the first case of a GF of 4m and R=12m is shown in Figure 46. A comparison between the cases of run-up of 5m and 12m is illustrated in Figure 47.

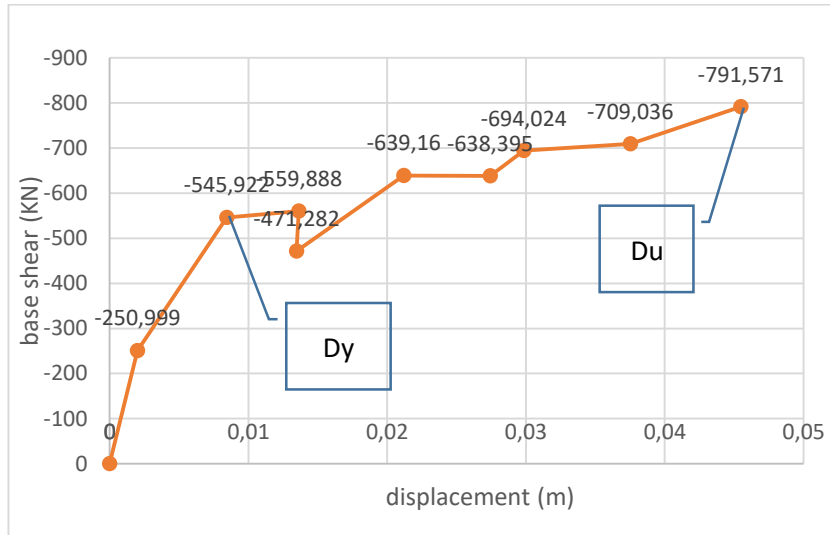


Figure 46: capacity curve for case GF=4m, R=12m

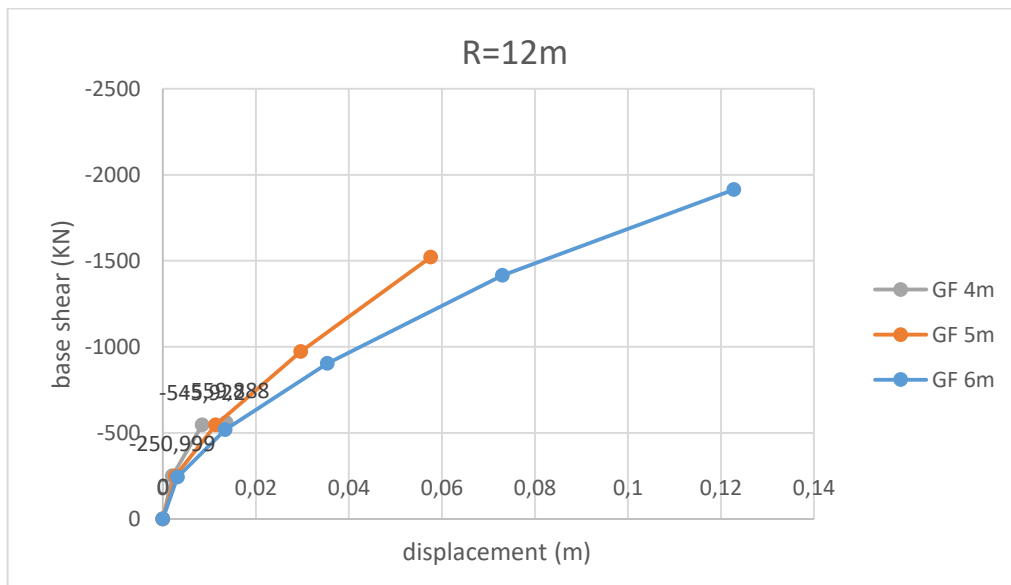
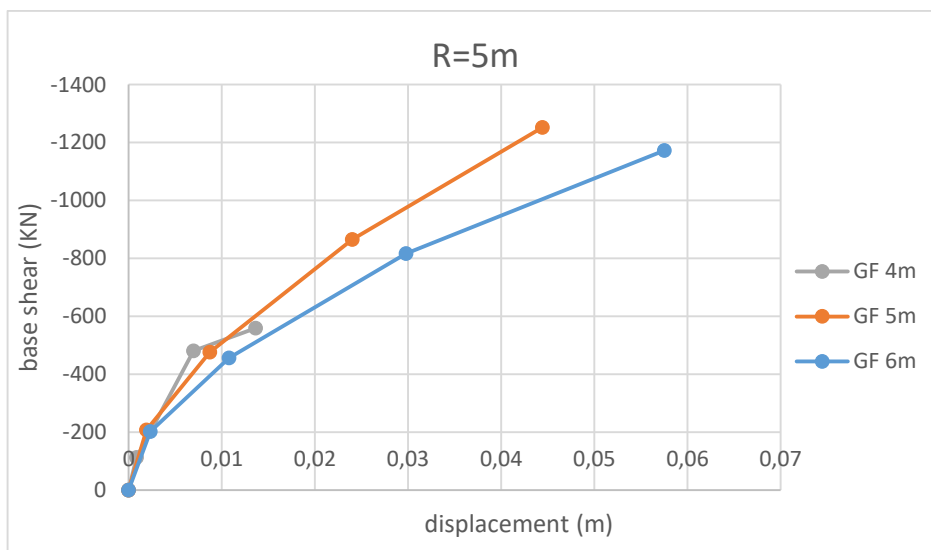


Figure 47: comparison between capacity curves (restricted to ground height) for run-up of 5m and 12m with different Ground Floor heights

Figure 46 shows how the layout of the curve indicates the domains of elasticity and plasticity of the building under tsunami forces. The yield point is located approximately for the displacement of 1cm and a base shear of 600KN. The ultimate point, which describes the point of failure could not be specified from the curve because the plastic range doesn't seem to stop at a rupture point characterized by a sudden drop of the curve layout. The analysis is stopped at the effective height step of 10m because the building has a total height of 10m.

The two charts of Figure 47 shows a comparison of the response of the building towards tsunami wave impact for different ground floor's heights. For the case of a run-up of 5m for example, the curves show that the maximum displacement of the building increases if the ground floor height increases. The analysis focuses on the reaction of the building up to the ground floor height but doesn't continue for higher floors, in order to make the comparison reasonable because the tsunami run-up is just 5m. For a given base shear force, ie tsunami force, the yield force recorded for different cases increases as soon as the ground floor height increases. This result is understandable due to the fact that the building, which can be modeled as a system with a single degree of freedom, is put under a so alike uniform lateral load (Figure 48). The deflection is calculated as follows:

$$f = \frac{-px^2}{24EI} (6l^2 - 4lx + x^2)$$

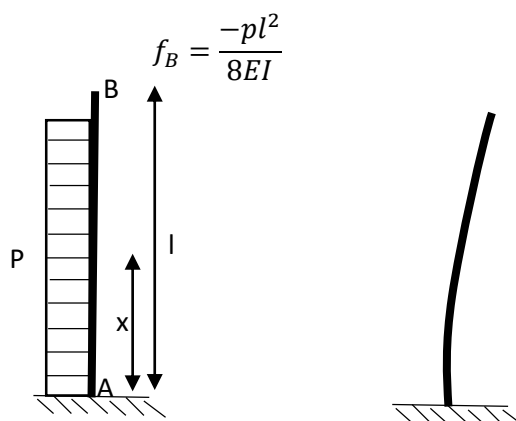


Figure 48: deflection of a single DOF system with fixed restraint

So, the maximum displacement increases as the length l increases.

The expression of the deflection proves also that displacement increases with the tsunami force. A comparison between the two charts of Figure 47 indicates that, for the same ground floor height, the displacement recorded for the case of a run-up height of 12m is approximately double than the one of case of 5m. The trend of the two curves remains similar.

5.4.4.3. Fragility curve

In order to plot the fragility curves, we should retrieve information about the yield point and the ultimate point, as well as defining the damage scenarios and their characteristics. Chapter 3.3 described the methodology of RISKUE and the steps that should be followed in order to correctly plot the fragility curves. In this section, the RISKUE methodology is adopted and specifically the LM2 method, because it is based on analytical data, rather than statistical ones.

The capacity curve of Figure 46 is chosen as basis for plotting the fragility curves. As mentioned in chapter 3.3, the conditional probability of exceeding a certain damage state (ds) is calculated as follows:

$$P(ds > Sd) = \Phi \left[\frac{1}{\beta_{ds}} \ln \left(\frac{S_d}{S_{d,ds}} \right) \right]$$

with S_d is the spectral displacement and $S_{d,ds}$ is spectral displacement value corresponding to the damage state (ds), and equals to:

$$S_{d1}=0.7 D_y$$

$$S_{d2}=D_y$$

$$S_{d3}=0.5 D_y+0.25 D_u$$

$$S_{d4}=D_u$$

and the parameters β_{ds} (lognormal standard variation) equal to:

$$\beta_{ds1}=0.25+0.07\ln(\mu_u);$$

$$\beta_{ds2}=0.2+0.18\ln(\mu_u);$$

$$\beta_{ds3}=0.1+0.4\ln(\mu_u);$$

$$\beta_{ds4}=0.15+0.5\ln(\mu_u)$$

where D_y and D_u are the displacements of the yield and ultimate points respectively, which are provided by the capacity curve. The parameter μ_u equals D_u/D_y .

For the current case of Figure 46, $D_y=0.01\text{m}$ and $D_u=0.05\text{m}$. The plot of fragility curves is shown in Figure 49. Different damage states introduced: "slight", "moderate", "extensive" and "collapse". Each damage state is characterized by its corresponding spectral displacement $S_{d,ds}$ and the parameters β_{ds} (lognormal standard variation). A comparison is held between the obtained results and fragility curves retrieved from statistical data of the Great tsunami of Japan (2011) illustrated by (Suppasri et al. 2013). Authors have determined six damage states (P_{xi}) and also expressed the fragility curves by inundation depth.

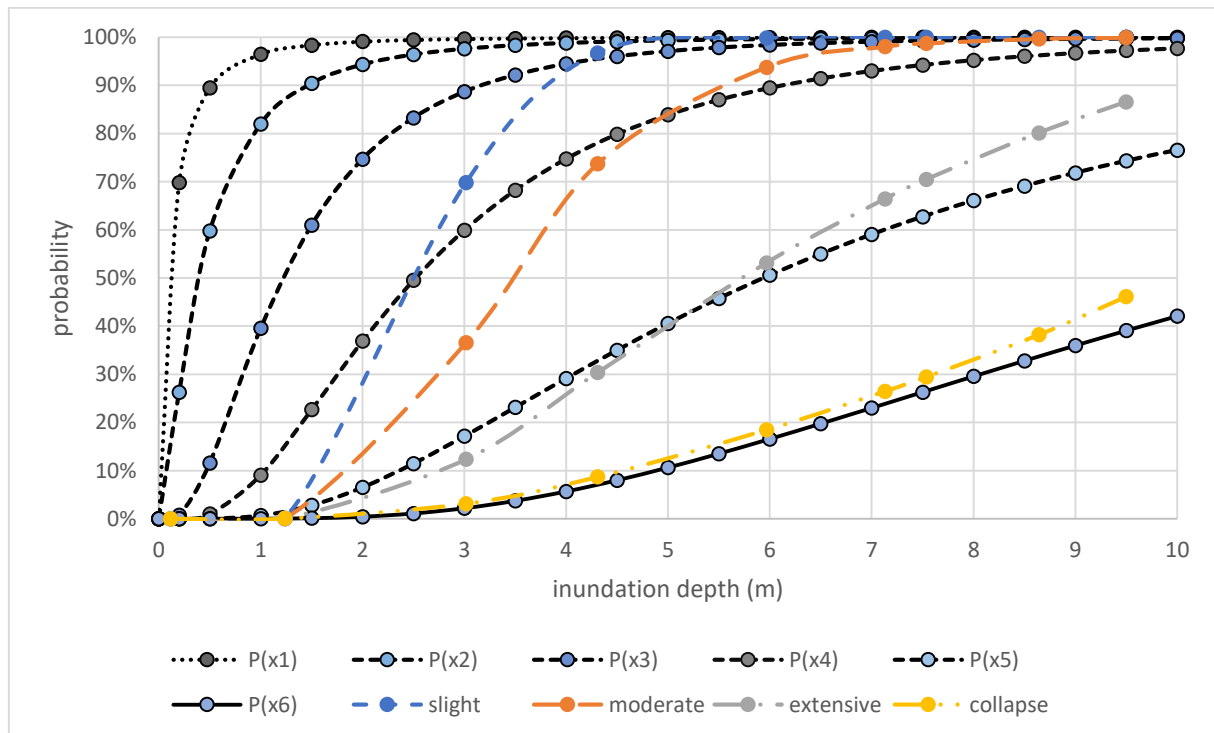


Figure 49: fragility curves computed for different damage states and a comparison with statistical observed data of the 2011 Great tsunami of Japan (Suppasri et al. 2013)

The damage curve that concerns the structural elements, i.e. the extensive and collapse curves, are well correlated to the P(x5) and P(x6) from the survey of Japan's 2011 tsunami. However, the two other curves that concern the non-structural elements (masonry walls) show a difference from data curves. This is due to the fact that statistical data illustrated by (Suppasri et al. 2013) regroup different types of buildings: Reinforced concrete buildings, Steel, Wood and other vulnerable structures constructed with light materials. This makes the comparison not accurate and not precise because we compare with an RC type only in our analysis. Moreover, not only water could destroy the non-structural elements, but also the debris with massive shell or a barrage of debris if concentrated on the local zone: the analytical results were restricted by considering only the hydrostatic, hydrodynamic and surge (impulsive) forces, while other forces such as debris and barrage debris are not considered.

From the frame perspective, the results illustrated are accepted in case of non-occurrence of other problems like the failure of a foundation or the presence of a dangerous scour. In these cases, the behavior of the building changes, and the frame elements suffer from additional stresses in their cross-sections, which is usually not admissible (except for tsunami evacuation buildings).

5.5. Conclusion

This chapter describes the analysis of a tsunami impact on an "ordinary" building of two floors. The work tried to determine the behavior of infill masonry walls for both types: out of plane and in-plane walls, to the strike of a tsunami wave. The available models and norm's recommendations as well as the theory behind the deflection of shells are introduced in order to understand correctly the vulnerability of infill masonry walls against the solicitation of tsunami. The FEM model helped also to recognize the areas with critical stresses and the failure modes of these walls. Next, The RC frame is analyzed with an illustration of the building's equation of motion, the identification of characteristics of time history implemented into the FEM model and the description of the analysis's steps.

Important results are exploited from the analysis: the determination of capacity curve of the building that describes the global ductility of the structure as well as the maximum displacements. A comparison between different cases of ground floor's heights helped measuring the influence of such parameter on the maximum displacement recorded. The fragility curves are established after identifying the yield and ultimate points. A comparison with statistical data retrieved from the Great tsunami of Japan 2011 helped validating the results while pointing the differences and similarities between this analysis method which is the analytical method, and the other statistical method.

This chapter helped to identify globally the reaction of the building to tsunami impact with the introduction of capacity curve and fragility curves. The next chapter tries to analyze the behavior of a school building with the same analytical method with a further comparison to the seismic solicitation.

6. Assessing tsunami vulnerability for a school building: comparison with seismic vulnerability

Content:

- 6.1. Introduction
- 6.2. Designing the test school building
- 6.3. Simulation of the inundation
- 6.4. RC frame
- 6.5. Conclusion

6.1. Introduction

After studying the response of a common two floors building, we investigate in this section the response of a strategic building with an important role in the immediate tsunami evacuation plan. This building is a school with three floors that may represent a fortified shelter for people threatened by an incoming tsunami wave. The strong construction of the school allows it to bear the loads of a large amount of population.

The first chapter is dedicated to the school building's design with the representation of its architectural plans in order to understand the global structure of the school. The frame elements' design is established by introducing the considered loads for school buildings and the calculations of cross sections for columns and beams of the frame.

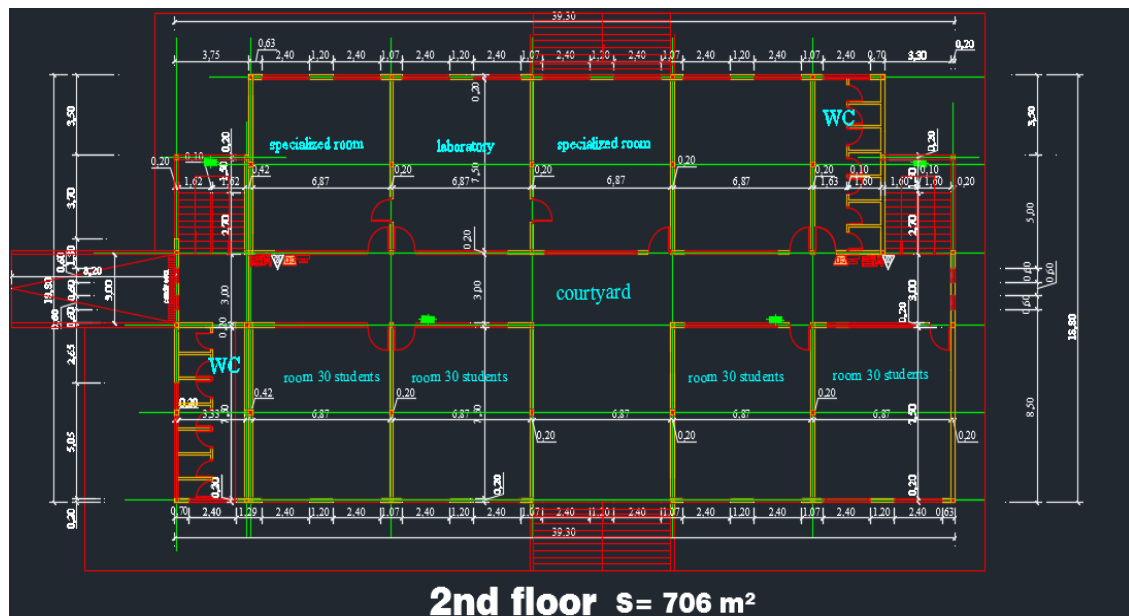
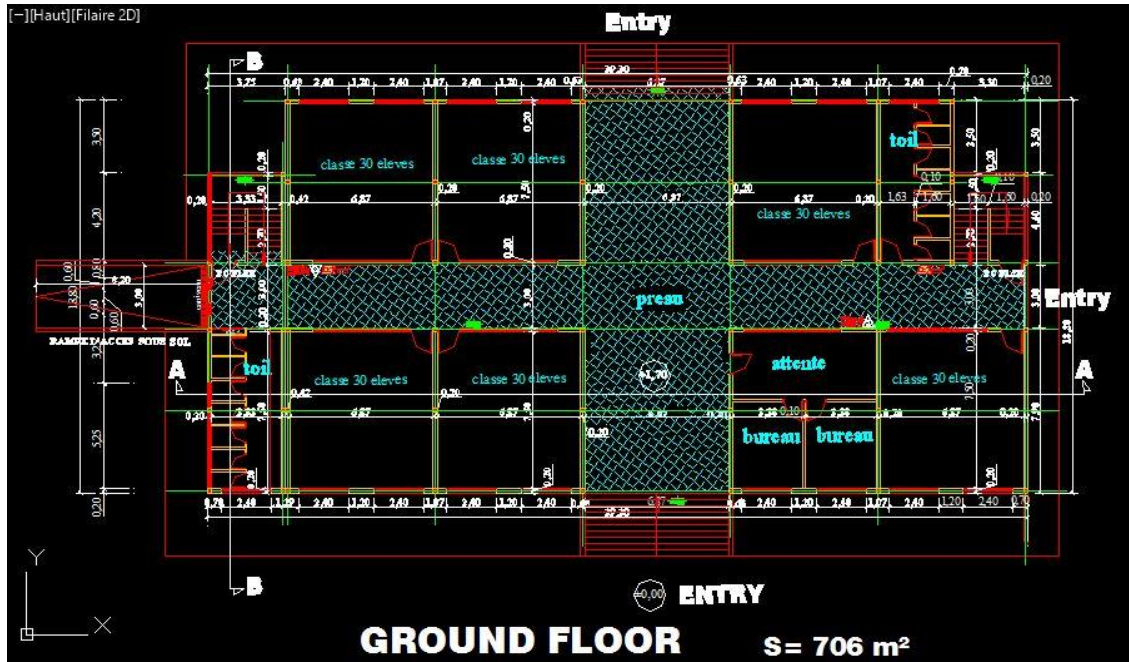
A simulation on a CFD program is then introduced. The CFD simulation can help understanding the flow trajectory and the intensity of pressure on surfaces. A 3D model of the school building is elaborated in a CAD program and integrated in the CFD simulation model. Other characteristics such as the fluid velocity and the materials of the school's 3D model are defined. Finally, an interpretation of the results of the CFD simulation is held with the illustration of the available features in the program results.

The third section investigates the RC frame behavior with the elaboration of capacity curve and fragility curves. A comparison to pushover curve and other fragility curves from statistical data of previous tsunami events is introduced in order to compare the tsunami and seismic actions on the building.

6.2. Designing the test school building

6.2.1. Architectural plan

The school building has eight or nine classrooms per floor for study purposes, laboratory or specialized rooms. The total area of each floor is 706m² with a length of 40m by 18m. The rooms have approximately the same dimensions of 6.87*7.80m². The original plan of the structure shows a parking place under the building but the model in this study does not take it into account. The terrace is not accessible.



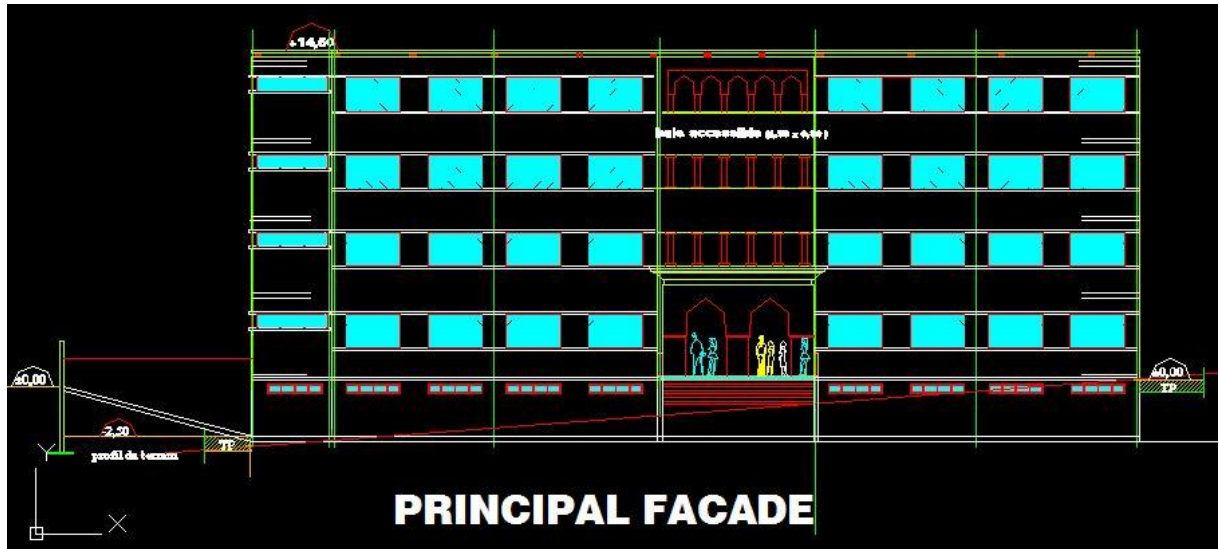


Figure 50: Ground floor, 2nd floor and principal facade architectural plans

6.2.2. Frame elements design

As proceeded for the regular building introduced in the first study case, this school building is designed according to the BAEL'1990 norm. As a reminder, this norm is based on the limit state design where the structure should satisfy two principal criteria: the ultimate limit state (ULS) and the serviceability limit state (SLS). The ultimate limit state (ULS) for the school building represents all the dead load of the RC frame, infill masonry, coat materials, tiles, etc. In the other hand, the serviceability limit state (SLS) considers the bearing loads like seats for classrooms, laboratory materials, library loads, seminar places loads, etc. A list of some loads considered when dimensioning a school building is presented in Table 5.

ULS loads (Ultimate limite state)			SLS loads (Service limite state)		
Load	Value	unit	Load	Value	Unit
Reinforced concrete (frame)	25	KN/m ³	classrooms	2.5	KN/m ²
Concrete (solid slab)	25	KN/m ² /cm	theater	3.5	KN/m ²
Concrete (hallow block slab:25+5)	3.6-4.00	KN/m ²	laboratory	2.5	KN/m ²
Infill masonry (brick clay)	10	KN/m ³	stairs	4.0	KN/m ²
Tiles	0.5	KN/m ²	Seminar places	4.0	KN/m ²
			library	4.0	KN/m ²

Table 5: loads considered for school design

The school building is designed with the structural analysis program (SAP2000) to provide the necessary dimensions of the frame sections as well as the required reinforcing rebars along the cross-sections. The combinations of loads are the same as the one mentioned in chapter 5.2.2. Additionally, the seismic loads are applied to the building and the least required configuration for seismic design is respected as well. The method applied for this seismic design is the linear static method, due to the regularity of the building. All the columns of the frame have a cross section of 30*50cm² except some columns in higher floors that have a cross-section of 30*40cm². All the Beams have a cross-section of 30*50cm².

6.3. Simulation of the inundation

6.3.1. Introduction

This section proposes an inundation simulation on the school building at a local scale (within the average order of the structure's dimensions). Although it is not part of this thesis objective to construct a model for inundation, this simulation could provide some interesting results to prove the rational methodology applied in this study which is based on FEMA'P646 expressions.

The simulation of inundation is carried through the CFD (computational fluid dynamic) analysis described in the first following section. The CFD program is presented and the model characteristics are defined such as the velocity of the tsunami wave and the boundary conditions. These different parameters are illustrated in the second section. Finally, results of this simulation are detailed in the last section without interpretation and comparison with the FEMA'P646 method.

6.3.2. Computational fluid dynamics (CFD)

Computational Fluid Dynamics is a branch of fluid mechanics that solves problems involving fluid flows through numerical analysis. A software helps simulate the interaction of liquids and gases with boundary conditions (structures, obstacles ...). An example of CFD problems is the Navier-Stokes equations that can be simplified and linearized in order to solve the fluid flow equations.

The basic procedure followed in a CFD problem could be summarized in these steps:

- First, geometry and physical boundaries are defined using a computer-aided design (CAD) like Autodesk AutoCAD program. This includes all the "obstacles" against the way of the wave such as barriers, buildings, ...
- The volume of fluid is discretized into cells or meshes. The technique of discretizing could be the finite volume method, finite element method or finite difference method.
- The equations of motion or fluid are defined
- Boundary conditions are defined such as the bounding surfaces of the fluid domain and the fluid behavior.
- The analysis of simulation is launched
- The results are visualized

In this section, a simulation of inundation on the school building is executed in the CFD program: Autodesk CFD 2017. We try to achieve the steps listed above.

6.3.3. Model characteristics

The first step in a CFD problem solving is the definition of geometry and physical bounds. In the case of this study, the obstacles are the school building, and specifically the infill walls, columns and for higher effective height of the wave: beams exposed to the impact of the wave. In order to consider

the various scenarios of the inundation, the CFD simulation is put under analysis for every effective height step. For each case, some important considerations must be respected:

- The infill masonry walls' collapse must be considered. As calculated earlier in chapter 5.3.1, the out of plane walls may collapse for a 1m effective height. The simulated school building should then have a ground floor without infill masonry walls (considering also the collapse of in-plane masonry walls, which is due to the infiltration of water). The ground floor would be emptied from obstacles but just columns, because they are structural elements.
- The fluid domain should respect the condition of the effective height of the wave. For each step, the level of the wave increases in order to satisfy this condition.
- Moreover, the fluid domain should not be very large so as not to include nearby buildings.

Characteristics of the wave such as the flow depth and the wave velocity could be provided by the studies of propagation and inundation of tsunami for large scales (Omira, Baptista, and Miranda 2011). This later study proposes that the velocity of the inundation in the Gulf of Cadiz is estimated to be 6m/s to 8m/s but differs from a region to another. In the CFD model, the velocity introduced is set as 6m/s as an average velocity value.

The school building model requires a 3D representation that can be admitted by the CFD program. For this objective, a CAD (computer-aided design) program is used in order to extrude the architectural plans into a 3D model of the structure: the "skeleton" of the ground floor from up view, which indicates the external boundaries, is retrieved from the architectural plans after removing unnecessary details. The "skeleton" is then extruded for the height of the floor. Windows and openings are integrated after by cutting and extracting its delimited volume from walls. The floors architectural plan is similar so the 3Dmodeled ground floor is duplicated in order to generate other floors. The final 3Dmodel is represented in Figure 52. As for considering the collapse of infill masonry walls, the delimited volume of these walls could be extracted as well. The remaining layout of the ground floor regroups just the columns.

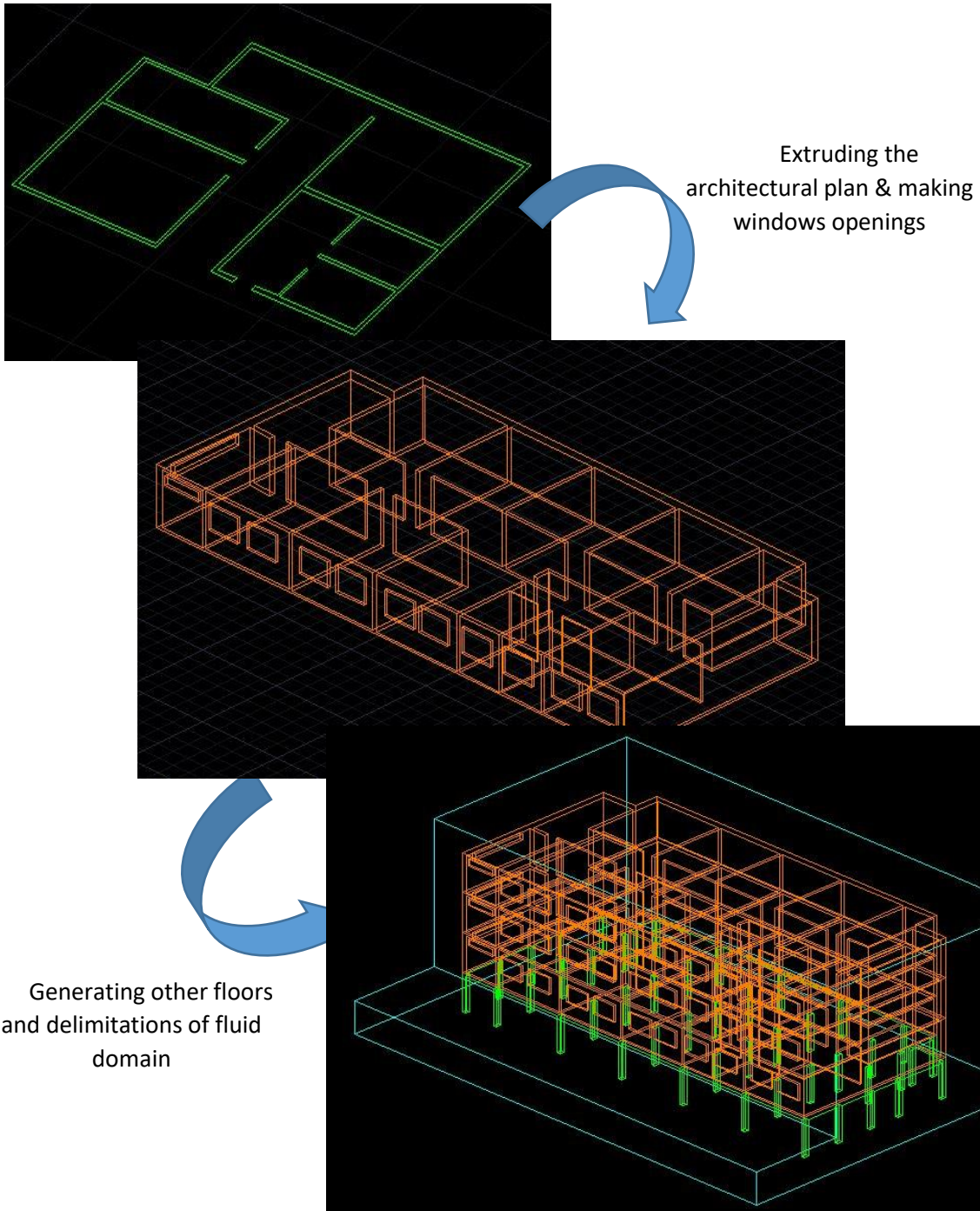


Figure 51: steps of creating the 3D CAD model of school building

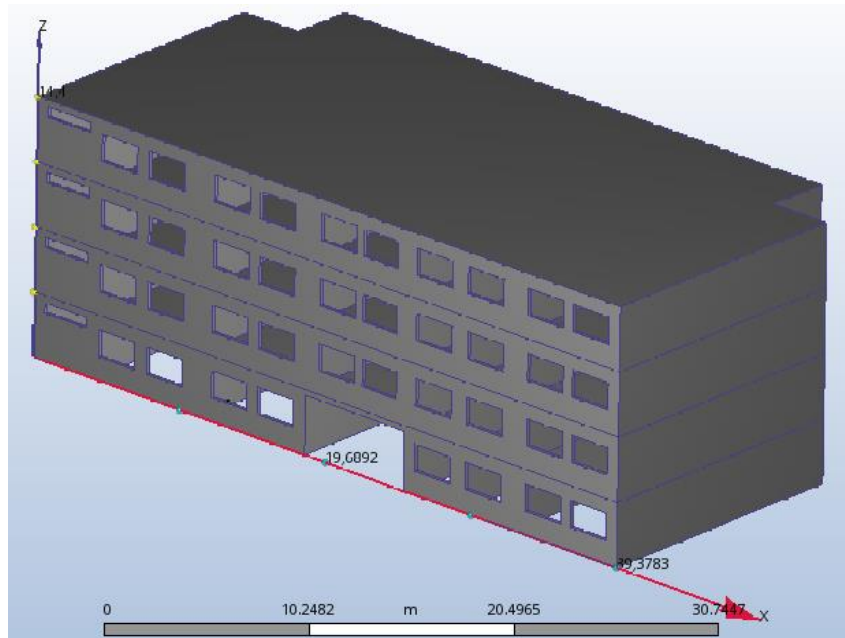


Figure 52: CFD 3D model of the school building

6.3.4. Results and interpretation

After defining the geometry and physical bounds (the school structure) with the necessary characteristics such as the material type of components (concrete for the school building and water for fluid), boundary conditions: velocity of 6m/s for incoming flow's surface, null pressure for the back-of-the-school surface, and finally the mesh discretization, the software provides detailed results about the inundation. The user could visualize the flow trajectory when the fluid passes through the building elements and exits from the null-pressure surface. Figure 53 and Figure 54 show the flow trajectory for two different views in order to understand the inundation of the tsunami wave.

The flow trajectory shows that all the columns of the ground floor are exposed to the impact of the wave. The turbulence signaled in the two figures next to the lateral sides of the building might be caused by the restriction on boundaries of fluid domain, which was set in order to not include closer buildings' influence.

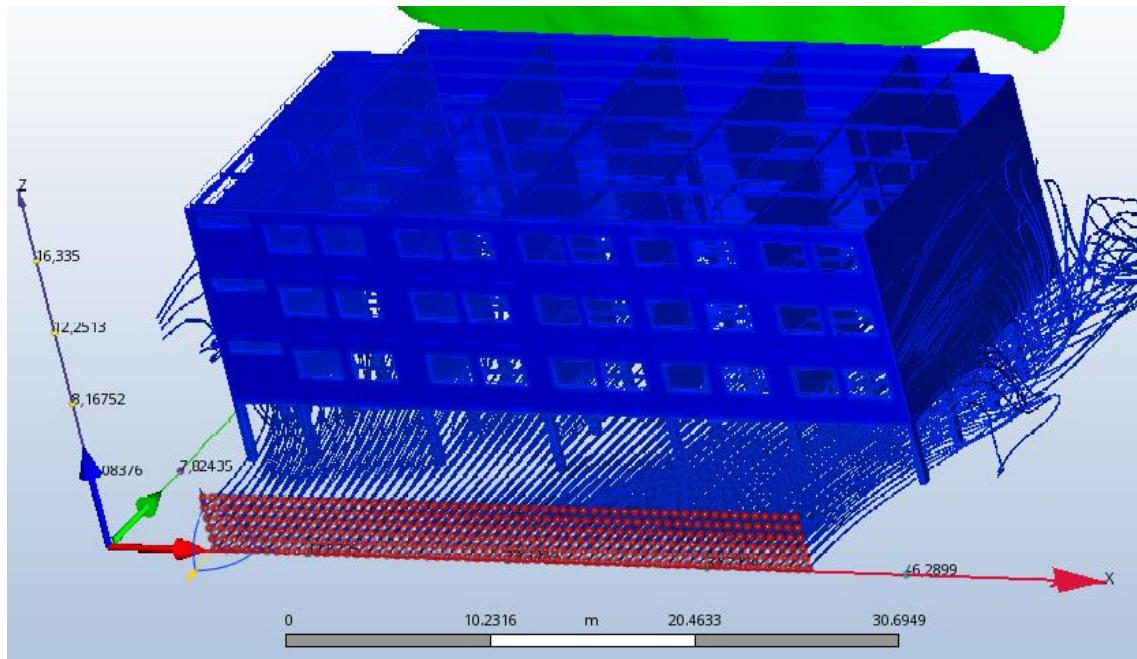


Figure 53: flow trajectory (front view)

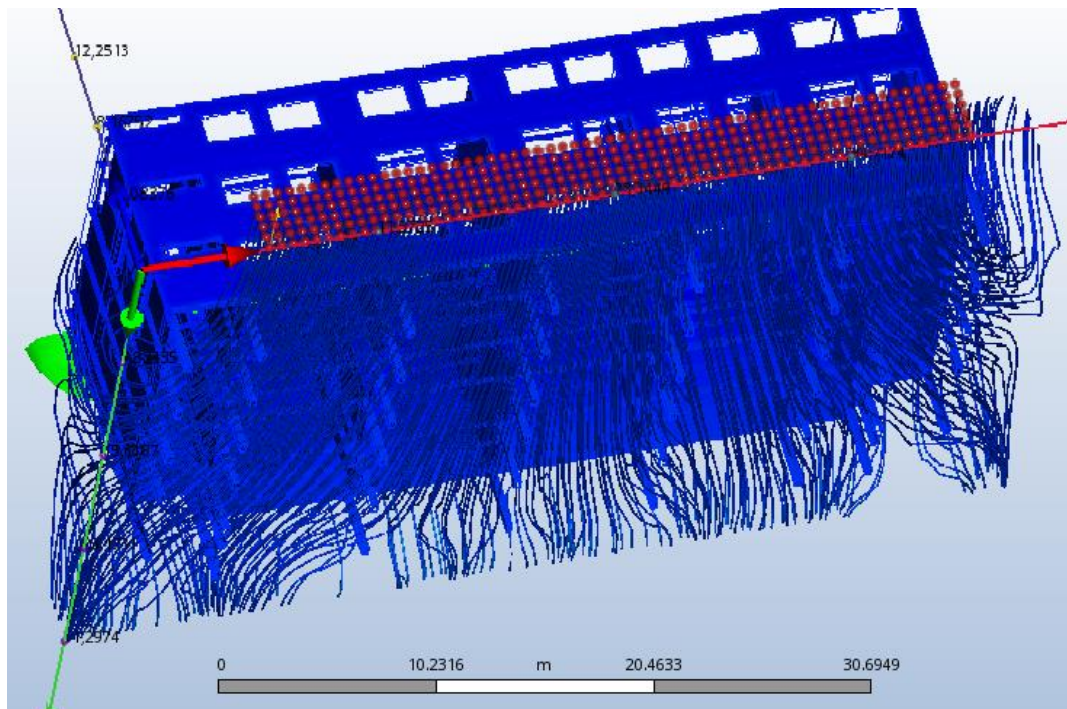


Figure 54: flow trajectory (bottom view)

Another interesting feature available on the results panel is the visualization of physical characteristics for a plane section such as total pressure, velocity amplitude, shear stress, etc. Figure 55 illustrates the variation of total pressure recorded on columns due to the fluid flow.

Studying the local characteristics of a column is provided by another feature of the CFD program, which allows measuring the named characteristic in a specified point of the column. This is a useful tool for analyzing the temporal variation of the characteristic (pressure, velocity, stress...). The measure of total pressure and shear stress (τ) on a mid-height point of a column chosen from the first row of columns struck by the wave is shown in Figure 56.

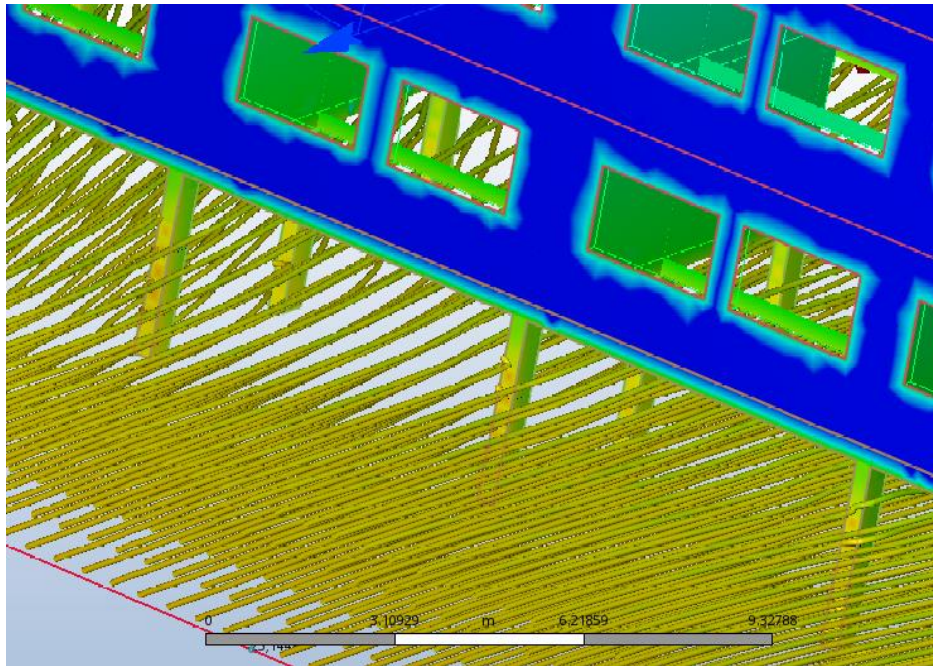


Figure 55: total pressure variation on the surface of columns

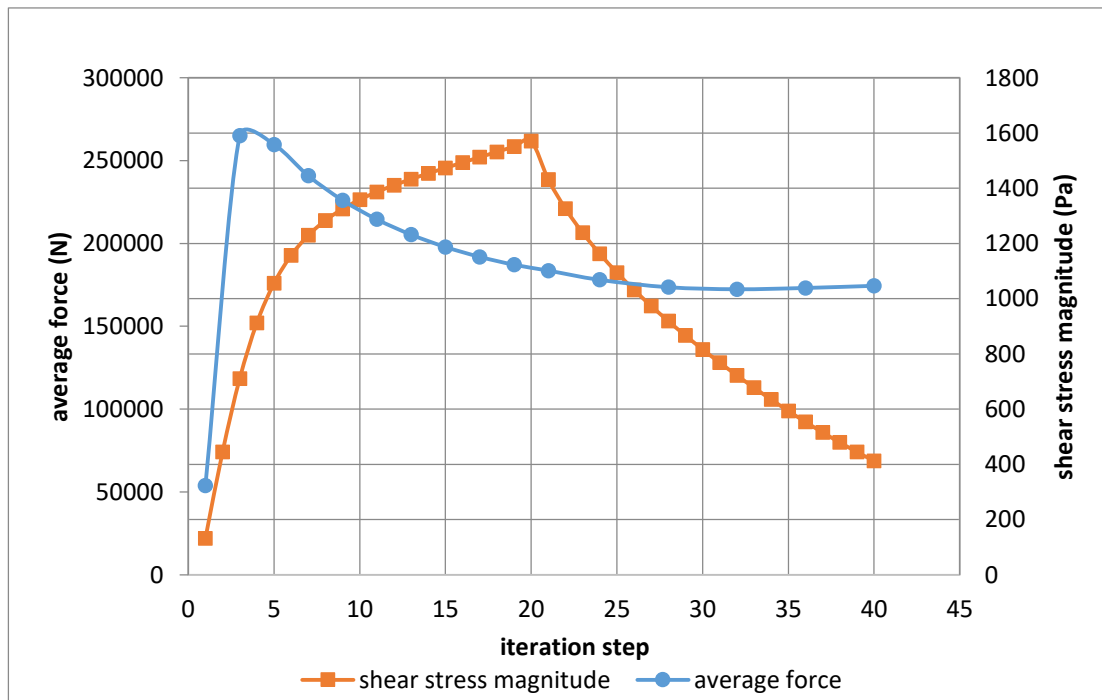


Figure 56: variation of average total force (N) and column's shear stress (tau) by time iteration

The curve of total pressure in Figure 56 is similar to the time history integrated in the structure analysis of the main study (described in chapter 5.4.2). This proves the logical reasoning of succession of tsunami forces, which starts with impulsive forces followed by hydrodynamic forces with less amplitude. The ratio of impulsive force to the hydrodynamic force may be compared by the FEMA-P646 suggestion and the CFD results: for FEMA-P646 the ratio is 1.5 while Figure 56 (average force) shows that:

$$\frac{F_i}{F_{hyd}} \approx \frac{265kpa}{172Kpa} = 1.54$$

This result proves the correctness of the FEMA-P646 estimation for the ratio of impulsive/hydrodynamic forces.

Going over 40 iteration steps is meaningless, since the concrete column collapses due to the drop of shear stress (τ) shown in Figure 56 (shear stress magnitude). The results after this iteration step cannot be considered reliable because the software is not a structural analysis program rather it is a pure CFD program.

This CFD study presents an interesting feature for analyzing the flow's trajectory but is still just a complimentary work because it does not rely on the structural elements behavior. One should understand that this software provides a helpful tool for measuring stresses in specified surfaces and mapping the intensity and pressure of the flow, but it does not unfortunately consider the collapse of masonry walls or other structural elements, which requires using a different approach taking into account the failure of these elements.

6.4. RC frame

In this section, we discuss the reaction of reinforced concrete frame in response to the strike of a tsunami wave. Masonry infill are not considered as resistant to tsunami forces according to the results of the first test building. Loads of tsunami are applied directly on the structural frame elements. This study shows the influence of tsunami actions on the structure backbone because it focuses on the impact on structural elements rather than analyzing the structure with its components. This later case could generate an erroneous image of what the real resistance of the building is and what the capacity provided by the structure could reach. The previous CFD model have attempted to simulate the inundation of tsunami fluids through the building, but in this phase of the study we try to understand the columns and beams behavior and malfunctioning. It tries also to analyze the vulnerability of the frame elements and provide the fragility curves that indicate the damage level. Later sections compare two hazards impact on the building: tsunami vs. earthquake, and discuss the characteristics of each case and its influence on the structure.

6.4.1. tsunami forces distribution

In this second study case, the front of the school building is chosen as the surface against the strike of tsunami wave. Columns of the ground floor are to be loaded successively by their ranks. The first loading is the impulsive force that last for a few seconds. Hydrodynamic and hydrostatic forces are distributed after impulsive forces through their respective time history, based on laboratory analysis. Figure 57 shows how the forces of tsunami are loaded in the model. In order to simplify the loadings on the program, we assumed a loading of two ranks simultaneously in place of one rank. Due is justified by the quick time of loading the wave's forces (seconds) and the short distance between column ranks compared to the building dimensions.

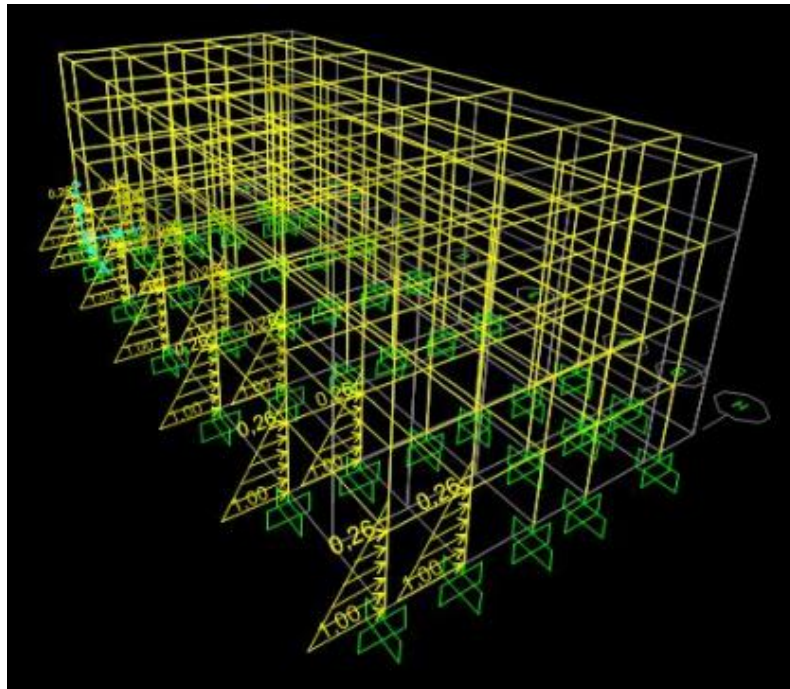


Figure 57: distribution of forces in the test school building

Fourteen cases were set to be analyzed. They correspond to each height step. While the distribution of hydrodynamic and impulsive forces is uniform through the height of the column, hydrodynamic forces are triangular and should be recalculated each time the height step is increased. Formulas of the three types of forces, as explained in the first chapter, are related to the height of the wave.

6.4.2. Pushover curve

The program analyzes firstly the static loads on the building, namely, the G: permanent loads and Q: service loads. Combinations are also set automatically as described by the standard code. After dimensioning the frame elements (beams and columns), a seismic dimensioning and verification is needed. The regularity of the building is checked but it is more advantageous to proceed with a pushover analysis. The loading of pushover load is placed on the roof joints and it is chosen automatically by the program proportionally to the height of the building.

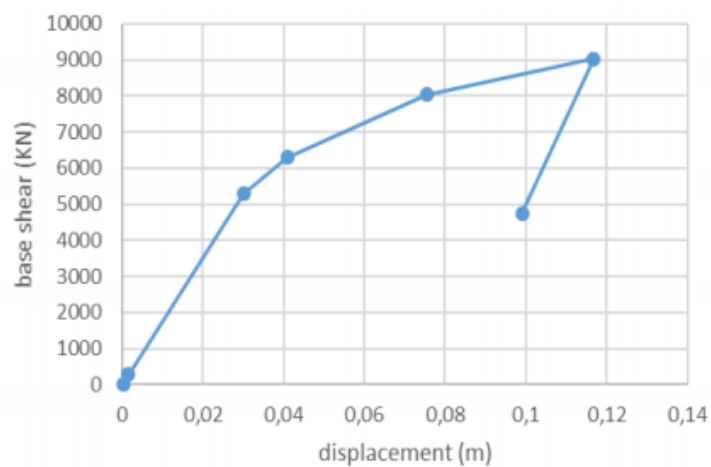


Figure 58: pushover curve for school building

Through the curve of pushover analysis, some observations could be signaled:

- A linear segment in the first part of the curve indicates the elastic domain boundaries. In this segment, the effects of displacement of the building are reversible. The yield point could be easily recognized (Y(3cm,5300KN)).
- A transition domain or an “elasto-plastic” domain appear next to the elastic domain. The building begins to bear a portion of the plastic deformation due to the excess of the push energy. Displacement after this domain are not reversible.
- A plastic domain where displacement are increasing rapidly by the increase of loading force. The building shows some fractures in the structural frame elements.
- A collapse section where the building can't bear the seismic load anymore and the resistance of the frame system is deteriorated. The ultimate point is recognized as the maximum point of the curve reach (U(12cm,9000KN))

6.4.3. Capacity curve for tsunami loading

In order to plot the capacity curve of tsunami loading, displacements and base shear forces should be retrieved from the program analysis results. As aforementioned, the fourteen cases of tsunami loading that correspond to wave level at the rate of one meter height step each, are put under analysis with the respective impulsive, hydrodynamic and hydrostatic forces values. For each case, maximum displacement and maximum base shear forces are indicated in the program results. Data regrouping max displacement vs. max base shear force help plotting the capacity curve of tsunami loading, similarly to the pushover technique. Figure 59 shows the plot of these data with a comparison to pushover curve.

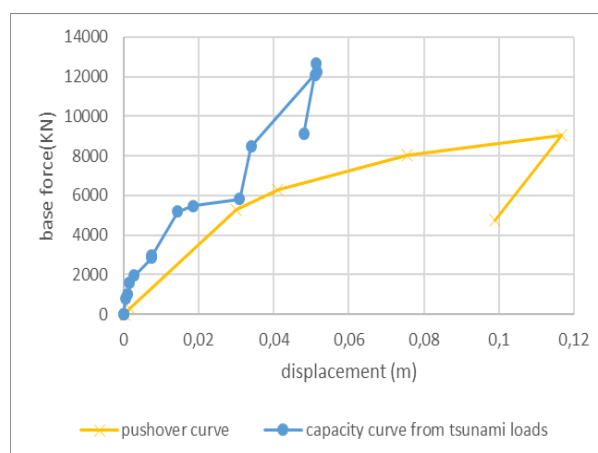


Figure 59: comparison between tsunami capacity curve and pushover curve

From the figure above, the yield displacement is localized at approximately $D_y=7.5\text{mm}$ which correspond to a wave height of 7.5m. The ultimate point in the other hand is localized for a $D_u=5.1\text{cm}$, which is recorded for a wave height of 14m (total building height).

The difference between pushover curve and tsunami capacity curve is various. It is illustrated by the following points:

- Slopes of the curves are distinct. In fact, the slope of elastic domain (K_y) that determines the yield point (D_y) is greater for the tsunami action than seismic loading. However, the yield domain is reached more quickly in the tsunami case than seismic case.

$$K_y(\text{tsunami}) > K_y(\text{earthquake})$$

$$D_y(\text{tsunami}) < D_y(\text{earthquake})$$

The same remarks are to be said about the ultimate domain slope (K_u) and the ultimate point (D_u):

$$K_u(\text{tsunami}) > K_u(\text{earthquake})$$

$$D_u(\text{tsunami}) < D_u(\text{earthquake})$$

- The tsunami forces variation is different from the seismic monotonous increase of force. While the pushover procedure is set by a stable increment of force value at the top joints of the building, tsunami forces increase exponentially. This is illustrated by Figure 60 where the approximate curve resembles a parabolic shape.

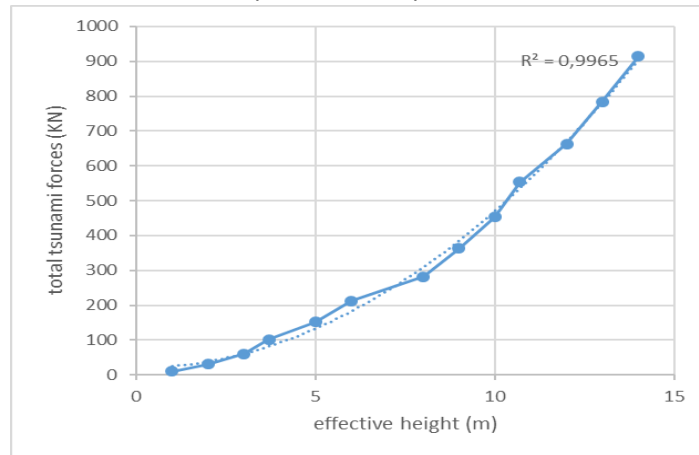


Figure 60: increase of tsunami force

In order to correctly interpret the remarks detailed above, it is necessary to bear in mind the distribution and value of forces of each hazard case as well as the mechanical laws regulating the reaction of the structure. Thus, a simplified representation of the action on the building is illustrated in Figure 61.

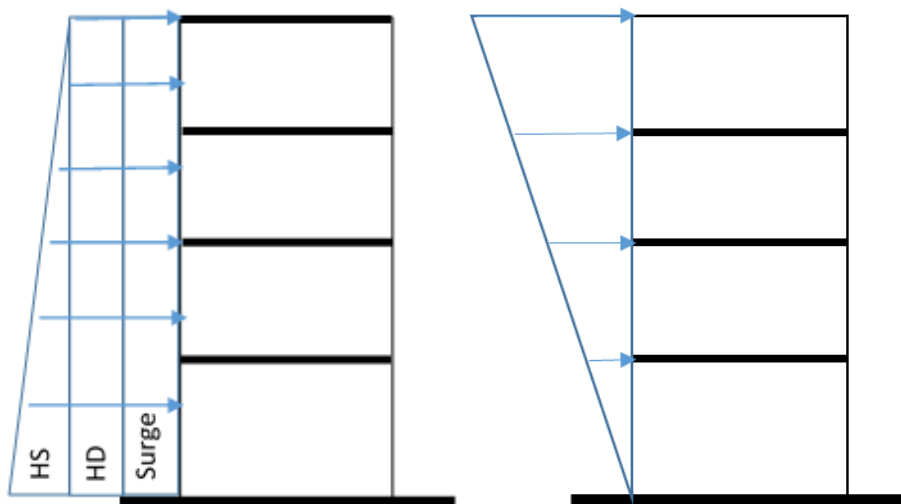


Figure 61: representation of actions of tsunami forces (left) and earthquake forces (right)

Tsunami actions are the main three forces: hydrostatic, hydrodynamic and surge force. While the hydrostatic force is triangularly distributed, hydrodynamic and surge force are uniform through all the height of the building. The total load on the building in tsunami case looks like forming a trapezoidal distribution where the point of action is located at lower levels. On the other hand, the theory of seismic action and the solicitation of the building by ground motion have justified a reversed triangular

distribution by the height of the building. The maximum force of earthquake is located in the top slab and the point of application of seismic solicitation is near the higher levels.

The difference in location of forces application point is the leading cause for the distinctive failure mode for both hazard cases. The tremendous forces of tsunami impact columns, especially the ground column. These later are usually dimensioned to resist the most important load from higher floors loadings and are subject to the most critical axial and shear forces as well as moment values. Engineers tend often to enlarge the dimensions of these columns in order to insure the capacity of bearing the descending loads, which is according to a single axial major load concept. However, in tsunami case, these columns suffer an excess of lateral loading and are subject to a composed flexion (axial force+ lateral force leading to positive moment) rather than a single axial force. Thus, steel reinforcement for columns in both cases (axial force/composed flexion) is different: while the longitudinal reinforcement is the most important rebar to take care of its dimension and position in the first case, transversal reinforcement and flexion rebars have to be considered as well in the composed flexion case. Lateral force causes a flexion in the column that tends to displace the middle area of the column and create an eccentricity of the axial force, which could easily threaten the stability of the column due the tremendous moment of $(\text{great axial force}) * (\text{eccentricity of the neutral axe})$. Moreover, if by chance a column fails at bearing the tsunami impact and its resistance drops, the near columns suffer additional loading because the distribution of descending load is changed. This emphasize the creation of a repeated failure of juxtaposed columns.

On the other hand, seismic loads have already been analyzed through laboratory tests. Results show that the seismic action needs a particular care for transversal reinforcing rebars as well as the adoption of a special constructive dispositions. The main important difference between earthquake and tsunami in this comparison is the fact that seismic forces are distant forces while tsunami forces are contact forces. Because of this argument, the structure tends in the seismic case to behave as a whole system reacting all together to the influence on seismic force. Thus, some structures have a reinforced concrete wall cage in usually elevator area or stairs walls in order to shield the seismic force and absorb its energy. This RC cage is placed often where the center of gravity and torsion is, so that the distant forces of earthquake should be focused on this part of the structure. Another important characteristic of seismic solicitation is the fact that it is accumulated where the important concentration of mass of present. Seismic solicitation is in fact related to the acceleration of the ground which is proportional to mass quantity. Consequently, the main forces of earthquake are applied to floor slabs. This is the reason why the lateral force distribution in the equivalent static method (linear static method illustrated in previous chapters) focuses the seismic forces on floors levels, not taking attention to column interaction, because it is negligible. Because of that, cracks happens to walls with an X shape fracture due to the relative displacement between successive floor levels. Columns also are displaced by the shear force and show some fractures in the edges if the solicitation is important. However, it is to be said that the whole system of two floor slabs+ wall+ two columns (which defines a closed frame) work simultaneously to absorb the seismic action and reduce displacements, while in tsunami case, the first rank of columns suffers the most from the impact and bear the important load. Moreover, the frame system in tsunami case does not work as a unit but by rank of exposition and the type of loading.

In order to justify the explained interpretation listed above, the graphic results of the SAP2000 program shows clearly the difference of the structure reaction to the two hazard solicitations. Figure 62 makes a comparison between the two cases.

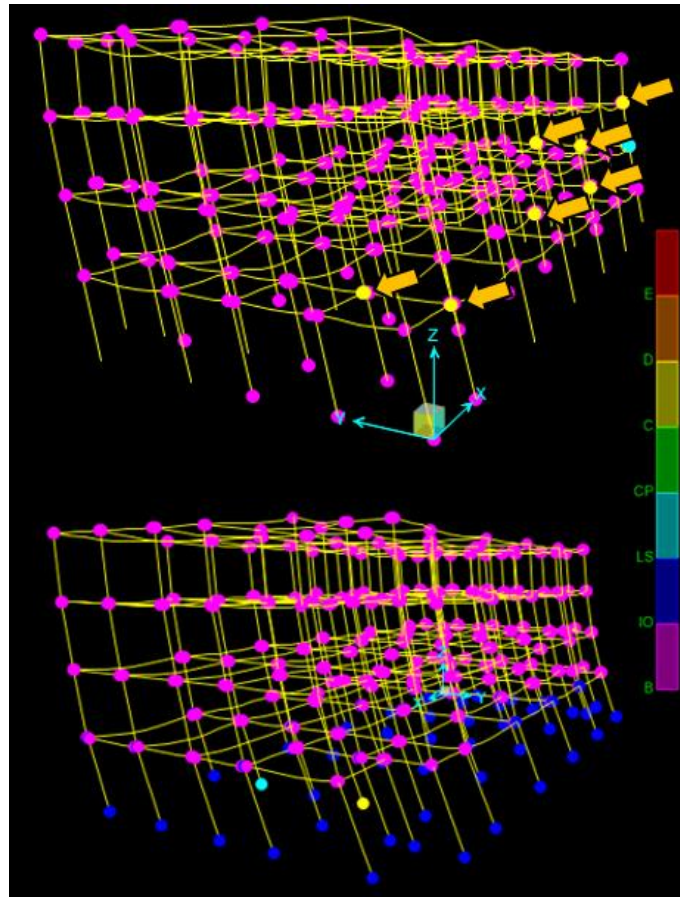


Figure 62: hinges plastification in columns (top: tsunami case ,bottom: seismic case)(B-C-D&E: degrees of plastification of hinges, IO-LS&CP: Acceptance criteria of hinges(immediate occupancy, life safety and collapse prevention))

It is important to highlight the meaningful use of nonlinear hinges. As explained in previous chapters, non-linear hinges are tools for measuring the plastic state of an element according to the applied moment value and the axial force value. The hinges are chosen then to interact according to a composed flexion behavior. The software calculates the axial force P , moment M_2 and moment M_3 and compares to the base data allowed for the type of column according to the specifications gained by laboratory results. Moreover, the program classifies the plastification of the element to three sub-domains which are: IO: immediate occupancy, LS:life safety, CP: collapse prevention. Danger of failure of the frame element is residing just after the collapse prevention plateau which mean it's the most critical of the element.

Figure 62 shows a comparison between the hinges results of the two hazards. In the tsunami case, the observer could notice the yellow state of some hinges, which indicate that they have already reached the failure state. While other columns haven't reached the plastification zone (still between B and IO domain which is the elastic domain), the rupture of columns with yellow hinges state demonstrates the interpretation that have been discussed earlier. This shows also that tsunami forces are focused on a single frame element rather than targeting the whole system. This is a dangerous results because constructions designed to resist tsunami hazard should be strengthened not only as a system mechanism but for each element alone. Another remark is that crushed columns are all in the first raw of columns. This shows also the dangerous first impact of tsunami wave and the great influence of the surge force.

On the other hand, the earthquake case confirms that the frame system interact with the seismic solicitation as a unit. Plastification occurs firstly for ground floor columns but all columns reach the

same state. Columns in higher levels are not affected and are still in the elastic phase. Additionally, the seismic energy is supposed to be absorbed by columns (especially ground columns). This is why the pushover curve indicates that the building reaches an advanced value of max displacement before failure compared to tsunami case. The unified work of columns allows a good distribution of energy with a small quantity to each column, which allows also a long resistance of the building before the collapse point.

6.4.4. Fragility curve analysis

Fragility curves are plotted similarly to the method of RISK-UE LM2 method. Data retrieved from capacity curve helps distinguishing between four levels of vulnerability. It is explained above according to the four values of beta, parameter in the probability equation. The obtained curves are shown in Figure 63 and Figure 64. Figure 63 shows the fragility curves by max recorded displacement, while Figure 64 illustrates fragility curves by height level and shows also a comparison to the results of [suppasri & al \(2013\)](#) about the data of great Japan tsunami 2011.

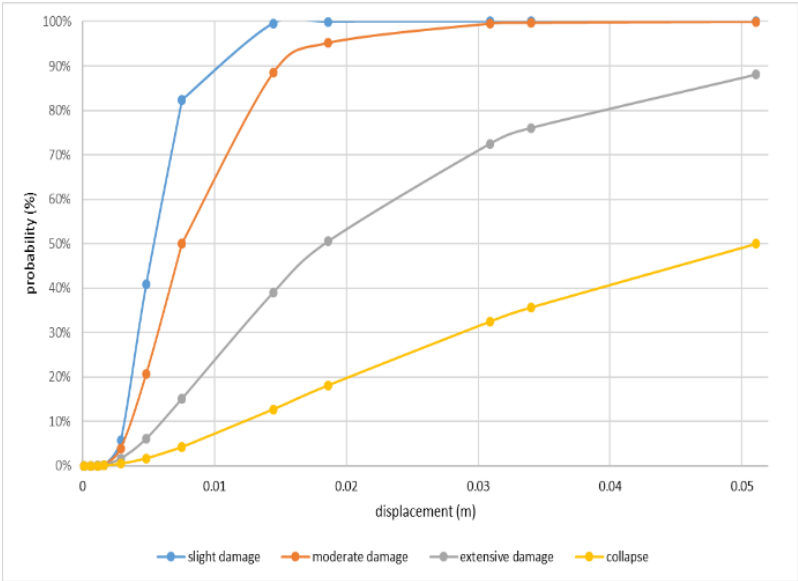


Figure 63: fragility curve by max displacement value

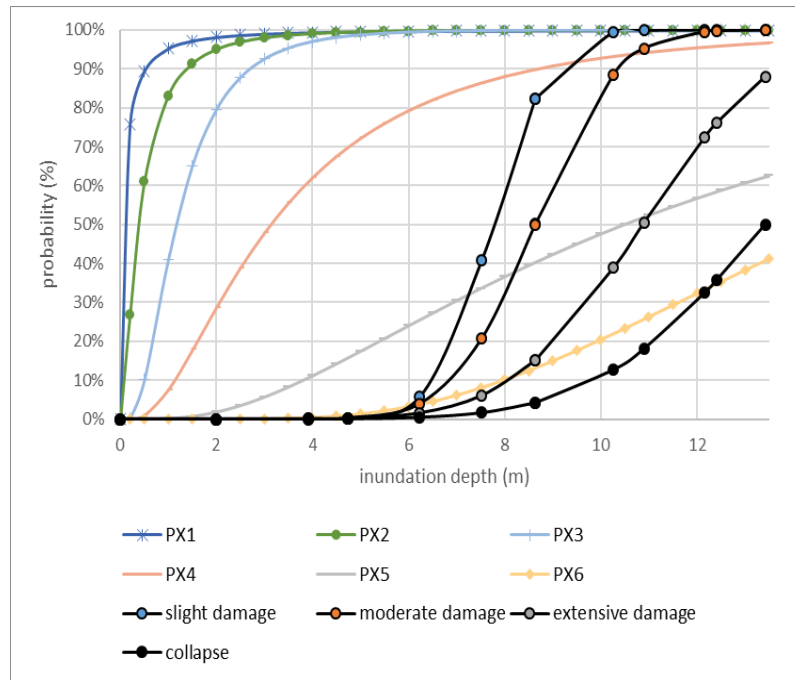


Figure 64: fragility curves (black) and comparison to suppasri data (PXi) compiled from the great 2011 Japan tsunami

Figure 64 shows our most interesting results since it highlights and compares the real observed data to our findings. In fact, differences between the curves are clearly apparent. The only case where the curves could be said to approximately correlate is the collapse scenario and the PX6 curve. Suppasri's statistical curves start to increase from low high levels of inundation depth, while the results of the school building are barely noticed until the 5.5m height. Moreover, Suppasri results are composed of six types of fragility curves which is more detailed, because the main objective of fragility curves is the four cases explained in the RISK UE method and that extend from the non-structural medium/critical levels to structural medium/critical levels. The differences between the results could be justified by the following arguments:

- The study case is a school building. This type of structure is a specific type. The method of dimensioning a school building is not similar to regular buildings (loads are greater than regular buildings loads).
- Statistical data regroup the classes of "G+3Fs" and above in the same type. This means a mixture of types that don't interact with tsunami in the same manner. In fact, the descending load from a high building is greater than the one of low buildings and consequently needs greater ground columns' dimensions.
- The present study focuses on three main forces only: hydrostatic, hydrodynamic and surge forces. It doesn't take into account the debris action and the debris dam pressure, as well as projected objects impact.
- The suppasri statistical data classifies fragility curves according to the building level: "G+1F", "G+2F" and "G+3F" and above. It doesn't specify the geometry of types, the weak inertia of the buildings and the height/surface ratio.

Although there are differences in results of statistical data and our findings are distinct, one could easily recognize the importance of school structures to resist to tsunami impact compared to the reaction of other regular buildings. Because the threat is not important until an inundation in depth of 5.5m high, the school building can be recognized as a good option of immediate tsunami evacuation plan and a good shelter until the hazard passes.

6.5. Conclusion

The assessment of tsunami vulnerability for the school test building has shown interesting results about the behavior of the building and the expected degree of vulnerability towards the wave's strike. The building was dimensioned for dead and usual loads as well as seismic loads, with a high attention to security coefficients due to the important function of this structure on bearing scholar loads. Fortunately, this fortified dimensioning helps considerably in resisting the strike of tsunami waves and protecting the population inside. The school building thus, appears through the results achieved by this study of vulnerability, as a strategic solution for immediate tsunami evacuation plans and an important temporary shelter.

7. General Conclusion and direction for future research

In this work, we have studied the vulnerability of building against tsunami waves. Two types of buildings are considered in this study: a "regular" building with a ground floor+ two floors, and a school building composed of GF+3floors. The work tries to focus on the response of the tested buildings to a tsunami attack through numerical simulation of the inundation on a structural analysis program. The methodology of the study resides fundamentally on structural engineering perspective rather than statistical or surveys viewpoint. This methodology focuses on the mechanical behavior of the buildings' frame elements and the quantification of vulnerability through plotting fragility curves.

The study of the first building investigates the behavior of infill masonry walls and the estimation of its degree of vulnerability. Two types of infill masonry walls are recognized: out-of-plane and in-plane walls. For each type, the analysis tries to take advantage and benefit from existing models of these walls using different levels of modelling: micro, meso or macro modelling. The analysis also tried to adapt these studies into the case of tsunami solicitation because the previous works focused essentially on the seismic response of infill masonry walls. Some explanation about the mechanical behavior of the walls for a lateral or in-plane loading is introduced in order to logically understand the mechanism of failure. The Eurocode'6 recommendations and directions are illustrated also. Finally, the analysis shows the results of resistance and failure of the infill masonry walls through analytical reasoning or FEM method.

With the exploitation of results of infill masonry walls, the reinforced concrete frame is analyzed by a structural analysis software. The equation of motion that governs the mechanical behavior of the building is explained and detailed, as well as the time history integrated in the program in order to identify the variation of tsunami forces through time. The method of analysis is explained step by step. The results retrieved after running the analysis show interesting facts about maximum displacements recorded, bending moments distribution, nonlinear hinges reactions, stresses fluctuation and measure and also the decrease of the building's stability due to the irreversibility of the stiffness matrix. The capacity curve of the building for tsunami solicitation is illustrated and presented. Fragility curves are then plotted based on the capacity curve's layout and parameters. The results about fragility curves

are extremely important due to its utility in estimating the vulnerability of the building. These curves are compared to statistical data of previous tsunami events in order to retrieve and explain the points of similarities and differences.

The final section focuses on the school building analysis and the assessment of vulnerability for this structure. This type of building is chosen due to its importance in immediate tsunami evacuation plans. The architectural plan is described and the frame elements' cross-sections are designed. Moreover, in order to comprehend the flow trajectory and the fluid movement across the school building, a CFD (computational fluid dynamic) analysis is held. The 3D model of the school structure is established with regards to different cases of failure of infill masonry walls. The CFD simulation, although it is introduced as a complementary study, shows some interesting results about the flow pattern, stress of elements, and temporal variation of the fluid characteristics such as the total pressure and the velocity amplitude. The analysis of the RC frame through FEMA-P646 guideline with the structural analysis program is then investigated. Comparisons are established between the capacity curve of tsunami solicitation and the pushover curve in order to compare tsunami and seismic actions on the structure. Another comparison is established between fragility curves from this analysis and from the statistical data of the great tsunami of Japan 2011, with a description and interpretation of the findings.

The main objective of this work, which is the assessment of vulnerability of buildings against tsunami solicitation (in the Gulf of Cadiz), could be considered mostly achieved. The main study of buildings' behavior towards tsunami wave impact as well as the elaboration of the methodology for constructing tsunami's capacity curve and fragility curves have been illustrated by this thesis work. However, there still remains several points for development and more investigation:

- The actual work has some limitations in considering only the main tsunami forces: hydrostatic, hydrodynamic and impulsive forces. More investigation about the debris impact and debris barrage influence could be foreseen.
- Other types of building are to be analyzed: this study worked on RC buildings due to their abundance on the urbanism build. However, steel, wood, masonry and other types of structures could be analyzed.
- The work emphasizes a local analysis focused on a single building. This could be developed in order to assess the vulnerability with numerical tools for a large area of the scale of districts or cities. Although it is useful for analyzing single structures, this method may be interesting when making a mapping of vulnerability through a wide zone.

This study of vulnerability, though the limitations and restrictions, could still be judged as helpful and useful for plans of understanding and making awareness of the threat of tsunamis on coastal areas. It provides, not only the full comprehension of buildings' capacity to resisting tsunami waves impact, but also a complete explanation of the behavior of structures solicited by such waves, with a methodology based on objective, logical and analytical methods, which supports its accuracy and reliability.

Conclusion Générale

Dans ce travail nous avons étudié la vulnérabilité des bâtiments contre l'impact du tsunami. Nous avons étudié deux types de structures : Un bâtiment régulier de trois niveaux et une école de quatre niveaux. L'analyse de la vulnérabilité tsunamique se fait par les simulations numériques pour déterminer la réponse de la structure. La méthode de ce travail réside fondamentalement sur les lois de la mécanique et le contexte de l'ingénierie génie civil au lieu des sondages et des jugements subjectives apportées dans d'autres études. La vulnérabilité est déterminée selon l'analyse de la réaction des bâtiments et la réalisation des courbes de fragilité.

L'étude de la première structure est focalisée sur la réaction des murs de remplissage en maçonnerie et l'estimation de leur degré de vulnérabilité. Deux types de chargement de ces murs sont étudiés : le chargement hors-plan et le chargement dans le plan des murs.

Pour chaque type de chargement, l'étude analyse les modèles existants des murs de remplissage en maçonnerie suivant les différentes échelles de modélisation : micro, méso ou macro-modèle . Pour le chargement hors-plan, le bâtiment R+2 est introduit dans le logiciel pour simuler la réaction structurelle suite à l'impact de tsunami. Toutes les caractéristiques physiques et géométriques des éléments constructifs sont présentées. Selon le plan architectural du bâtiment, nous avons repéré les murs de maçonnerie selon leur type et selon leurs dimensions.

Suite aux nombreuses recherches sur les murs de maçonnerie, nous avons comparé nos résultats aux courbes de comportement de ces murs (pression appliquée/déplacement mesuré).

Pour encore vérifier la certitude des résultats, une explication selon la norme de l'Eurocode est présentée et les résultats sont exploités pour caractériser le mode de rupture du mur de maçonnerie dans notre cas de recherche. Ce qu'est important est de comparer la demande de tsunami (l'impact de la vague) et la résistance du mur (capacité du mur), et c'est ce qui est présenté graphiquement en rapportant la variation de la pression mesurée à la hauteur effective (depuis la base du bâtiment jusqu'au niveau de la vague).

La constatation majeure conclue par cette étude est l'écroulement total des murs de maçonnerie sauf pour des cas particuliers où le mur a par exemple une hauteur effective inférieure à 1m avec un run-up inférieur à 3m, et c'est ce qui est dû à une vitesse relativement faible de la vague pour ce run-up.

Pour la zone d'étude qu'est le golfe de Cadix, les simulations ont indiqué une hauteur du run-up de 7-8m, donc les murs de maçonnerie ne peuvent pas résister à l'impact de tsunami selon ces simulations.

Pour le chargement dans le plan d'incidence de la vague, une étude comparative entre la sollicitation sismique et tsunamique est établie. On conclue par une confirmation de la non-validité du modèle de la barre de compression diagonale puisqu'elle est adaptée au calcul sismique et ne correspond pas aux conditions tsunamique. Une simulation par éléments finis est faite et la comparaison des zones de développement des contraintes indique que les sollicitations tsunamiques écrasent le mur de maçonnerie.

En résumé et en tenant en compte de l'effet des charges latérales des inondations dans le plan du mur, les murs ne résistent pas à l'impact de tsunami.

Dans la suite du travail l'analyse du portique structurel est poursuivie en ignorant l'effet des murs de maçonnerie. L'équation de mouvement est présentée et développée et les déplacements des nœuds du portique sont calculés.

Pour le calcul numérique, on a besoin d'un histogramme temporel de sollicitations. Les mesures faites sur des prototypes de structures étudiés par d'autres recherches et les comparaisons rationnelles entre eux nous ont fourni un diagramme détaillé de la force sur la face des poteaux.

Le modèle de la structure est introduit par la suite dans le logiciel SAP2000 avec les sollicitations extérieures calculées et l'histogramme simplifié de la variation des forces. Toutes les forces de la vague, mentionnées dans le rapport de FEMA P646, sont indiquées. Les étapes de calcul sont aussi présentées.

Différents résultats sont exposés : les courbes de développement temporel des contraintes des poteaux, les déplacements des niveaux, les zones de développement des rotules non-linéaires dû à la plastification des matériaux et finalement le taux de stabilité décroissant suivant la hauteur effective d'inondation.

Les courbes de capacité indiquent la corrélation entre la réaction du bâtiment à la base et son déplacement maximum. Deux cas de run-up sont comparés : Un run-up de 5m et de 12m ainsi que trois cas de hauteur de rez-de-chaussée : 4m-5m et 6m.

La justification satisfaisante des résultats de ces comparaisons est présentée suivant le modèle simplifié de la structure représentée selon un seul degré de liberté.

L'analyse de la vulnérabilité du bâtiment est couronnée par l'établissement des courbes de fragilité à partir des courbes de capacité, par la méthodologie de RISKUE pour le risque sismique est adaptée, dans notre cas, pour le risque tsunamique. La probabilité de dépassement d'un degré de dommage prédéfini (ds) est rapportée à la hauteur effective d'inondation. La comparaison avec les résultats de sondage du grand tsunami du Japon de 2011 a validé les résultats numériques. Selon cette comparaison, les probabilités de dépassement des dommages extrêmes et de rupture coïncident suffisamment avec les résultats de sondage.

Dans la seconde section de cette thèse, l'analyse de la vulnérabilité est portée sur une structure d'une importance stratégique pour les plans d'évacuation immédiate lors d'un tsunami : une école de trois étages avec une superficie totale de 706m². Comme la section précédente a montré, la faible résistance des murs au tsunami, nous avons ignoré les effets des murs dans la suite des études. L'école est dimensionnée depuis les premières étapes de détermination de l'inventaire des charges permanentes, d'exploitation et les charges sismiques, jusqu'à la fixation des caractéristiques des éléments des portiques (poutres et poteaux). Ensuite, une simulation d'inondation est établie suivant la CFD méthode (computed fluid dynamics) qui se base sur les relations de Navier stocks pour le mouvement des fluides. Le modèle de l'école est dessiné sur le programme CAD et transféré vers le programme Autodesk CFD. La comparaison des résultats avec ceux du rapport de FEMA P646 montre que le rapport entre les forces impulsive et dynamique est approximativement identique pour la FEMA P646 et le CFD programme. Cependant, le programme CFD n'aide pas à connaître les réactions du portique et ne répond pas aux questions de la vulnérabilité structurelle du bâtiment. L'analyse CFD a

satisfait plutôt le besoin d'une vérification numérique des suggestions de la FEMA P646 et a donné une représentation 3D du mouvement probable de la vague.

Structurellement parlant, le modèle de l'école est introduit dans le logiciel de structure SAP2000 et les distributions des forces tsunamique sont appliquées. Quatorze cas d'étude sont établis en tenant compte du pas d'un mètre 1m, de la hauteur effective sur toute la hauteur du bâtiment. Pour chaque cas, les forces de tsunami et les distributions sont calculées et introduit au logiciel. On détermine la courbe de capacité tsunamique en rapportant la réaction totale du bâtiment à son déplacement pour chaque pas de hauteur. En parallèle avec cette étude, nous avons aussi tracé la courbe de capacité sismique dite: Pushover. Nous avons par la suite comparé les deux courbes de capacité tsunamique et sismique et nous avons relevé les différences entre eux.

La constatation principale réside dans les distributions de chargement du bâtiment qui se caractérise dans les deux cas par des propriétés différentes : la magnitude de force, les zones d'application des forces, le travail d'ensemble des éléments de portique pour la dissipation d'énergie, etc. Ces différences ont influencé sur les courbes de capacité soit dans les pentes remarquables soit dans les limites d'élasticité et de plasticité.

Après avoir déterminé la courbe de capacité tsunamique, nous avons tracé les courbes de fragilité qui estiment la vulnérabilité de la structure de l'école vis-à-vis l'impact de tsunami en s'inspirant des méthodes de RiskUE. Quatre probabilités sont déterminées : dommage mineur, modéré, extrême et finalement la rupture. Ces probabilités sont rapportées à la hauteur effective d'inondation et sont comparées aux courbes de fragilité établis selon les sondages du Grand tsunami du Japon en 2011. Finalement, on trouve que l'école représente un abri stratégique lors d'une inondation de tsunami vue que les sollicitations de la vague n'ont aucun effet significatif sur la structure du bâtiment lorsque la hauteur effective d'inondation atteint les 5-6m.

Cette étude de vulnérabilité des bâtiments vis-à-vis l'impact de tsunami nous a révélé le comportement des structures et les dommages prévus suite à cette catastrophe côtière. L'étude a démontré les zones de vulnérabilité d'une structure donnée et elle a apporté analytiquement des analyses tangibles et rationnelles comparant les sollicitations tsunamiques et sismiques. L'étude a aussi montré l'importance des bâtiments comme l'école dans les plans d'évacuation immédiate du tsunami. Certes, l'analyse de vulnérabilité des structures face au tsunami nécessite des efforts encore poussés tenant compte des projectiles et des débris en toutes forme qui peuvent attaquer les bâtiments notamment ceux du premier rang. En plus, cette étude peut être développée afin de traiter les problèmes d'affouillement, l'influence de l'effet de masque et le comportement de la structure lors du retour de la vague (phase run-down).

Practical example

Here an example of the assessment of tsunami vulnerability based on this thesis findings.

Let's take the location of Tangier city: many numerical simulations have been applied to this region in order to determine the limits of the inundation and to relocate the red zones where the danger of the tsunami attack is alarming. Some of these studies have been mentioned earlier in this report. To sum up these simulations output, the maximum height expected of the wave is approximately 6-7m.

To analyze the vulnerability of a structure, one must proceed through the methodology described in chapter 5.4.3. Modelling the structure on a structural software firstly, applying the tsunami forces and their respective distributions secondly, retrieving the maximum displacements and base shear for each height step thirdly, and plot the tsunami capacity curve in the fourth place could finally lead to plot the fragility curves that report the probability of a certain damage state to the inundation height. If the two buildings mentioned in this report are taken as example, the fragility curves are shown in Figure 65.

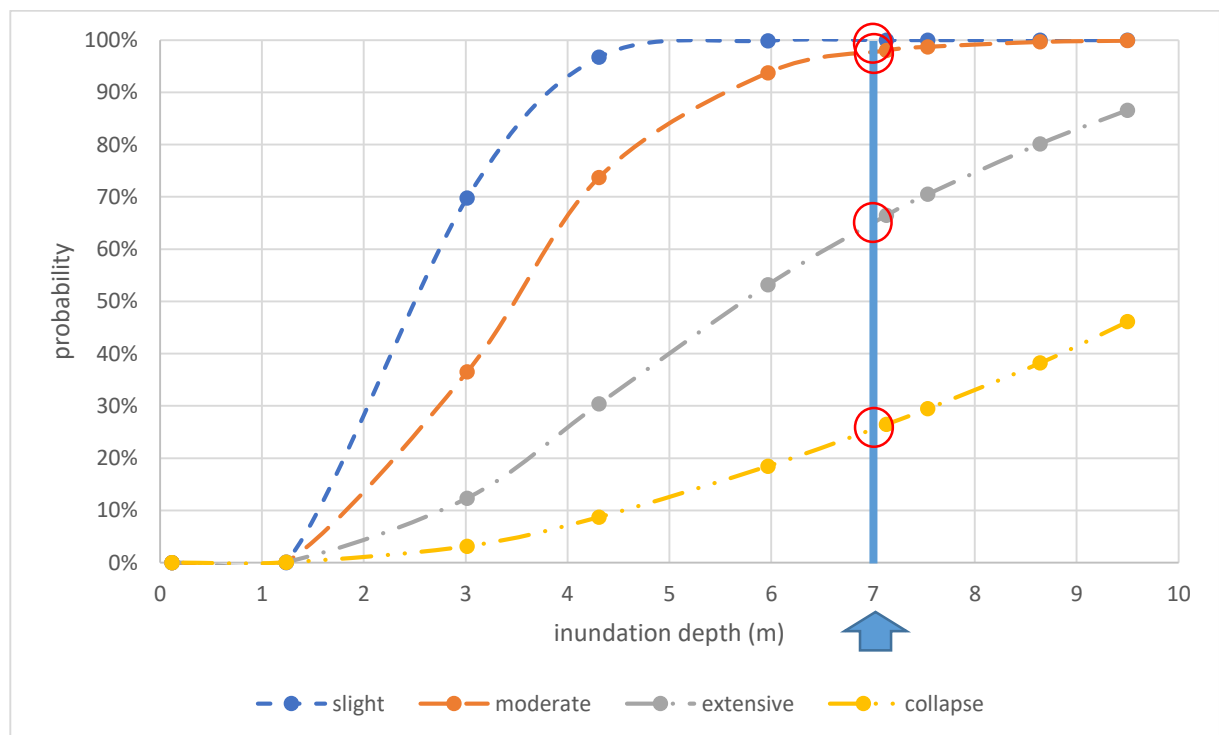


Figure 65: fragility curves of the first building

From Figure 65, the probabilities are retrieved as follows: 100% for slight damage, 98% for moderate damage, 65% for extensive damage and 25% for collapse.

For the school building, the fragility curves are shown in Figure 66. The recorded probabilities are: 22% for slight damage, 13% for moderate damage, 4% for extreme damage, and finally 1% for collapse.

The comparison between the two results shows how the school building resist more to the tsunami impact and how the probability of collapse is reduced.

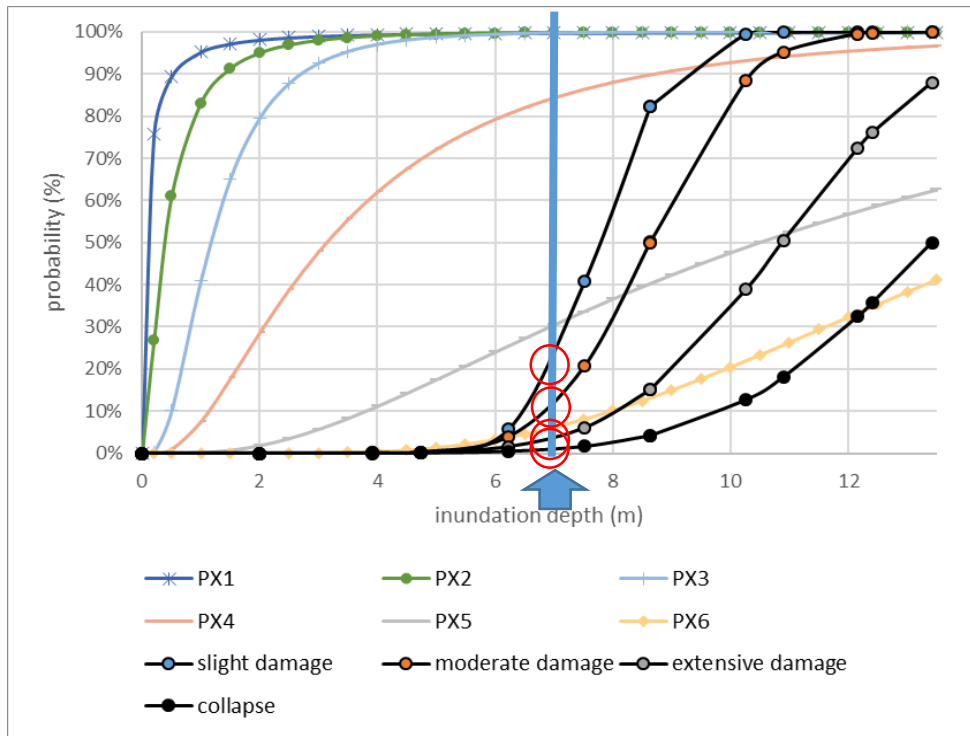
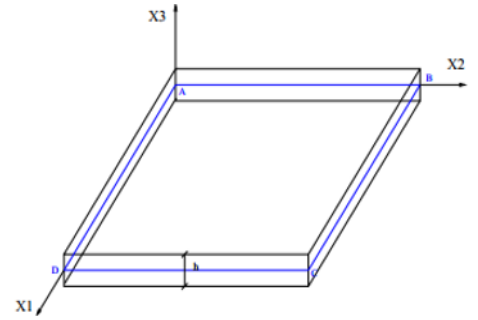


Figure 66: fragility curves for the school building

Appendix

This appendix illustrates the theory of plates mentioned in section 5.3.1.2 for lateral loading of masonry out-of-plane walls. We consider a plate which is a plane structural element with a small thickness h compared to plate planar dimensions.

ABCD is the mid-surface and the material is supposed isotropic and homogeneous.



We assign:

- f_{v1} , f_{v2} and f_{v3} : forces per unit of volume in x_1 , x_2 and x_3 directions.
- f_1 , f_2 , f_3 , m_1 and m_2 : forces and moments per unit of surface with:

$$f_1(x_1, x_2) = \int_{-h/2}^{h/2} f_{v1} dx_3 \quad f_2(x_1, x_2) = \int_{-h/2}^{h/2} f_{v2} dx_3 \quad f_3(x_1, x_2) = \int_{-h/2}^{h/2} f_{v3} dx_3$$

$$m_1(x_1, x_2) = \int_{-h/2}^{h/2} x_3 f_{v1} dx_3 \quad m_2(x_1, x_2) = \int_{-h/2}^{h/2} x_3 f_{v2} dx_3$$

Axial forces N_1 , N_2 and N_3 (N/m) are:

$$N_{11}(x_1, x_2) = \int_{-h/2}^{h/2} \sigma_{11} dx_3 \quad N_{22}(x_1, x_2) = \int_{-h/2}^{h/2} \sigma_{22} dx_3 \quad N_{12}(x_1, x_2) = \int_{-h/2}^{h/2} \sigma_{12} dx_3$$

Where σ_{11} , σ_{22} are stresses perpendicular to x , y planes respectively and σ_{12} is the shear stress.

Bending moments M_{11} , M_{22} and M_{12} (Nm/m) are:

$$M_{11}(x_1, x_2) = \int_{-\frac{h}{2}}^{\frac{h}{2}} x_3 \sigma_{11} dx_3 \quad M_{22}(x_1, x_2) = \int_{-\frac{h}{2}}^{\frac{h}{2}} x_3 \sigma_{22} dx_3$$

$$M_{12}(x_1, x_2) = \int_{-h/2}^{h/2} x_3 \sigma_{12} dx_3$$

Shear forces T_1 and T_2 (N/m) are:

$$T_1(x_1, x_2) = \int_{-h/2}^{h/2} \sigma_{13} dx_3 \quad T_2(x_1, x_2) = \int_{-h/2}^{h/2} \sigma_{23} dx_3$$

Due to the fact that:

- The thickness doesn't change, $\varepsilon_3 = 0$
- The stress σ_{33} is negligible compared to other stresses

The Hooke law that describes the stress-strain relation is:

$$\begin{bmatrix} \sigma_{11} \\ \sigma_{22} \\ \sigma_{12} \end{bmatrix} = \frac{E}{1-\vartheta^2} \begin{bmatrix} 1 & \vartheta & 0 \\ \vartheta & 1 & 0 \\ 0 & 0 & 1-\vartheta \end{bmatrix} \begin{bmatrix} \varepsilon_{11} \\ \varepsilon_{22} \\ \varepsilon_{12} \end{bmatrix}$$

E is the young modulus and ϑ is the Poisson ratio.

In a point (x_1, x_2, x_3) , the equilibrium equation should satisfy:

$$\begin{cases} \sigma_{11,1} + \sigma_{12,2} + \sigma_{13,3} + f_{v1} = 0 & (A1) \\ \sigma_{21,1} + \sigma_{22,2} + \sigma_{23,3} + f_{v2} = 0 & (A2) \\ \sigma_{31,1} + \sigma_{32,2} + \sigma_{33,3} + f_{v3} = 0 & (A3) \end{cases}$$

The general equilibrium over the thickness of the plate is:

$$\int_{-h/2}^{h/2} \{equations(A1, A2 \& A3)\} dx_3 = 0$$

So:

$$\begin{cases} N_{11,1} + N_{12,2} + f_1 = 0 \\ N_{11,1} + N_{12,2} + f_2 = 0 \\ T_{1,1} + T_{2,2} + f_3 = 0 \end{cases} \quad (S1)$$

The equilibrium of moments about x_1 and x_2 axis is:

$$\int_{-h/2}^{h/2} x_3 \{equations(A1 \& A2)\} dx_3 = 0$$

By considering that $\sigma_{13} = \sigma_{23} = 0$ for $x = \pm h/2$

$$\begin{cases} M_{11,1} + M_{12,2} - T_1 = 0 \\ M_{12,1} - T_2 = 0 \end{cases} \quad (S2)$$

By combining the equations in (S1) and (S2) we obtain the equation of Lagrange:

$$M_{11,11} + 2M_{12,21} - M_{22,2} + f_3 + m_{1,1} - m_{2,2} = 0$$

By exploiting the stress-strain relations, we have:

$$M_{11}(x_1, x_2) = \int_{-\frac{h}{2}}^{\frac{h}{2}} x_3 \sigma_{11} dx_3 = \frac{E}{1-\vartheta^2} \int_{-\frac{h}{2}}^{\frac{h}{2}} x_3 (\varepsilon_{11} + \vartheta \varepsilon_{22}) dx_3$$

So:

$$M_{11}(x_1, x_2) = \frac{E}{1-\vartheta^2} \int_{-\frac{h}{2}}^{\frac{h}{2}} x_3 (u_{,1} + \theta_{2,1} x_3 + \vartheta (v_{,2} - \theta_{1,2} x_3)) dx_3$$

Where u, v are displacement in x_1, x_2 directions and θ_1, θ_2 are rotations about x_1, x_2 axis.

The plate is symmetric about the neutral plane (x_1, x_2) so:

$$M_{11}(x_1, x_2) = D(\theta_{2,1} - \vartheta\theta_{1,2})$$

Where: $D = \frac{h^3 E}{12(1-\vartheta^2)}$ is the flexural stiffness of the plate.

The hypothesis of the plate of Kirchhoff which considers that points in a cross-section perpendicular to the neutral axis stay in this cross-section even after deformation leads to $\theta_1 = w_{,2}$ and $\theta_2 = -w_{,1}$ where w is the deflection of the plate. So:

$$M_{11}(x_1, x_2) = -D(w_{,11} + \vartheta w_{,22})$$

The same results for other moments is written as:

$$M_{22}(x_1, x_2) = -D(\vartheta w_{,11} + w_{,22})$$

$$M_{12}(x_1, x_2) = -D(1 - \vartheta)w_{,12}$$

By replacing in the equation of Lagrange we obtain:

$$w_{,1111} + 2w_{,1212} + w_{,2222} = \frac{f_3}{D}$$

Or

$$\Delta^2 w = \frac{f_3}{D}$$

A load f_3 could be written with the Fourier double trigonometric series equation as:

$$f_3(x_1, x_2) = \sum_{m=1}^{\infty} \sum_{n=1}^{\infty} a_{mn} \sin\left(\frac{m\pi x_1}{a}\right) \sin\left(\frac{n\pi x_2}{b}\right)$$

Where a_{mn} is a fourier coefficient given by :

$$a_{mn} = \frac{4}{ab} \int_0^b \int_0^a f_3(x_1, x_2) \sin\left(\frac{m\pi x_1}{a}\right) \sin\left(\frac{n\pi x_2}{b}\right) dx_1 dx_2$$

The solution by Fourier series leads to:

$$\omega(x, y) = \frac{1}{\pi^4 D} \sum_{m=1}^{\infty} \sum_{n=1}^{\infty} \frac{a_{mn}}{\left(\frac{m^2}{a^2} + \frac{n^2}{b^2}\right)^2} \sin\left(\frac{m\pi x}{a}\right) \sin\left(\frac{n\pi y}{b}\right)$$

Bibliography

- Al-Chaar, G. (2002). *Evaluating Strength And Stiffness Of Unreinforced Masonry Infill Structures* (No. Erdc/Cerl-Tr-02-1). Engineer Research And Development Center Champaign Il Construction Engineering Research Lab.
http://www.researchgate.net/publication/235149444_Evaluating_Strength_and_Stiffness_of_Unreinforced_Masonry_Infill_Structures.(as of November 9, 2018)
- Applied Technology Council (ATC). (1996). ATC-40 Seismic Evaluation and Retrofit of Concrete Buildings. (November 1996): 612. <https://www.atcouncil.org/vmchk/Rehabilitation-of-Engineered-Buildings/Seismic-Evaluation-and-Retrofit-of-Concrete-Buildings/flypage.tpl.html>.(as of November 9, 2018)
- Asteris, P. G., Antoniou, S. T., Sophianopoulos, D. S., & Chrysostomou, C. Z. (2011). Mathematical macromodeling of infilled frames: state of the art. *Journal of Structural Engineering*, 137(12), 1508-1517.
- Atillah, A., El Hadani, D., Moudni, H., Lesne, O., Renou, C., Mangin, A., & Lorito, S. (2011). Tsunami vulnerability and damage assessment in the coastal area of Rabat and Salé, Morocco. *Natural Hazards & Earth System Sciences*, 11(12).
- Baptista, M. A., Miranda, J. M., Chierici, F., & Zitellini, N. (2003). New study of the 1755 earthquake source based on multi-channel seismic survey data and tsunami modeling. *Natural Hazards and earth System Science*, 3(5), 333-340.
- Benchekroun, S., Omira, R., Baptista, M. A., El Mouraouah, A., Ibenbrahim, A., & Toto, E. A. (2015). Tsunami impact and vulnerability in the harbour area of Tangier, Morocco. *Geomatics, Natural Hazards and Risk*, 6(8), 718-740.
- Benchekroun, S., Omira, R., & Baptista, M. A. (2013, April). Tsunami Vulnerability in the NE Atlantic: Towards a new approach to estimate the damage grade on coastal buildings. In *EGU General Assembly Conference Abstracts* (Vol. 15).
- Bendada, A., El Hammoumi, A., Gueraoui, K., Sammouda, M., Ibenbrahim, A., & El Mouraouah, A. (2015). On the Vulnerability of Coastal Buildings in the Gulf of Cadiz under Tsunami Forces. *Contemporary Engineering Sciences* · January 2016 DOI: 10.12988/ces.2016.59275
- Bendada, A., El Hammoumi, A., Gueraoui, K., Sammouda, M., Ibenbrahim, A. (2017). Vulnerability Analysis of a School Building under Tsunami Loading in the Gulf of Cadiz. *International review of civil engineering IRECE* (January). DOI: <https://doi.org/10.15866/irece.v8i1.10912>
- Borrero, J., Cho, S., Moore, J. E., & Synolakis, C. (2006). The Regional Economic Cost of a Tsunami Wave Generated by a Submarine Landslide Off of Palos Verdes, California. *Infrastructure Risk Management Processes: Natural, Accidental, and Deliberate Hazards*, 1, 67.
- Buhan, D. P., & Felice, D. G. (1997). A homogenization approach to the ultimate strength of brick masonry. *Journal of the Mechanics and Physics of Solids*, 45(7), 1085-1104.
- Bui, T. T. (2013). *Etude expérimentale et numérique du comportement des voiles en maçonnerie soumis à un chargement hors plan* (Doctoral dissertation, Lyon, INSA). <https://tel.archives-ouvertes.fr/tel-00963611/document> (as of November 12, 2018)

- Dominey-Howes, D., & Papathoma, M. (2007). Validating a tsunami vulnerability assessment model (the PTVA Model) using field data from the 2004 Indian Ocean tsunami. *Natural Hazards*, 40(1), 113-136.
- El Mrabet, T. (1991). La sismicité historique du Maroc (en arabe). These d'état de 3ème cycle, Faculté des lettres et des Sciences et Humaines, Université Mohammed V, Rabat.
- EN 1052-1 (1998). Methods of Test for Masonry–Part 1: Determination of Compressive Strength. *European Committee for Standardization, Brussels*.(
<https://www.boutique.afnor.org/norme/nf-en-1052-1/method-of-test-for-masonry-part-1-determination-of-compressive-strength/article/760901/fa029727> (as of November 12, 2018)
- FEMA. (2011). FEMA P-55 Coastal Construction Manual Coastal Construction Manual.(
<https://www.fema.gov/media-library/assets/documents/3293> (as of November 9, 2018)
- FEMA, 356. (2000). Commentary for the seismic rehabilitation of buildings. *FEMA-356, Federal Emergency Management Agency, Washington, DC*.
<http://sharif.edu/~ahmadizadeh/courses/strcontrol/CIE626-2-FEMA-356.pdf> (as of november 9,2018)
- FEMA P-646. (2008). Guidelines for Design of Structures for Vertical Evacuation From Tsunamis. *Jetty.Ecn.Purdue.Edu* (June): 176. <ftp://jetty.ecn.purdue.edu/spujol/Andres/files/15-0021.pdf>. (as of november 12,2018)
- Gazzola, E. A., & Drysdale, R. G. (1986, September). A component failure criterion for blockwork in flexure. In *Advances in analysis of structural masonry* (pp. 134-154). ASCE.
- Kaabouben, F., Baptista, M. A., Iben Brahim, A., Mouraouah, A. E., & Toto, A. (2009). On the moroccan tsunami catalogue. *Natural Hazards and Earth System Sciences*, 9(4), 1227-1236.
- Kaushik, H. B., Rai, D. C., & Jain, S. K. (2006). Code Approaches to Seismic Design of Masonry-Infilled Reinforced Concrete Frames: A State-of-the-Art Review. *Earthquake Spectra*, 22(4), 961-983.
- Kawatsuma, S., Fukushima, M., & Okada, T. (2012). Emergency response by robots to Fukushima-Daiichi accident: summary and lessons learned. *Industrial Robot: An International Journal*, 39(5), 428-435.
- Kumar, S. M., Western, J. J., & Satyanarayanan, K. S. (2017). Analytical Study On Nonlinear Performance Of Rc Two Bay Three Storey Frames With Infill. *Asian Journal Of Civil Engineering (Bhrc)*, 18(1), 133-149.
- Lourenço, P. B. (2000). Anisotropic softening model for masonry plates and shells. *Journal of structural engineering*, 126(9), 1008-1016.
- Lukkunaprasit, P., Ruangrassamee, A., & Thanasisathit, N. (2009). Tsunami loading on buildings with openings. *Science of Tsunami Hazards*, 28(5), 303.
- Luque, L., Lario, J., Civis, J., Silva, P. G., Zazo, C., Goy, J. L., & Dabrio, C. J. (2002). Sedimentary record of a tsunami during Roman times, Bay of Cadiz, Spain. *Journal of Quaternary Science: Published for the Quaternary Research Association*, 17(5-6), 623-631.
- Mainstone, R. J., and Weeks, G. A. (1970). The influence of bounding frame on the racking stiffness and strength of brick walls. Proc., 2nd Int. Brick Masonry Conf., Building Research

Establishment, Watford, England, 165–171.

Milani, G. (2011). Simple homogenization model for the non-linear analysis of in-plane loaded masonry walls. *Computers & Structures*, 89(17-18), 1586-1601.

Milani, G., Lourenço, P., & Tralli, A. (2006). Homogenization approach for the limit analysis of out-of-plane loaded masonry walls. *Journal of structural engineering*, 132(10), 1650-1663.

Nistor, I., Palermo, D., Nouri, Y., Murty, T., & Saatcioglu, M. (2010). Tsunami-induced forces on structures. In *Handbook of coastal and ocean engineering* (pp. 261-286).

Norwegian Geotechnical Institute. (2013). UNISDR Global Assessment Report 2013 - Tsunami Methodology and Result. Geneva, Switzerland,.

Omira, R., Baptista, M. A., Miranda, J. M., Toto, E., Catita, C., & Catalao, J. (2010). Tsunami vulnerability assessment of Casablanca-Morocco using numerical modelling and GIS tools. *Natural hazards*, 54(1), 75-95.

Pande, G. N., Liang, J. X., & Middleton, J. (1989). Equivalent elastic moduli for brick masonry. *Computers and Geotechnics*, 8(3), 243-265.

Papathoma, M., & Dominey-Howes, D. (2003). Tsunami vulnerability assessment and its implications for coastal hazard analysis and disaster management planning, Gulf of Corinth, Greece. *Natural Hazards and Earth System Science*, 3(6), 733-747.

Piatanesi, A., Tinti, S., & Bortolucci, E. (1999). Finite-element simulations of the 28 December 1908 Messina Straits (southern Italy) tsunami. *Physics and Chemistry of the Earth, Part A: Solid Earth and Geodesy*, 24(2), 145-150.

Puglisi, M., Uzcategui, M., & Flórez-López, J. (2009). Modeling of masonry of infilled frames, Part I: The plastic concentrator. *Engineering Structures*, 31(1), 113-118.

Ramsden, J. D. (1993). Tsunamis: forces on a vertical wall caused by long waves, bores, and surges on a dry bed.

Ringot, E. (2014). cours de dynamique de structure 2eme partie réponse à un séisme M1-Dynamique Part2. (<https://sites.google.com/site/sciencespouringenieur/home/dynamique-et-parasismique> (as of november 9,2018)

Risk-Ue. (2003). An Advanced Approach to Earthquake Risks Scenarios with to Applications Different European Towns, WP4: Vulnerability of Current Buildings.

RMSI. (2012). Morocco Natural Hazards Probabilistic Risk Analysis and National Strategy Development Tsunami Hazard Report.

RPS2000 v2011. règlement de construction parasismique (<http://www.sodibet.com/telechargement/RPS2011.pdf>)

Standard 2005. Eurocode 6: Design of masonry structures—Part 1-1: General rules for reinforced and unreinforced masonry structures. *Comité Européen de Normalisation: Brussels, Belgium*(<https://www.boutique-formation.afnor.org/2018/construction-reglementation-et-ingenierie/conception-technique/eurocodes/c3662>)

Standard 2005. Eurocode 8: Design of structures for earthquake resistance-part 1: general rules, seismic actions and rules for buildings. *Brussels: European Committee for Standardization*. (<https://www.boutique-formation.afnor.org/2018/construction-reglementation-et-ingenierie/conception-technique/eurocodes/c3636>)

Suppasri, A., Mas, E., Charvet, I., Gunasekera, R., Imai, K., Fukutani, Y., & Imamura, F. (2013). Building damage characteristics based on surveyed data and fragility curves of the 2011 Great East Japan tsunami. *Natural Hazards*, 66(2), 319-341.

Yeh, H. (2007). Design tsunami forces for onshore structures. *Journal of Disaster Research*, 2(6), 531-536.

Zucchini, A., & Lourenço, P. B. (2002). A micro-mechanical model for the homogenisation of masonry. *International journal of Solids and Structures*, 39(12), 3233-3255.

List of figures

Figure 1: project organization	13
Figure 2: response spectrum (after Ringot, E. 2014)	22
Figure 3: capacity curves required to define the strength degradation (after ATC 40).....	25
Figure 4: capacity curve with global strength degradation modeled (after ATC 40).....	25
Figure 5: acceleration response spectrum (after Ringot, E. 2014).....	26
Figure 6: displacement response spectrum (after Ringot, E. 2014).....	26
Figure 7: Acceleration-displacement response spectrum (ADRS) (after Ringot, E 2014)	27
Figure 8: example of fragility curves (after Risk-Ue 2003).....	30
Figure 9: principal steps to plot fragility curves (after Risk-Ue 2003).....	30
Figure 10:Tsunami damage in Thailand and Indonesia (December 2004 Indian Ocean tsunami): (a)severe structural damage, Khao Lak, Thailand; (b) column failure of a reinforced concrete frame, Thailand; (c) column failure due to debris impact, Banda Aceh, Indonesia; (d) failure of infill walls, Banda Aceh, Indonesia. (after Nistor et al. 2010)	33
Figure 11: The shallow water, long waves, approximation for tsunami propagation. presents the free surface elevation, h denotes the water depth and u and v are the velocity components in x - and y - directions, respectively.(after Piatanesi & al 1999).....	34
Figure 12: computed extreme water surface from South West Iberia source to local areas (after RMSI 2012)	35
Figure 13: Omira 2011 model: (a) maximum wave heights and flow depths generated from South West Iberia source (b) inundation onshore(after Omira & al 2011)	36
Figure 14: hydrostatic force distribution and location of resultant.....	39
Figure 15: calculation of drag coefficient on rectangular columns due to hydrodynamic force (after Arnason 2005)	39
Figure 16: runup and z elevation parameters.....	40
Figure 17: hydrodynamic force distribution.....	40
Figure 18: bore formation offshore (FEMA P646).....	41
Figure 19: surge form when tsunami rush up on shore (after FEMA P646)	41
Figure 20: experiment simulating the tsunami wave impact on a building prototype (after Lukkunaprasit & al 2009).....	43
Figure 21: time history of base shear forces (up) and pressure (above) (after Nistor et al. 2010)	43
Figure 22: time history of maximum sensed force and different pressures detected (after Lukkunaprasit & al 2009).....	44
Figure 23: architectural plan of the test building.....	46
Figure 24: micro model proposed by (Milani, Lourenço, and Tralli 2005).....	49
Figure 25:recording of the displacement of the wall's center due to the pressure p (after Lourenço 2000).....	49

Figure 26: results of analysis at pressure p equals 6.6Mpa (peak) (a) deformed mesh (b) principal moments (c) plastic strain in bottom and (d) in top face. (after Lourenço 2000).....	49
Figure 27: failure modes of unreinforced masonry: (left) parallel or (right) perpendicular to bed joints (after Eurocode 6).....	51
Figure 28: failure for a simply supported masonry panel (WII) (after Bui 2013)	52
Figure 29: determination of f_{xk1} and f_{xk2} characteristics according to EN 1052-2 norm (see EN 1052-2 norm for more details).....	52
Figure 30: FEM in "3DEC" software to determine f_{xk1} and f_{xk2} (after Bui 2013)	53
Figure 31: behavior of masonry panels simply supported by 3 edges (after Bui 2013)	53
Figure 32: Variation of pressure of the impulsive force for different run-ups by the effective height, W_{edmax} is the maximum bearable pressure.	55
Figure 33: change in lateral load transfer mechanism by in-plane walls (after kaushik & al 2006).....	56
Figure 34: diagonal strut model for masonry walls following (after Mainstone & al 1970).....	57
Figure 35: all failure modes of in-plane infill masonry (after Kumar & al 2017).....	57
Figure 36: force application pattern for (top) seismic and (bottom) tsunami solicitations.....	58
Figure 37: stress distribution in (top) seismic and (bottom) tsunami solicitations at the same time step (KPa).....	59
Figure 38: time history in the FEM model.....	61
Figure 39: time history for each row of columns considering the delay of impact (F. impulsive and F. hydrodynamic).....	62
Figure 40: maximum displacement of the building frame (case of 7m effective height at the top floor)	63
Figure 41: bending moments in columns (case of 7m effective height).....	63
Figure 42: deformed shape of the building frame and state of hinges (case of 7m effective height)	64
Figure 43: acceptance criteria (IO, LS and CP) for a force-deformation interaction of hinges (after SAP2000 help menu)	64
Figure 44: S11 stress recorded in a ground floor column for a 4m and 5m effective height cases	65
Figure 45: decrease of building stability by level of effective inundation height	65
Figure 46: capacity curve for case GF=4m, R=12m	66
Figure 47: comparison between capacity curves (restricted to ground height) for run-up of 5m and 12m with different Ground Floor heights	66
Figure 48: deflection of a single DOF system with fixed restraint	67
Figure 49: fragility curves computed for different damage states and a comparison with statistical observed data of the 2011 Great tsunami of Japan (Suppasri et al. 2013).....	68
Figure 50: Ground floor, 2nd floor and principal facade architectural plans	72
Figure 51: steps of creating the 3D CAD model of school building.....	75
Figure 52: CFD 3D model of the school building.....	76

Figure 53: flow trajectory (front view)	77
Figure 54: flow trajectory (bottom view)	77
Figure 55: total pressure variation on the surface of columns	78
Figure 56: variation of average total force (N) and column's shear stress (tau) by time iteration	78
Figure 57: distribution of forcises in the test school building	80
Figure 58: pushover curve for school building	80
Figure 59: comparison between tsunami capacity curve and pushover curve	81
Figure 60: increase of tsunami force	82
Figure 61: representation of actions of tsunami forces (left) and earthquake forces (right)	82
Figure 62: hinges plastification in columns (top: tsunami case ,bottom: seismic case)(B-C-D&E: degrees of plastification of hinges, IO-LS&CP: Acceptance criteria of hinges(immediate occupancy, life safety and collapse prevention))	84
Figure 63: fragility curve by max displacement value	85
Figure 64: fragility curves (black) and comparison to suppasri data (PXi) compiled from the great 2011 Japan tsunami	86
Figure 65: fragility curves of the first building	93
Figure 66: fragility curves for the school building	94

List of tables

Table 1 : methods of evaluation of a seismic action	21
Table 2:coefficients of the empirical method for period determination.....	22
Table 3: characteristics of materials	47
Table 4: characteristics of masonry material (after Bui 2013).....	53
Table 5: loads considered for school design	72

Résumé

La présente thèse traite le sujet d'analyse de la vulnérabilité tsunamique des structures en se basant sur des méthodes précises s'appuyant sur les règles d'ingénierie et les lois de la dynamique des structures.

Les trois éléments principaux de l'étude sont décrits : la connaissance du tsunami, ses forces et ses caractéristiques, les normes de dimensionnement des structures en béton armé et la méthode des éléments finis. En outre, une description de l'analyse de la vulnérabilité sismique est introduite puisque elle aide à comprendre la réaction de la structure suite à une sollicitation extérieure. Les caractéristiques du tsunami, les charges qu'appliquent la vague et la distribution de ces charges sur les obstacles rencontrés sont illustrées. En se basant sur ces éléments, une analyse détaillée sur la vulnérabilité tsunamique est développée sur deux niveaux: pour les bâtiments réguliers et pour les structures stratégiques pour l'évacuation comme les écoles. Plusieurs éléments de cette analyse sont traités, comme la réaction des murs en maçonnerie, l'étude de mouvement des éléments des portiques, ...etc. La déduction des déplacements et les déformations nous permet d'établir la courbe de capacité et les courbes de fragilité qui indiquent les probabilités des dommages que subiront les éléments structuraux et non structuraux et déterminent la vulnérabilité du bâtiment.

Mots-clefs (5) : vulnérabilité, bâtiment, tsunami, analyse sismique, pushover.

Abstract

This work investigates the tsunami vulnerability of structures through numerical simulations of the impact. Our method is based on a structural analysis of the building frame and the exploitation of mechanical behavior results. Objective judgments of the building state in case of a tsunami attack is conducted through engineering references and methodologies like the displacement-base shear analysis, known for seismic analysis as the pushover curve. Interesting findings from the analysis of two test buildings introduced in this study provide a considerable asset in the assessment of tsunami vulnerability. One branch of the study develops an analysis of infill masonry walls' response for both types: in-plane and out-of-plane walls, while another branch details the reinforced concrete frame response as well as a CFD analysis of the tsunami attack. The RC behavior is fully discussed through an expanded explanation of results of the maximum displacements recorded, bending moment's distribution, nonlinear hinges reactions, and the decrease of building's stability.

Setting the assessment of tsunami vulnerability as the main objective, this study has reached its goals of illustrating seismic pushover curve, plotting tsunami capacity curve and fragility curves as well as justifying the findings with a logical interpretation and detailing the discussion of results.

Key Words (5) : vulnerability, building, tsunami, seismic analysis, pushover.